Hydrological and geochemical characterization of shallow aquifer water following a nearby deep CO_2 injection in Wellington, Kansas

by

Ian E. Andree

B.S., Temple University, 2012

A THESIS

submitted in partial fulfillment of the requirements for the degree

MASTER OF SCIENCE

Department of Geology
College of Arts and Sciences

KANSAS STATE UNIVERSITY
Manhattan, Kansas

2017

Approved by:

Major Professor
Saugata Datta

Copyright

Abstract

Domestic and irrigation well water quality in south-central Kansas is threatened by multiple sources of contamination including CO_2-EOR activities, evaporite dissolution and oilfield brine release. This research identifies potential groundwater flow paths for contaminant migration in a concentrated area mixed with oil, injection, irrigation and domestic wells. Groundwater (GW) sampling took place before and after CO_2 injections into the Mississippian in to assess temporal changes in water quality in a ~2 mile radius around injection well KGS 2-32. Samples were analyzed for stable isotopes, rare earth elements (REE), major and trace ions, dissolved organic carbon (DOC) with a select few analyzed for dissolved CO_2 and hydrocarbons. Results of major ion chemistry reveal an evaporite control on geochemistry in wells screened within the paleoterrace as opposed to the incised valley. Bedrock channeling due to erosional scouring of the paleovalley is speculated to have led to secondary porosity thereby increasing GW flow. Similar stable isotopic and Br/Cl mass ratios between SW-3, Shepherd and Zehr indicate water is similarly sourced; lower total dissolved solids within incised valley could result from dilution from infiltration through overburden sediments. Br/Cl, SO_4/Cl, Na/Cl and (Ca+Mg)/Na ratios indicate Shepherd, Zehr and SW-3 are possibly impacted by a recent salt plume movement through this portion of the shallow aquifer. An increase in total dissolved solids and Mg/Ca ratios with temperatures less than 25°C over a 25 to 200 ft. depth interval into the Permian Shale of the uplands could have resulted from increasing calcitization and reduction in effective porosity. Dissolved REEs showed most domestic and surface waters contain similar signatures, indicating similarly sourced water. Additionally, there was no CO_2 leakage found within the sampling timeframe and a future leaked plume may be impeded by decreasing porosity from current secondary mineralization processes taking place in the Permian Shale.

Table of Contents

List of Figures

List of Tables

Acknowledgements

These last two years were a hard fought emotional journey that would not have been successful without the help of a number of people. First, I would like to thank those at the Kansas Geological Survey (KGS) namely Lynn Watney for his help coordinating field events, enthusiasm and willingness to address all of our concerns; Tiraz Birdie for his endless generosity, assistance with sampling plans and providing answers and data when we needed it most; Donald Whittemore for taking the time out of his day to meet with me and share his infinite wisdom; Tandis Bidgoli for meeting with me to answer my long list of questions. I'd like to thank those at Berexco for their incredible help and flexibility out in the field and for setting a world record for the fastest standpipe replacement on SW-3. I would like to thank Kansas State University (KSU) undergraduate Trenton Bortz for his assistance in the field and bearing with my nose to the grindstone mentality on those scorching hot July Summer days; Brooks Ryan for helping gather and organize field supplies and acid bathing a million bottles always with a smile.

I would like to specially thank my funders, in particular KSU Geology alumni Paul and Deanna Strunk and Mr. Darrow for their generous donations which saved me financially and helped me feel like a valued part of the KSU Geology family; the Geological Society of America (GSA) and Kansas Geological Foundation (KGF) for their research investment funds, without them we would not have been able to afford analyses, field/lab supplies, hotel, etc.

I would like to thank Karen Johannesson at Tulane University for taking time out of her day countless times to address my numerous and often times repetitive questions about correct REE pre-concentration procedures and for carefully analyzing my samples and providing exquisite data. I would also like to thank Darren Chevis at Tulane who courteously offered his

assistance with REE pre-concentration steps occasionally over the phone with the utmost patience.

I would like to thank those in the KSU Geology Dept. namely my committee members, Dr. Pamela Kempton for her incredibly helpful writing critique, Dr. Matthew F. Kirk for being a great friend and fellow scientist through humor and personal guidance and helping me get unstuck in my research and providing Ion Chromatography assistance sometimes at no cost; Dr. Sambhudas Chaudhuri for sharing his experience and wisdom with me and providing insight that changed the way we look at this research. I would like to thank the graduate students for letting me let loose and unwind with them after long weeks, in particular Grant Zwiefelhofer, Jacob Hughes, Michelle Berube, Sam Berkelhammer, Beth Morter and Kyle Marquart; a special thanks to Colleen Gura for long days in the XRD lab working with me and being a great mentor providing general advice.

I would like to thank my parents Gloria and Ed Andree and Jackie and Junichi Miura for their endless support and righting my motivation. I'd like to lend a heartfelt thanks my fiancé Lauren Knox who endured this journey with me despite difficult circumstances and Mandy for her goofy antics and bringing a smile to my face after long days.

Last but furthest from least, my advisor and great friend Dr. Saugata Datta, thanks for everything. Dr. Datta provided the idea for this research and helped frame it by coordinating with others to plan field events, analyses, meetings, conferences, etc. He pushed me to present this research at every opportunity and helped improve me as a geologist but more importantly as an individual. He helped out with costs when we needed it most, and made time for me when he didn't have it. Thank you, Dr. Datta, for being a great friend, for learning to laugh with me when we were beyond stressed and for endless encouragement inside and out of the department.

Chapter 1 - Introduction

Water salinity, attributed to the rise in total dissolved solids (TDS), is a form of water quality degradation which can result from numerous sources. The source in question may be natural or anthropogenically-related with the true signal difficult to discern using limited geochemical tools. In an area afflicted by multiple potential salinity sources, tracing the source, particularly in the subsurface, can be further obfuscated by the complicated pathways which groundwater migrates and the role that geology plays on impacting water composition. It is therefore understood that hydrology/hydrogeology is inherently related to geochemistry and investigative efforts to understand contaminant distribution in a hydrogeologic setting would benefit by exploring both.

In terms of groundwater, there are a variety of ways to define contamination. One such way is delimitation via enforceable standards established by an authorizing agency such as the EPA to control the level of quality for the consumer. Other water quality criteria such as TDS or individual major ions are less restricted, although some less severe adverse effects on human health, crops or livestock have been previously studied. With respect to groundwater used for irrigation, high sodic content can adversely affect the structure of the soil and osmotic potential of the plant resulting in over stress and quicker wilting (Grattan, 2002). According to Michael Cahn, Irrigation and Water Resource Advisor at Monterey County UCCE, the 100% yield potential irrigation water TDS threshold for a variety of common crops ranges from 1,984 to 384 mg/L. Water monitoring for irrigation supplies is not controlled at the government level due to its indirect impact on human health, although its significance is bequeathed at the state and local economic level.

Subsurface water contamination may be prompted by anthropogenic pollution or natural accumulation of hazardous constituents that infiltrate the aquifer in a variety of ways. Examples of serious aquifer water quality degradation include trace metal release from sediment surfaces (Mandal & Suzuki, 2002; Mohan & Pittman, 2007; Dixit & Hering, 2003; Smith et al., 2000; Nordstrom, 2002) or salinization; the latter of which can be exacerbated by weathering of road salt stockpiles, extensive water-rock interaction or oilfield brine intrusion (Da Lio et al., 2015; Baba & Tayfur, 2010; Whittemore, 1995). In areas where oil production is high, the risk of water contamination by oilfield brine increases (Whittemore, 1995). Surficial oil spills from erupted pipelines, low-profile hydrocarbon releases, leaky pits near oil wells from historically poor disposal practices or underground migration of oilfield brines through open networks are common ways to substantially raise the TDS of a shallow groundwater system (Jackson et al., 2013; Ivshina et al., 2015). Salinization prompted by weathering of industrial salt stockpiles in heavily snow-laden areas produces the potential to mobilize chloride plumes as a continual point source (Granato et al., 2015). Transportation agencies have been known to store up to 3×10^5 kg of NaCl, $CaCl_2$ or $MgCl_2$ outdoors for winter highway de-icing (Ostendorf et al., 2006). Evapotranspiration concentration of salts in shallow soil profiles driven by low rainfall averages and arid to semi-arid climates is considered to be a major mechanism for salinity control. Irrigation water pulling from this source combined with leaching of nitrogen-based fertilizers or pesticides used in cropland management may incite local groundwater contamination. Over time, the contaminants may percolate and diffuse underground through the aquifers at rates dependent on lithology and hydraulic conductivity. Natural sources of chloride include dissolution of highly soluble evaporite deposits within subsurface rock formations or intrusion of brine. In south-central Kansas, irrigation and potable water are threatened by the presence multiple salinity

sources, which may ultimately pose a risk to human health (Whittemore, 1995; Watney et al., 2015; Anderson et al., 1994). Agricultural business, which accounts for the majority of land use in this region, is adversely affected by salinized irrigation water through plant growth prohibition, soil nutrient deficiency, phosphate availability and Ca transport (Grattan, 2002; Grattan, 1998). Groundwater/surface water quality is in turn adversely affected by cropland management negligence through infiltration or runoff of chemically-treated and salinized irrigation water into the hydrologic cycle.

Recent advances in the characterization of shallow aquifer salinity in Wellington, Kansas, have emerged from the Wellington Oil Field Small Scale Carbon Dioxide (CO_2) Injection Project led by the Kansas Geological Survey (KGS). This project was initiated to investigate the ability of the Mississippian and Arbuckle systems to receive CO_2 for the purpose of enhancing oil recovery (Mississippian) and CO_2 storage (Arbuckle). Injected CO_2 assumes the form of supercritical phase, i.e. a phase that contains characteristics of a gas and liquid, to initiate increased solubility and mass-solute transfer rates. Leakage occurs through migration pathways due to pressure gradient changes and the presence of localized faults, fractures or joints in the caprock above the repository. The outcome, depending on relative formation pressure, is exertion of fluid into shallower zones (Jessop & Subramaniam, 2007; Chang et al., 2008). Caprock failure due to exceedance of capillary breakthrough pressure and subsequent Darcy flow has been documented to occur during CO_2 reposition efforts, leaving implications for uncertainty of long term CO_2 storage (Wollenweber et al., 2010). An escaping plume is exposed to declining ambient pressure and temperature conditions, resulting in a phase change to gaseous CO_2, which further enables mobilization through a reduction in density and solubility (Wilkin, 2010). Moreover, waters with lower TDS have higher adsorption with CO_2 than saline water, resulting

in solubility variation with salinity (Wilkin, 2010). The environmental concern over a CO_2 intrusion into a shallow aquifer is through prolonged CO_2-water interaction and resulting water acidification via carbonic acid dissociation and subsequent leaching of trace elements from aquifer sediments in potentially hazardous quantities. An underground source of drinking water (USDW) is defined by the EPA as any aquifer of which a portion currently supplies water to potable wells or public water systems or contains less than 10,000 mg/L of TDS. Frequent monitoring of this resource, although not mandated for smaller-scale injections, is necessary to ensure preservation and protection of potable supplies.

This research identifies the potential of a miscible CO_2-EOR (Carbon Dioxide Enhanced Oil Recovery) intrusion into a shallow aquifer through a hydrogeochemical time series development approach from pre- to post-injection. Additionally, a major theme of this research is to use a variety of geochemical proxies to identify and trace salinity sources that will allow us to demarcate flow boundaries. The study site is focused around the CO_2-EOR injection well delineated by sensitive receptors such as surface reservoirs or domestic wells within Wellington Field in Central Sumner County, Kansas. Development of water quality characterization will be integrated using a variety of analytical approaches that address the areas of potential contamination. The key underlying tone is to provide an in-depth analysis of water quality and underline geochemistry as a proxy for interpretation of groundwater flow and behavior. Water bodies of interest to this study include surface waters, shallow groundwater and deeper oilfield brine. Water chemistry representation will be shown in graphical format, mostly in relation to sample depth to compare local conservative mixing trends. Complete evaluation includes an analysis of water-rock interaction through understanding local geologic changes. This research does not include sampling and analysis of shallow aquifer sediments to provide physical

qualities, such as solid mineralogical and elemental distribution constraints. Instead, local studies are juxtaposed for geochemical comparison to discuss larger-scale effects on flow behavior and compositional influence due to geologic differences. In terms of the CO_2-EOR aspect, it is understood that the working timeframe to complete this thesis does not envelop the likely timeframe for a CO_2 leakage event. This research will therefore attempt to confirm CO_2 security within the provided timeline through geochemical analysis and establish the basis for comparison against future water studies of potentially CO_2-contaminated waters in the local Wellington area. Thus the societal significance and purpose of this research is to wholly characterize water quality and identify current ports of contamination and pathways hydraulically connecting sample locations using a vast suite of geochemical tools in an effort to provide a detailed narrative of contributing saline sources, extent of water-rock interaction and aquifer connectivity.

Chapter 2 - Background

2.1 Previous Work

This research began in conjunction with an ongoing project implemented by the KGS who first pursued the Wellington Oil Field Small Scale CO_2 Injection Project in early 2010. The project started with the impetus to inject CO_2 for two purposes: (1) to enhance oil recovery of the Mississippian System and (2) to test the CO_2 sequestration potential of the Arbuckle Saline Aquifer. Injection wells KGS 1-28, 1-32 and 2-32 were installed to achieve those purposes; KGS 2-32 was installed for CO_2-EOR in the Mississippian limestone play "pay zone", whereas KGS 1-28 & 1-32 were installed to identify stratigraphic zones that show viable carbon storage potential in the Arbuckle. The KGS began CO_2-EOR injections into the Mississippian pay zone of KGS 2-32 in January 2016 with an average injection volume of 120 tonnes per day at a depth of 3664'-3706' below ground surface (BGS) spanning a total of 5 months until completion. This work does not address the shallow impact of CO_2 sequestration activities in the Arbuckle, as it has not occurred yet.

The primary motive for initiating the small-scale carbon storage project was to gain a fundamental understanding of the scientific process behind carbon storage using advanced characterization and modeling techniques (KGS, 2016). As such, this research was initially centered on the potential shallow water quality impact from a CO_2 leakage event. Barker (2012) laid the foundation of the work by conducting a mineralogical and geochemical investigation of the Arbuckle through SEM, XRD and CT as well as flow-through simulations to identify the ideal injection zone. The work was completed under DOE DE-FE-0006821 with the task to accurately characterize and determine highest carbon storage potential within the investigated injection zones. A zone of low porosity that defines the upper Arbuckle, deemed the baffle zone,

was identified through mineralogical findings of pervasive microcrystalline chert with substantially lower porosity than surrounding geologic layers. This baffle zone would become the cap rock above the injection zone to provide impedance for the CO_2 plume.

Before CO_2 sequestration activities within the Arbuckle could be launched, the KGS identified the need to test CO_2 injections within the Mississippian to enhance oil recovery. A geochemical and structural analysis of the Mississippian injection zone was first investigated prior to injections. KGS open-file report 2016-29 (Holubnyak et al., 2016) reported rock quality index results, calculated and measured capillary pressures, relative permeability and fault structure assessment—all of which validated the predicted success of CO_2 confinement within the Mississippian. This work allowed the KGS to identify the injection intervals and confirm the security of the CO_2 injectant in the long term.

Although monitoring of the shallow USDW is not mandated by the EPA for small-scale CO_2-EOR operations, the presence of sensitive receptors within the area of concern emphasizes the necessity to ensure security of shallow water quality. As such, the research documented in this thesis began under the jurisdiction of a Quality Assurance and Surveillance Plan implemented by KGS and EPA officials to monitor the shallow aquifer and report water quality changes that may be diagnostic of a CO_2 intrusion. Investigation was pursued on the basis of water quality characterization for the detection of mostly inorganic contaminants released by geochemical reactions involving CO_2-water interaction.

2.2 Current Work and Purpose

In October 2015, the first groundwater sampling event of this research was conducted by KSU alongside KGS and EPA personnel for the purpose of collecting and characterizing pre-injection water samples. Water samples were extracted from nearby potable wells and surface

water access points, as well as three monitoring wells installed by the KGS. The water chemistry that was characterized from the October 2015 sampling round served as the baseline reference for the pre-injection composition and comparison against post-injection samples. A later groundwater sampling event conducted in July 2016 was implemented to monitor the same sample locations following the start of CO_2 injections to serve as the basis for post-injection water composition. However, seismic surveys and mole fraction predictions based on porosity variations within the Mississippian conducted by the KGS in June 2016 reported that the plume was successfully confined within safe limits of the injection zone. As such, the goal of this research was amended to include comprehensive geochemical characterization and groundwater flow path connectivity of the shallow aquifer.

A secondary objective of this research is to identify and differentiate the primary salinity sources contributing to the high salinity gradient within the shallow aquifer of the study area. Prior to 1935, oil and gas practices in the state of Kansas did not regulate disposal of oilfield brine or involuntary release from incompetent well design (Jones, 1950). Further legislature administered by the state of Kansas in the late 1940s required containment of brine waste and written consent from the state for injection into deep repositories in an effort to protect local freshwater (Whittemore, 2007). The outcome was a generally successful prevention of oil and gas release by 1950, although years of negligence allowed for the release of large quantities of pollutants that are still sweeping through geologic layers today. Additional sources of salinity within the region include salinized irrigation water used in cropland management, dissolution of evapotranspiration concentration deposits, and evaporite minerals within regolith and bedrock strata. The significance of identifying salinity sources within the shallow aquifer of south-central Kansas is therefore predicated within the potential for obscurity. Whittemore (1995) used

fundamental conservative geochemical tracers to assist with tracking and differentiating salinity sources of south-central Kansas; sources such as oil brine, halite/evaporite deposits, industrial road salt and natural soil evapotranspiration concentration provided distinct signatures from which mass balance endmember mixing could be calculated.

Prior work conducted in Wellington, Kansas, by KGS personnel indicated abnormally high TDS values for some shallow wells and low TDS for others of similar depth nearby. As a result, this research has employed a comprehensive geochemical investigation that will assist in tracing source waters to help establish aquifer connectivity through the utilization of conservative relationships. The conservative nature of the Cl ion, i.e. its resistance to redox reactions and water-rock interaction, as well as the pervasiveness and variability of Cl sources enables environmental tracers such as Br/Cl and SO_4/Cl relationships to be useful. Since the majority of producing oil wells in Wellington Oil Field screen the Mississippian pay zone, the target repository interval for CO_2-EOR, this research is interested in characterizing Mississippian oilfield brine samples in an attempt to identify and correlate the fingerprint.

2.3 Geochemical Investigations

2.3.1 Major Ions

A detailed groundwater study is blind without a thorough look at the major ion distribution. Approximately 90% of the TDS in groundwater are comprised of eight major elements: Na^+, Ca^{2+}, K^+, Mg^{2+}, Cl^-, HCO_3^-, SO_4^{2-} and CO_3^{2-} (Hem, 1989). These elements contribute to the majority of the TDS and ionic strength of the solution, and form the basis of most water quality investigations. Previous studies in the area (Barker, 2012) have mapped the major ion distribution of the Arbuckle potential injection zone at varying intervals (Figure 2.1).

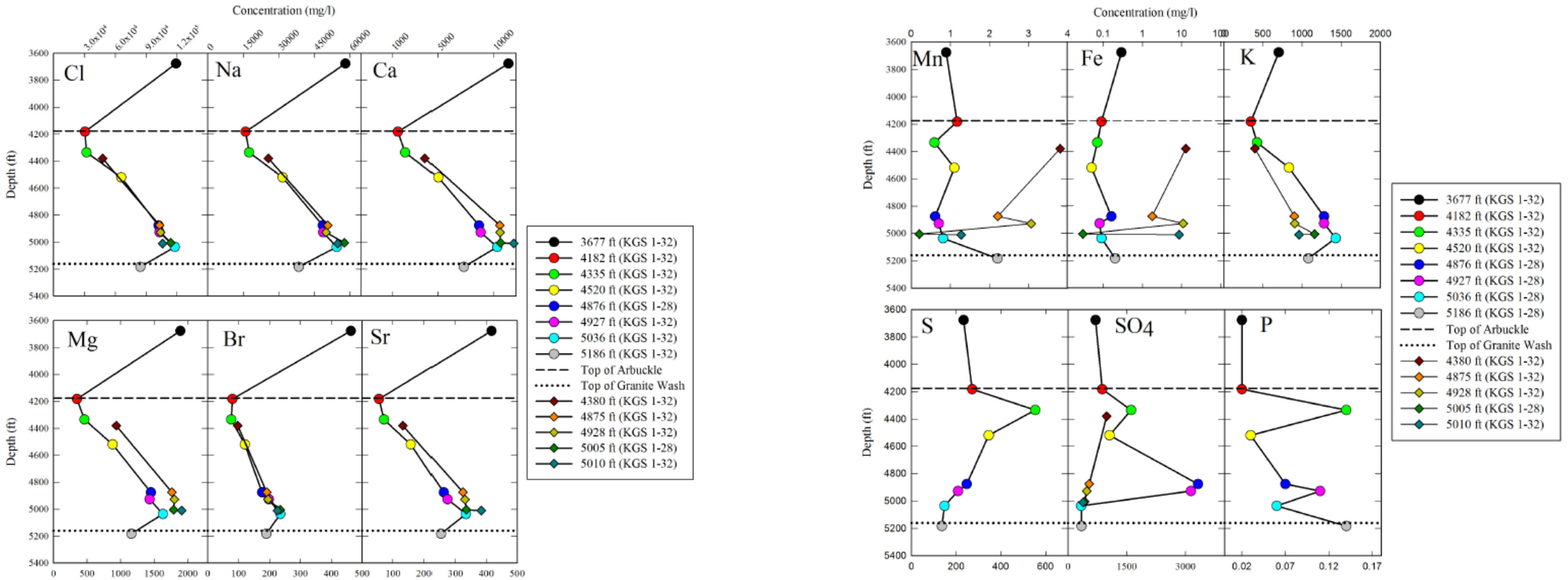

Figure 2.1 Major ion variation with depth through Arbuckle and Mississippian showing linear trending ions (left) and a non-linear trend (right) (Barker, 2012).

A significant finding of this work, as shown in Figure 2.1, was the observation of a nearly linear increase of some major ions such as Cl, Na, Ca, Mg and Br with depth. Piper diagrams were constructed to show hydrochemical facies transition between intervals (Figure 2.2). Barker (2012) purports that enriched Ca^{2+} and Sr^{2+} relative to depleted Mg^{2+} and SO_4^{2-} is representative of localized calcite dolomitization within the upper Arbuckle. This interpretation has been confirmed through SEM and CT imaging of the core mineralogy, as well as synchronicity of seawater evaporation curve placement as a function of chloride concentration (Barker, 2012).

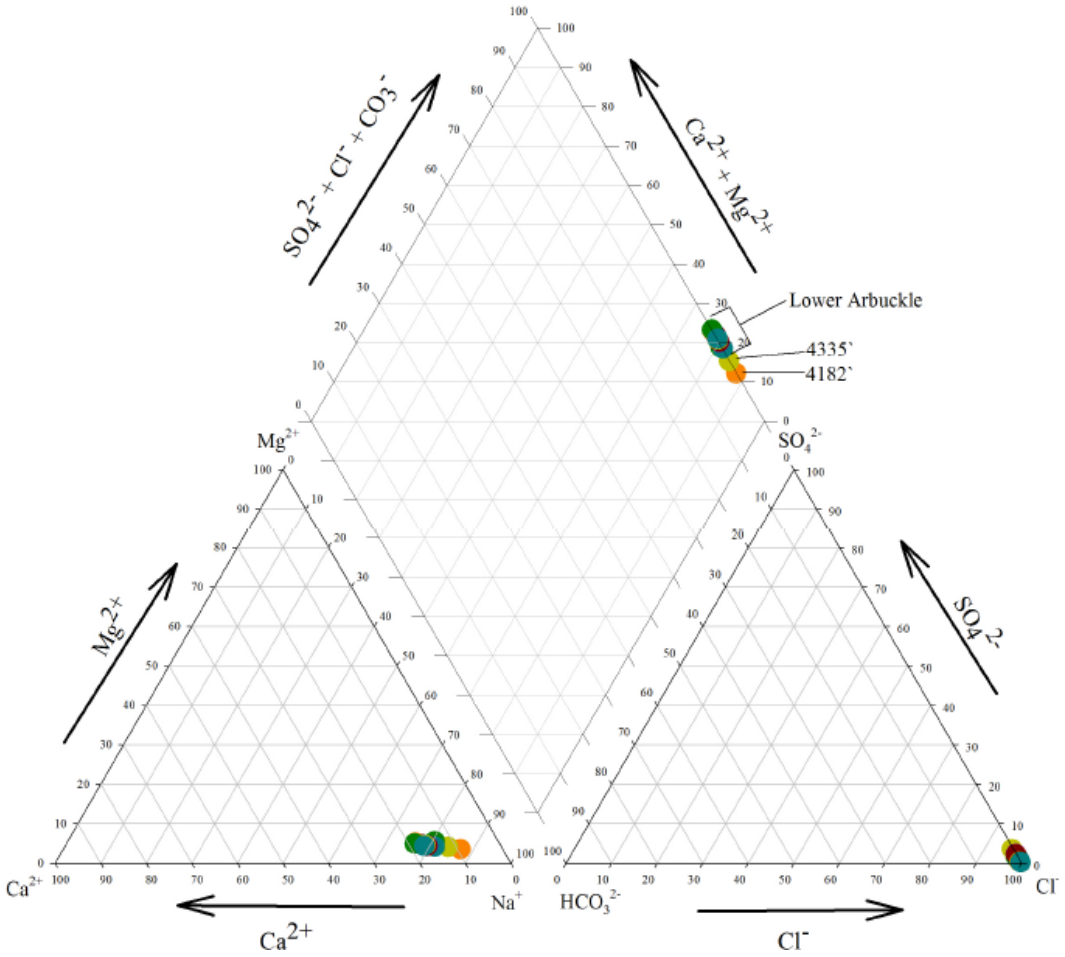

Figure 2.2 Piper diagram illustrating variation in hydrochemical facies with increasing depths through the Arbuckle (Barker, 2012).

Furthermore, as discussed in Chapter 2.2, major ionic conservative relationships such as Br/Cl, SO_4/Cl, Na/Cl and (Ca + Mg)/Na are of interest to this research, as they help to distinguish the salinity source using methods outlined by Whittemore (1995) (Figure 2.3). Brine disposal practices prior to the mid-20th century increased brine runoff in surface reservoirs. Subsequent infiltration into shallow aquifers progressed for the following decades. Periods of increased pumping from nearby irrigation wells increased lateral migration of the oilfield brine particularly during times of low flow (Whittemore, 2007). Anthropomorphized salinity on the basis of oilfield brine contamination is evidenced through mass balance mixing calculations of Br and Cl mass values. For the majority of shallow waters in south-central Kansas, salinity is sourced from natural evaporite deposits as shown in Figure 2.3.

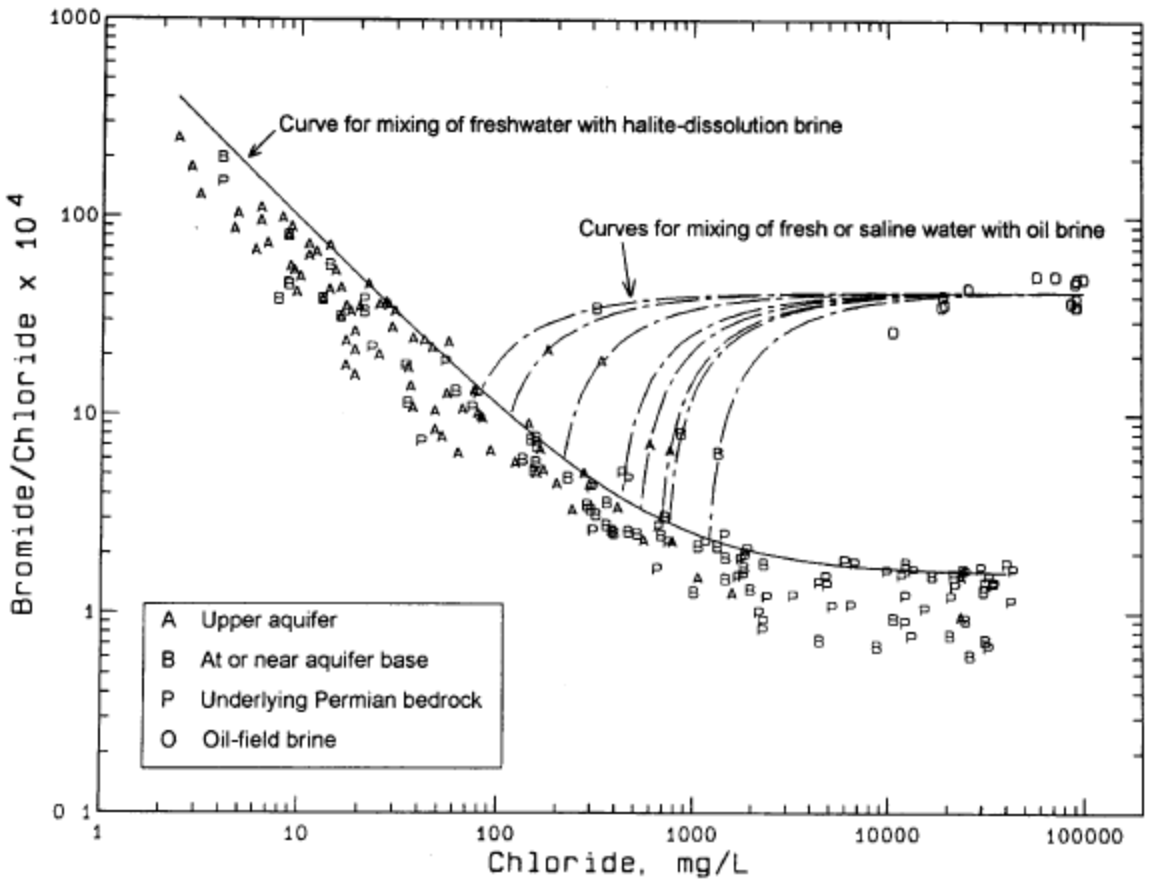

Figure 2.3 Br/Cl mass ratios of upper Permian waters in south-central Kansas as shown in Whittemore (1995). Water samples plotted within the mixing curve of freshwater and halite-dissolution brine represent naturally contaminated water.

2.3.2 Stable Isotopes

Stable isotopes are a key part of a comprehensive groundwater study for identification of water source relation. Water circulation on Earth is a cyclical process, storing valuable tracking information in stable isotopic signatures during different phases of water movement or mixing. The low mass of hydrogen and oxygen yield greater isotopic mass fractionation than heavier elements, leaving behind more distinct signatures in the fluid that render them useful as geotracers in water flow path behavior studies (Sharp, 2007). In general, evaporative processes tend to enrich the fluid with respect to ^{18}O and ^{2}H content relative to ^{16}O and ^{1}H, respectively.

Deep infiltration of water into the subsurface may be evident through more positive $\delta^{18}O$ and $\delta^{2}H$ ratios. The conventional expression of stable isotopes is per mil (‰) deviation from Vienna Standard Mean Ocean Water (VSMOW), an accepted standard used to normalize data (SAHRA, 2005; Craig, 1961a). In general there are two types of fractionation, equilibrium and kinetic isotope effects (Kendall et al., 1995).

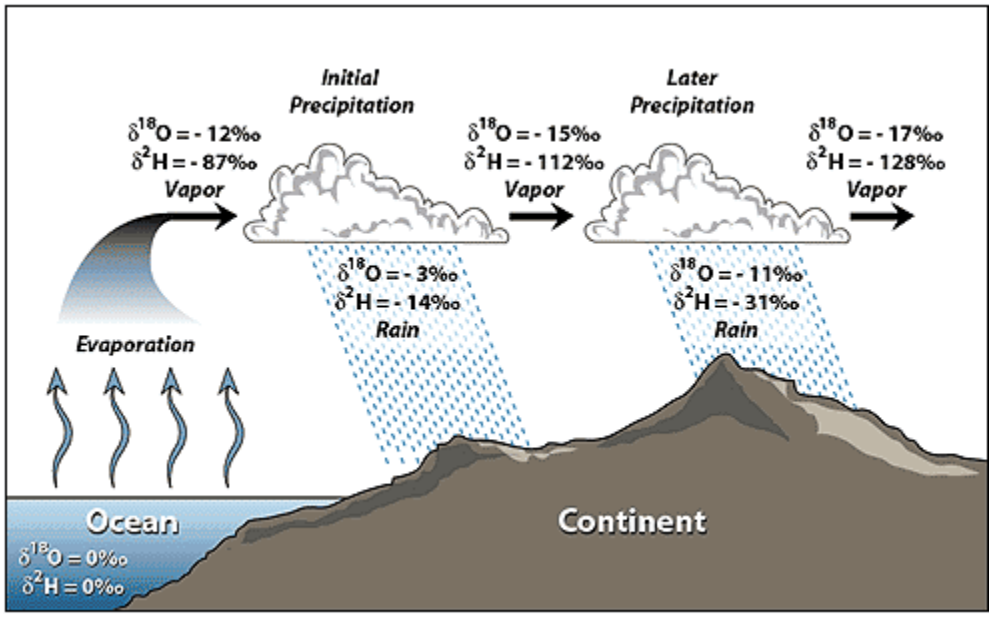

Figure 2.4 Isotope fractionation with distance from evaporation source (SAHRA, 2005).

The extent of fractionation depends on degree of mass partitioning. The lighter oxygen and hydrogen isotopes (^{18}O, ^{2}H) have significantly higher kinetic velocities and weaker bonds compared to their heavier counterparts (Melander, 1960). Therefore, these isotopic ratios are highly sensitive to fractionation effects providing distinct signatures that reflect their original source. Additionally, lighter isotopes are depleted in $\delta^{18}O$ relative to $\delta^{2}H$ in mid-continental areas due to mass partitioning as evaporative water vapor migrates from coastal areas to the plains (Figure 2.4 & Figure 2.5).

Together, hydrogen and oxygen isotopes may be used to constrain regional-scale mixing trends for groundwater flow pathway identification. In general, stable isotopic composition of water is only altered by evaporation or high-temperature geothermal processes, owing to their conservative value through a resistance to chemical reactions during transport though fractionation is appreciable (Muir & Coplen, 1981). Since a high proportion of the mass is contributed by oxygen, mixing between waters is a function of mass balance. Significant alteration of $\delta^{18}O$ ratios is therefore a result of large compositional differences between the original water and the contaminant. Distinct isotopic signatures would be apparent in geologic settings where prolonged water-rock interaction has precluded recharge and groundwater flow.

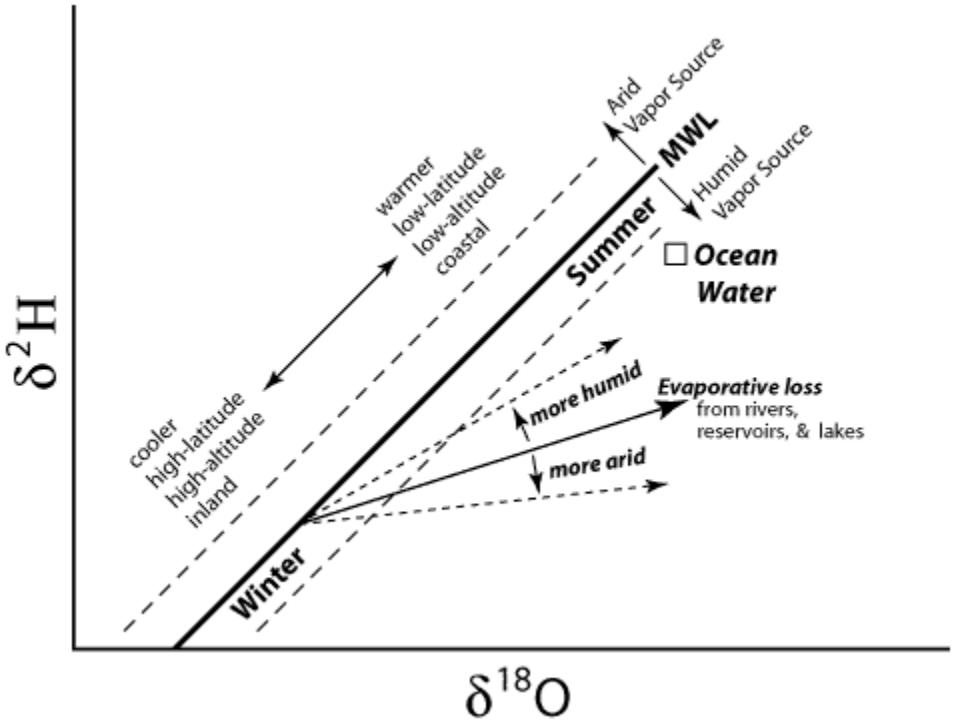

Figure 2.5 Isotopic deviation from a MWL reference with precipitation/evaporation processes (SAHRA, 2005).

The isotopically lighter fraction in water molecules contain higher translational kinetic velocity allowing faster water surface tension breakthrough, resulting in a higher contribution to the

lighter stable isotopic ratio in the water vapor phase. When compared to a Global or Local Meteoric Water Line reference (GMWL/LMWL) on a graphical plot, their relative location can assist in determining relative humidity and precipitation/evaporation processes of the collection area based on enrichment/depletion trends. If waters contain similar stable isotopic signatures, it may indicate a common source water origin allowing for the resolution of subsurface fluid migration pathways.

Barker (2012) previously mapped stable isotopic distribution of the Arbuckle injection zone within the study area from drill stem tests (Figure 2.6). A progressive ^{18}O-enrichment was observed with depth which was interpreted to have resulted from restrictive vertical hydraulic communication among sample intervals. Impermeable strata would preclude hydraulic connectivity implicating little inter-horizon transport and immobility for CO_2-brine uptake. This finding helped establish the competence of the cap rock overlying the injection zone to prevent pore-space transport.

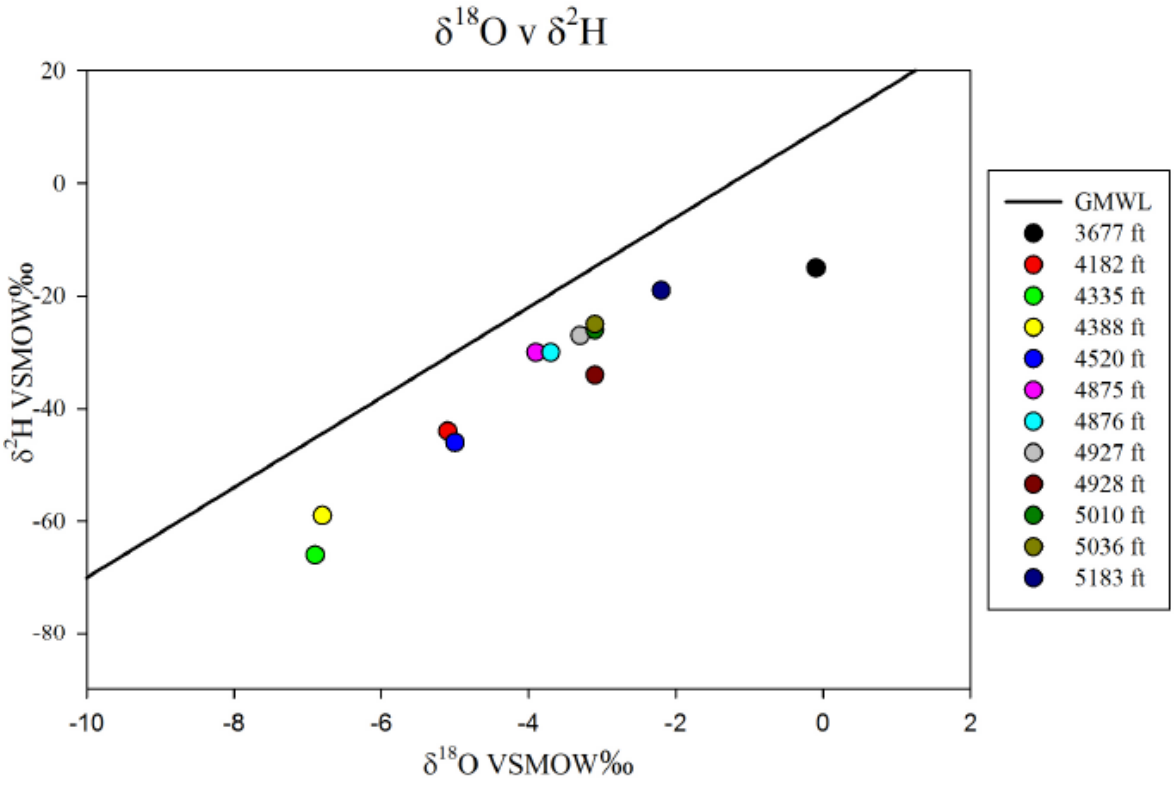

Figure 2.6 Arbuckle and Mississippian stable isotope deviation from GWML (Barker, 2012).

Additionally, $\delta^{13}C$ Dissolved Inorganic Carbon (DIC) analyses are an interest to this work as there are multiple sources within the shallow aquifer that could be contributing to higher DIC, namely weathering of calcitic deposits and presence of CO_2. Upon a leakage scenario, $\delta^{13}C$ DIC will increase due to dissolution of the intruding CO_2 (Sharp, 2007). The Mississippian interval, as shown by work conducted by Barker (2012), contains elevated $\delta^{13}C$ DIC values as a result of carbonate dissolution and voluminous additions of CO_2 by EOR activities. Biogeochemical cycling of DIC may obfuscate the signal of a foreign intrusion thus prompting the need for a time series observation to more thoroughly understand carbon budget. In essence, knowledge of $\delta^{13}C$ distribution can be used as a means of tracing water sources.

2.3.3 Trace Elements

A major potential health risk from acidified waters is the concurrent elevation of dissolved toxic metals. The higher surface area of finer aquifer sediments enables increased sorption stability with trace elements. Mobilization of trace metals into the fluid phase is a pH-dependent property. Solubility has an inverse relationship with pH; a lower pH will increase solubility and dissolve more ions into solution (John & Leventhal, 1995). As a result, water quality can quickly degrade with increased trace metal concentration; of particular interest are metals that are regulated by the EPA. Physicochemical processes of weathering or alteration result in the breakdown and transport of the trace elements from sediment surfaces, depending on the availability of complexing ligands and extent of surface protonation (Brickler & Jones, 1995; Pope et al., 1999). Speciation of major ions within groundwater depends on pH, availability of organic/inorganic ligands, ionic strength and cationic character of the water (Pope et al., 1999; Allard, 1995).

The source of trace elements in groundwaters, whether natural or anthropogenic, is difficult to ascertain. A comprehensive evaluation of the site detailing human activity and geologic history is required for this. In general, urban areas are more victimized from anthropogenic influence than suburban or rural areas due to greater human activity. Water supplies are affected as a result of industrial effluent releases, chemical erosion from coated buildings and combustion of fossil fuel from automobiles (Pope et al., 1999). Areas high in agricultural activity may observe a particular increase in copper concentrations in groundwater due to copper-containing pesticide sprays used in cropland management (Pope et al., 1999). As a result of lower population, rural areas tend to be the geographical target for studies such as CO_2 sequestration. Previous research has shown trace metal mobilization through CO_2 dissolution; in

particular, Cd, Cu, Fe, Pb, As and Cr are preferentially released (Kampman et al., 2014; Frye et al., 2012; Melhorn et al., 2016; Lawter et al., 2016). This effect has been shown to be buffered through the weathering of carbonates and subsequent bicarbonate release (Frye et al., 2012).

Previous trace metal water quality research of Quaternary deposits in south-central Kansas (Pope et al., 1999) documented the prevalence of Al and Ba in the shallow aquifer with some elemental concentrations that exceed EPA standards (Figure 2.7 and Figure 2.8). The majority of the constituents of concern were found to be below standard, with most falling below the reporting limit, although Al and Ni displayed limited variations in concentration. Contrary to what is expected for a highly agriculturalized area, Cu concentrations fell significantly below the Maximum Contaminant Limit (MCL) with median values just above the reporting limit.

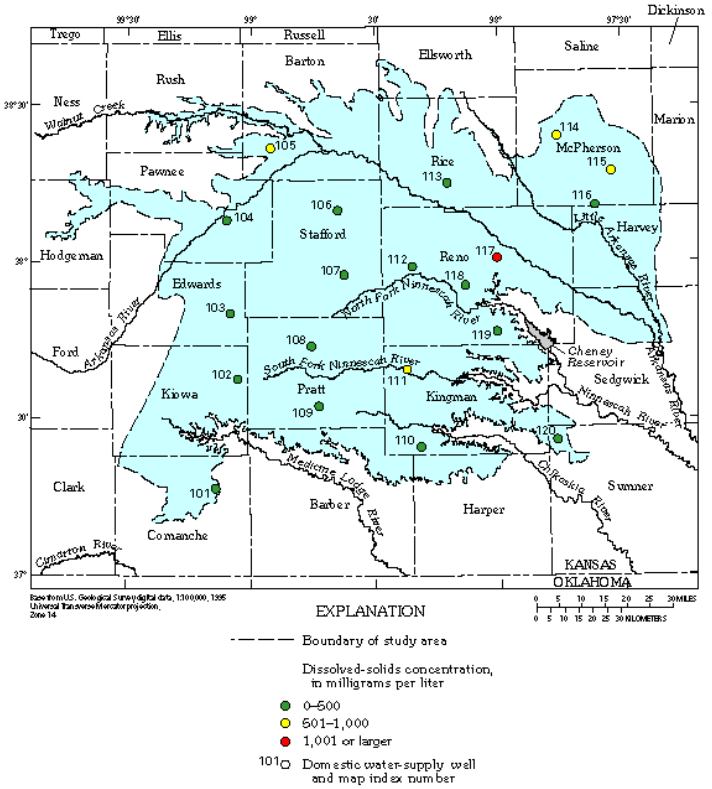

Figure 2.7 Map of geologic extent of Quaternary deposits in south-central Kansas and related shallow wells with their respective TDS concentration from Pope et al. (1999).

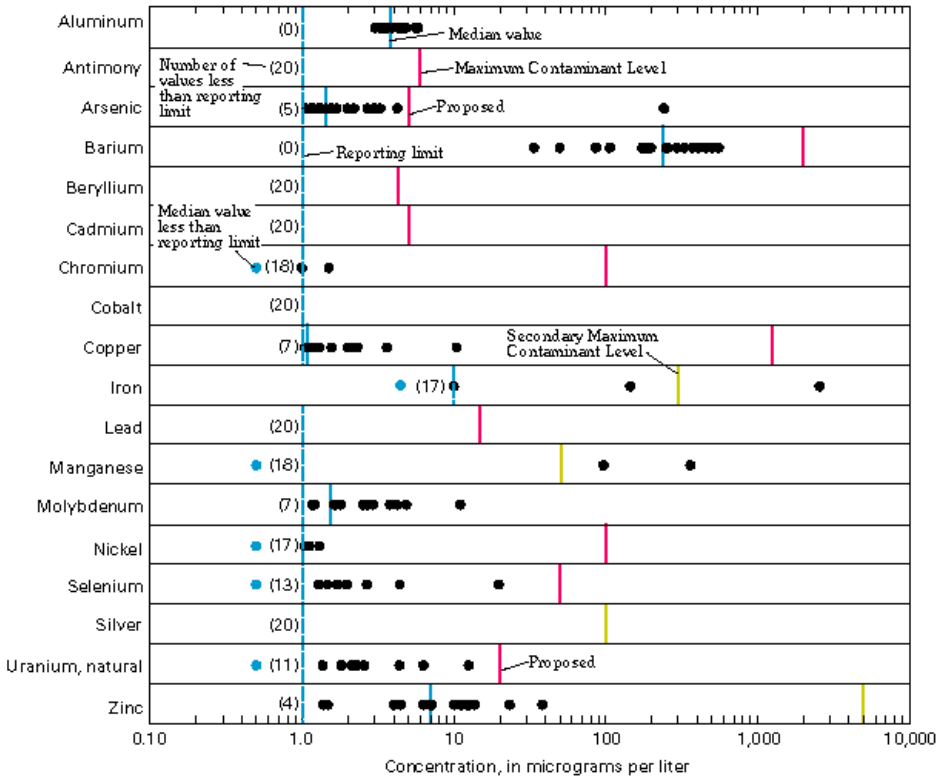

Figure 2.8 Trace elements (µg/L) from groundwaters sampled within Quaternary deposits in south-central Kansas (Pope et al., 1999) amalgamated with EPA MCL.

Excessive Mn, Fe and As concentrations within the shallow Quaternary deposits were explained by concomitant low dissolved oxygen values, indicating active reductive dissolution of Fe-containing (oxyhydr)oxides. Pope et al. (1999) determined there was little evidence to suggest trace elements were derived from an anthropogenic source and instead concluded accumulation in shallow groundwater is due to natural weathering of the local geology.

2.3.4 Rare Earth Elements

The REEs, also known as the lanthanide series, includes the 15 elements from La to Lu; Y and Sc are sometimes included due to similarities in their chemical behavior. The REEs are traditionally divided into a light REE (LREE) group consisting of La-Eu and a heavy REE (HREE) group from Gd-Lu and Y, although some studies separate out a middle REE (MREE)

group including Eu-Dy (Samson & Wood, 2004). The LREE are known to be incompatible during substitution with most other elements due to their large ionic radius. The consistent decrease in atomic radius with increasing atomic number is a phenomenon referred to as the lanthanide contraction. This results in fractionation patterns where HREE are more readily included in phases due to their smaller size, whereas LREE are excluded (Walters et al., 2011). The charges of all ions are exclusively trivalent with the exception of Ce (III/IV) and Eu (II/III). Typically REEs are used in igneous studies to determine fractionation patterns during crystallization of magma and are sought after in economically significant deposits; however, in the last 30 years REEs have increasingly become useful as geotracers in low temperature hydrological studies.

Groundwater flowpath behavior in addition to groundwater evolution can be characterized by differences in REE distribution (Jianfei et al., 2014; Johannesson et al., 1997; Johannesson et al., 1999; Tang & Johannesson, 2005; Leybourne & Cousens, 2005). Similar to some of the previously discussed trace metals, the distribution of REEs in waters is sensitive to pH changes owing to a strong, competitive complexation with ligands and relatively low free metal ion activity in solution (Johannesson et al., 1997). The chemical unity and conservative mixing behavior of REEs in waters can preserve a litho-signature indicative of past water-soil-rock interaction (Gosselin et al., 1992). The ability for REEs to serve as a tool for distinguishing different lithologic origins provides one means by which to detect displaced brine signatures. Notably, however, signals imparted by anthropogenic inputs may obfuscate the observed concentration (Noack et al., 2014). As REEs are weathered from the aquifer sediments/rock, they impart a signature on the fluid in the dissolved and particulate phase (Johannesson, 2005; Johannesson et al., 2005; Tang & Johannesson, 2005; Banner et al., 1988). The host

sediment/rock that was weathered by the fluid represents a control on the observed REE pattern. Hanson (1980) noted the importance of normalizing REE data to a reference standard due to the higher abundance of even atomic number REE relative to the odd atomic number REE owing to the Oddo-Harkins effect and processes originating back to nucleosynthesis. Typical normalizing materials include chondritic meteorites, Post-Archaean Australian Shale (PAAS), and North American Shale Composite (NASC). When normalized in this way, the alternating abundance patterns of odd and even numbered elements are removed and relative enrichments and depletions of interest can be observed.

A complete hydrochemical characterization of the waters includes the assessment of major ligands used for trace element transport. REEs will bind to complexing ligands due to the strong ionic bonding tendencies of their electronic configurations (Greenwood & Earnshaw, 1984; Aide & Aide, 2012). Transport occurs along the groundwater flow direction at rates dependent on the presence and concentrations of common REE-ligand complexes (CO_3^{2-}, PO_4^{3-}, HCO_3^-, OH^-, SO_4^{2-}, Cl^-, DOC, etc.) and hydrological/mineralogical constraints of the physical aquifer. In order to truly exploit REEs as natural tracers, one must understand their fractionation as a function of complexing ligand abundancy, ion exchange, pH variation, and colloidal partitioning (Gosselin et al., 1992). Their distribution via complex formation depends on sorption coefficient stability constants that vary with pH, salinity, ionic strength, pCO_2, etc. for each individual REE; these are experimentally-derived and can be used in solution complexation modeling to determine the relative sorption potential for each REE to understand transport mechanisms driving REE fractionation patterns (Tang & Johannesson, 2010; Johannesson et al., 2017). Typically, specific sorption sites have stronger binding potential than others, which affects REE distribution and behavior in the fluid (e.g. CO_3^{2-} versus SO_4^{2-}). REE-carbonate

complexes [$LnCO_3^+$] have potential to suppress carbonate precipitation through ion exchange with major binding ions such as Ca, Mg, Fe, etc. (Johannesson et al., 1997). Additionally, variations in the relative abundance of the different REEs relative to one another (e.g. heavy REE relative to light REE) can be attributed to specific hydrologic and geologic settings, leading to a general correlation of lithologic provenances. Although surface-complexing ligands are a substantial competitor with solution-complexing ligands, the former requires a firm understanding of the modal mineralogy and elemental distribution within the host aquifer to accurately model results. This thesis did not fully investigate the geochemistry of the shallow aquifer and, thus, surface complexation will not be considered.

REE complexation with DOC has been documented to be a strong competitor with other ligands. Solution complexations of REE-DOC are a poorly understood mechanism, given the complexity and variability of stability constants and abundancy of organic ligands (Tang & Johannesson, 2005). As such, this research does not evaluate the solution complexation of REE-DOC; however, the concentration of DOC relative to inorganic ligands is of interest in order to discuss the potential of DOC ligands to be a major complexing and transporting agent.

2.3.5 Dissolved Organic Carbon

As pointed out in section 2.3.1, DOC is used in trace element studies to evaluate the potential for organic ligands to be a major transporting agent in the absence of other strongly complexing ligands (Aiken, 2002; Allard, 1995). Additionally, DOC is used in general groundwater studies to assess the amount of available food source for microbially mediated reactions (Aiken, 2002). Microbial degradation of organic matter in the presence of a favorable electron acceptor can lead to the reduction of the acceptor through electron transfer (Lovley & Phillips, 1988; Bethke et al., 2011). Microbial respiration occurs as a function of favorable

(increasingly negative) [Gibbs] free energy release from oxidation-reduction reactions, with excess energy used to regulate their metabolic processes (Flynn et al., 2013). In general, microbial favorability of electron accepters to use as a substrate for transfer follows $O_2 > NO_3^- >$ Mn(IV) > Fe(III) > $SO_4^{2-} > CO_2$. This sequence has significant implications for water quality and microbially induced compositional changes with respect to increasingly anoxic settings. In oxygen-depleted environments, and with the absence of the other preferred electron acceptors, a CO_2 intrusion could be mitigated simply by microbial decomposition of the CO_2 molecule. In addition, organic matter degradation can increase bicarbonate concentration in acetotrophic reactions of reducing environments, thus increasing the buffer capacity of the groundwater during an intrusion event. Ferrous iron, manganous, hydrogen sulfide and methane are common byproducts from microbial reactions. Mobilization of arsenic through iron reducing reactions is a common source of natural contamination (Datta et al., 2011; Wang & Mulligan, 2006; Anawar et al., 2003) and should be monitored if DOC values are in excess.

Expected DOC values for groundwater not affected by outside contamination typically range from 0.5 to 2 mg/L (Leenheer et al., 1974; Drever, 1988). Soil filtration processes, including microbial leaching or precipitation of DOC complexes, remove the majority of DOC before the water table is reached (Drever, 1988). However, a shale aquifer contains significant proportions of DOC within lithified sediments, leaving accumulation likely sensitive to both allochthonous and autochthonous sources (Volk et al., 2002).

Sources of DOC besides that of organic contamination from landfill leachate or oilfield brine include soil leaching from the removal process as discussed above. Most forms of DOC in natural waters are present as humic or fulvic acids; in large quantities they can affect geochemical distribution of trace elements, redox reactions or water quality on the basis of odor,

smell, etc. (Hem, 1985; Pope et al., 1999). Pope et al. (1999) reports DOC values ranging between 0.3 and 1.5 mg/L with a median value of 0.4 mg/L for shallow waters that are contained within the Quaternary deposits of south-central Kansas. However, further analysis of the reported DOC data showed a DOC-contaminated blank and the values above could not be adequately validated.

2.3.6 Dissolved CO_2/Hydrocarbons

A secondary part of this groundwater investigation is the analysis of aqueous organic/inorganic dissolved carbon concentrations. Dissolved CO_2 within waters is an important consideration to an overall geochemical water quality assessment as it may provide information on inorganic carbon reactions related to carbonate minerals. Typically, dissolution of CO_2 happens such that:

(1) $CO_2(g) \rightarrow CO_2(aq)$
(2) $CO_2(aq) + H_2O \rightarrow H_2CO_3$
(3) $H_2CO_3 \rightarrow H^+ + HCO_3^-$
(4) $HCO_3^- \rightarrow CO_3^{--} + H^+$

Dissociation of carbonic acid (3) will yield increased acidity and bicarbonate concentration with further dissociation (4) leading to carbonate release accompanied by further acidification of the water. As carbonate is a highly reactive ligand, it may combine with various ions to precipitate a variety of carbonates. Additionally, CO_2 concentrations in excess of 50 mg/L may create a corroding environment with potential to mobilize trace elements from aquifer sediments (Hem, 1992).

Historical hydrocarbon releases have been documented in the general south-central Kansas region due to high oil productivity. Therefore, an assessment of dissolved hydrocarbons within waters in south-central Kansas would assist in the determination of point source pollution and salinity source differentiation. Analysis of a suite of hydrocarbons including methane,

ethane, ethene, propylene and propane would allow us to identify zones affected by anthropogenic or natural pollution. Implications of oilfield brine contamination in shallow groundwater include changes to water chemistry from microbial (methanogen) interaction, reduction via hypoxia and resulting trace metal mobilization from sediment surfaces as well as a general increase in TDS.

2.3.7 Water Quality Parameters

At the basic water quality assessment level, water chemistry can be characterized by parameters such as pH, turbidity, dissolved oxygen, oxidation-reduction potential, specific conductivity and temperature. This specific list of parameters has been standardized and mandated by the EPA for official groundwater sampling to ensure preservation of sample quality. Parameters must be collected by a properly calibrated meter as per ASTM D6452-99 (ASTM, 2012) to ensure accuracy of readings. Additionally, these parameters serve to track the water quality over time as they are sensitive to changing conditions from increased redox, water mixing or biological activity.

Chapter 3 - Geologic Setting

3.1 Surface Topography and Overburden

Shallow wells Shepherd, Becker and SW-3 partially screen the unconsolidated horizon above the bedrock at the study site (Figure 3.1 and Figure 3.2). To the SW, Slate Creek represents the topographic low of the site with elevation increasing NE. At the ground surface, the study area is described as an alluvial plain mantled by deep Bethany-series soil within the Wellington-McPherson lowlands (Watney et al., 2015). The red-dark brown mottled well-moderately-well-drained silt-silty clay loam was deposited as loess and alluvium in the

Pleistocene and is unconformably underlain by Permian-age shale in the NW quadrant of the site (Watney et al., 2015). Clay content ranges between 35-50% and is described as plastic with increasing proportions towards the base of the unconsolidated layer. These soils were lain down via drainage processes within the uplands through a network of summits and backslopes of paleoterraces. Following erosion of the SW quadrant, the stream network was discontinued and the 0-5 percent sloping surface with alluvial deposits was retained. A NE-SW elevation profile of transect A-A' and B-B' is shown in Figure 3.1 and Figure 3.2, respectively.

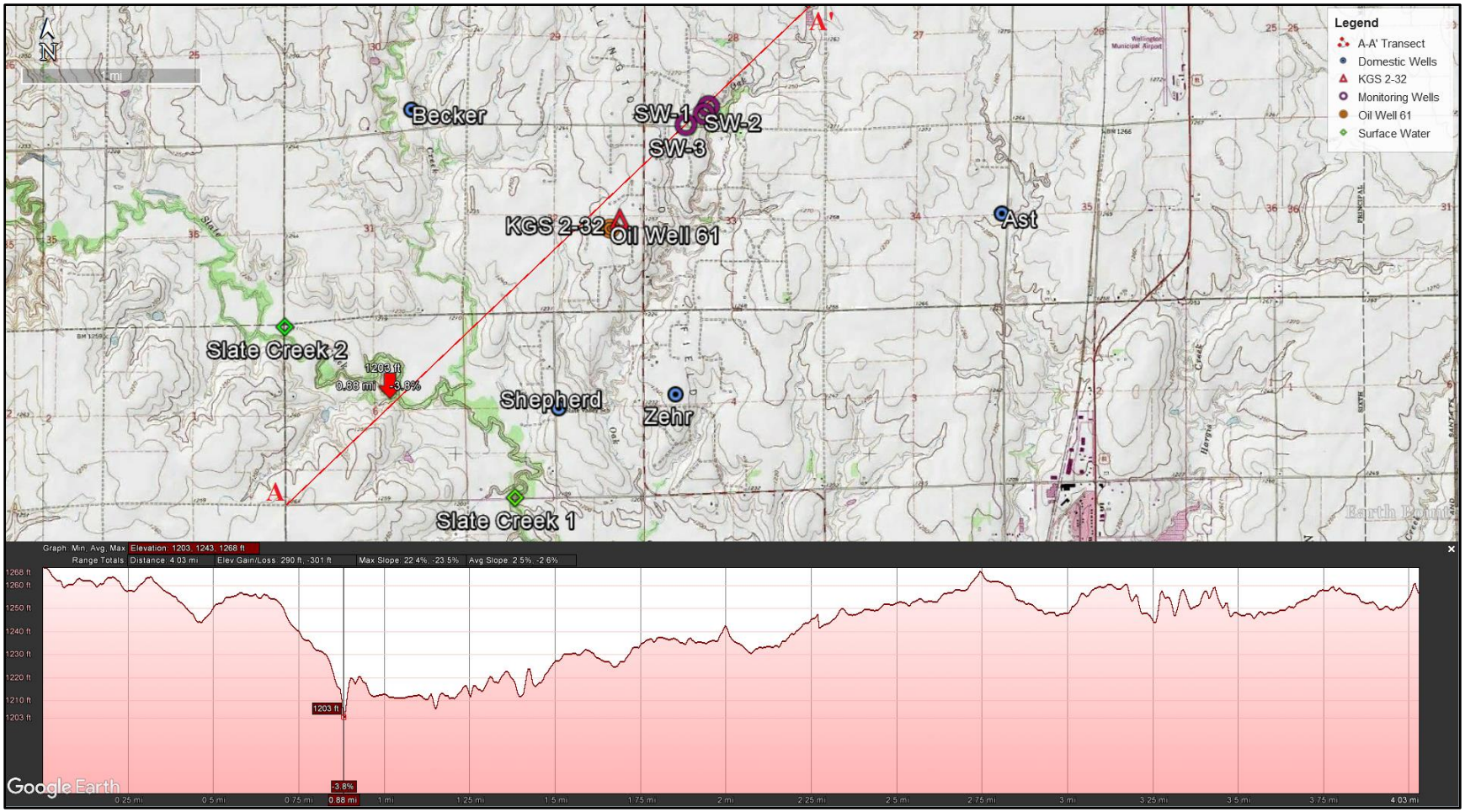

Figure 3.1 Transect A-A' showing surface topography throughout study area. KGS 2-32 is the CO_2-EOR injection well with Oil Well 61 being the most proximal and CO_2-charged Mississippian oil well. Becker, Shepherd, Zehr and Ast are domestic wells that represent the shallow 20-60' interval, Slate Creek 1 and Slate Creek 2 are surface water access points and SW-1, 2 & 3 are observation wells screened at various depths ranging between 25-200 ft.

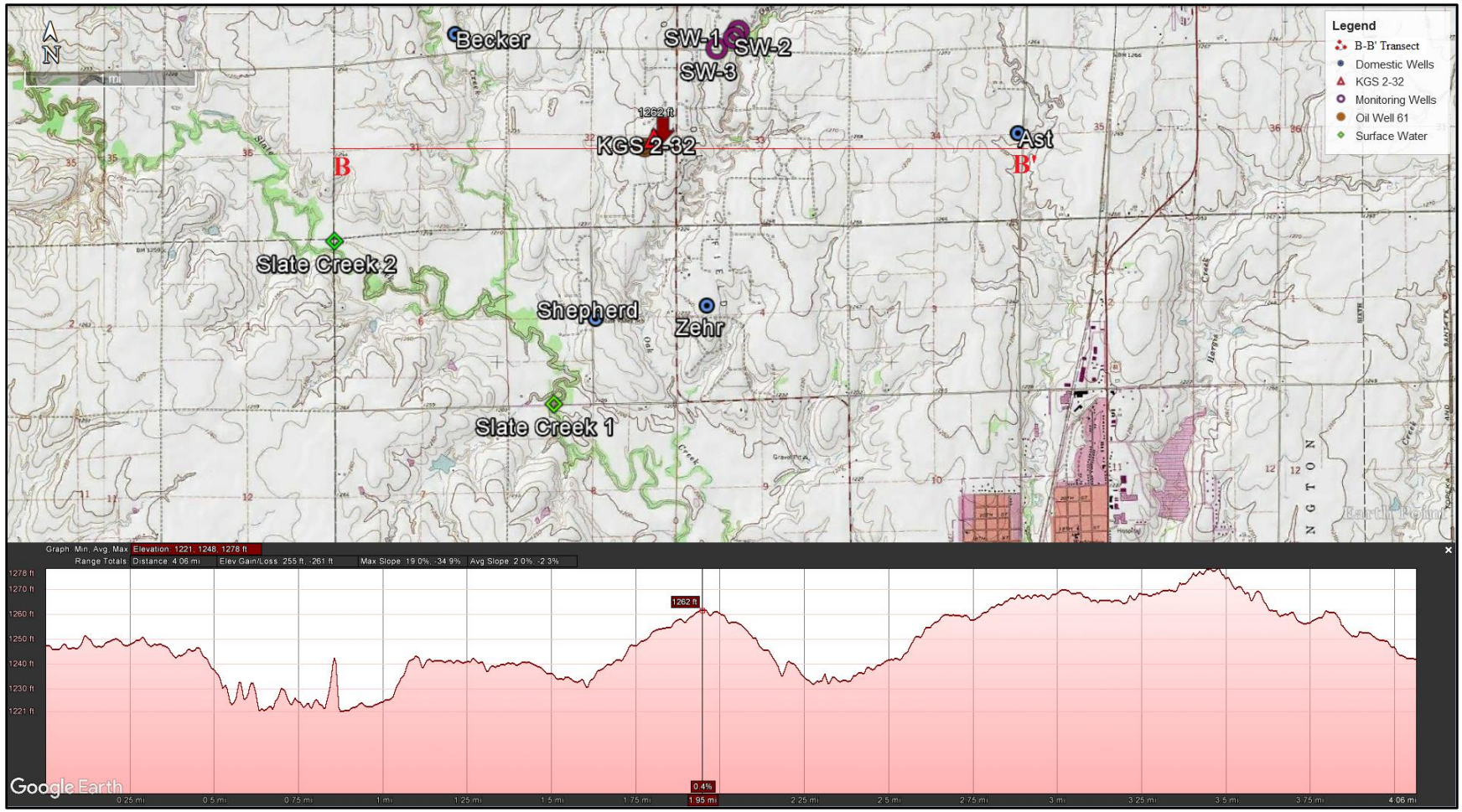

Figure 3.2 Transect B-B' showing surface topography throughout study area. KGS 2-32 is the CO_2-EOR injection well with Oil Well 61 being the most proximal and CO_2-charged Mississippian oil well. Becker, Shepherd, Zehr and Ast are domestic wells that represent the shallow 20-60' interval, Slate Creek 1 and Slate Creek 2 are surface water access points and SW-1, 2 & 3 are observation wells screened at various depths ranging between 25-200 ft.

There is a clear south-westward surface topographical sloping trend observed from the elevation profiles, indicating drainage and water flow takes place roughly to the southwest into Slate Creek. Previous interpretations of this relief gradient indicate the SW quadrant of the site was eroded to form an incised valley or 'paleovalley' as indicated by lower Holocene sand and gravel sediments in the overburden, whereas the higher relief NW quadrant retained the Pleistocene alluvial terrace silts and clays to form a 'paleoterrace' (Watney et al., 2015) (Figure 3.3).

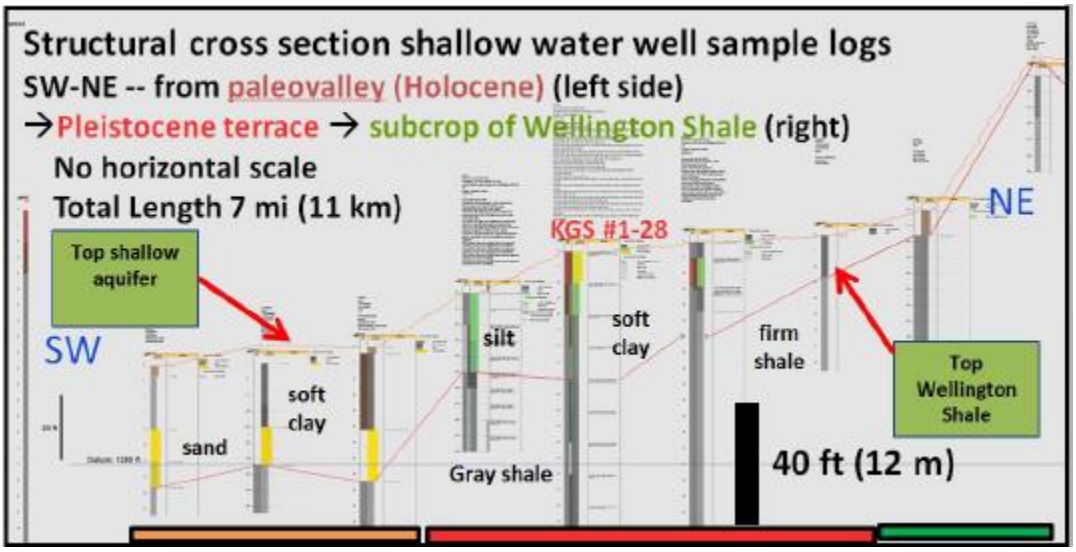

Figure 3.3 Cross section showing unconsolidated isopach variation with topographic relief throughout the Wellington, KS study area (Watney et al., 2015).

3.2 Hydrology of Study Area

Identification of source supply to the shallow aquifer in Wellington, Kansas, is necessary to assess recharge water controls on subsurface water chemistry. In general, aquifers are recharged mostly by inflow from surface water bodies and precipitation and discharged by outflow from groundwater and evapotranspiration (Viessman & Lewis, 2002). A hydrologic system maintains a balance of losses and gains through the processes of the hydrologic cycle.

The hydrologic budget of a region can be summarized as [P – R – E – T – G = ΔS]; where P is precipitation (also accounting for infiltration), R is surface runoff, E is evaporation, T is transpiration, G is groundwater flow and ΔS is change in water storage. Each of these weighted variables contributes to the net gain of the hydrologic system that can be described as either depleting or gaining. Based on the NOAA National Climatic Data Center, the national annual precipitation average of the U.S. (excluding HI and AK) is 30.21". The average for the state of Kansas is 28.9" and Wellington, Kansas, is 34.59", indicating a high annual precipitation within the study area in comparison to the state and national average.

The soil moisture regime of the soils are Udic-Ustic with implications towards a net gain from infiltration over water lost from evapotranspiration owing to the high local mean annual precipitation despite moderately high runoff and low permeability of overburden sediments in the uplands. The area is underlain by the Ozark Plateau Aquifer System (OPAS) consisting of carbonate sediments deposited between Cambrian and Mississippian periods (Jorgensen & Signor, 1981). Shallow groundwater is located within the Wellington Aquifer, named on the basis that groundwater interaction takes place solely with Wellington Formation regolith/rocks (Gogel, 1981). Slate Creek, a local tributary of the Chikaskia River, runs NW-SE on a Wisconsin-age terrace. It is underlain by high-yielding arkosic sand and gravel with minor silt and clay lenses. All drainage at the site comprises a portion of the Arkansas Salt Fort watershed (Moore & Buck, 1953). The general region communicates with the greater Mississippi River watershed which supplies large quantities of water to south-central Kansas and northern Oklahoma (Moore, 1964).

Hydrological assessment of the area (Figure 3.4) indicates that alluvial sand deposits beneath Slate Creek are hydraulically connected to the sand and gravel deposits that screen the

domestic wells (Watney et al., 2015). If CO_2 injected into the subsurface intrudes into the shallow Wellington Formation, the interconnected hydrologic systems between the domestic and observation wells could allow contamination to proceed uninterrupted. Additionally, a subsequent change in chemical balance and increase in pressure within the aquifer system from a CO_2 intrusion will influence other hydrologic factors such as pore-pressure or dispersive and diffusive potential.

Drainage patterns as a result of topographic relief indicate a general water flow direction to the W-SW of the site towards Slate and Spring Creeks (Figure 3.4). In general, water flows from the shallow monitoring well area to the SW towards domestic wells Zehr and Shepherd and ultimately to Slate Creek. The primary recharge area is assumed to be upgradient, NE of the study site.

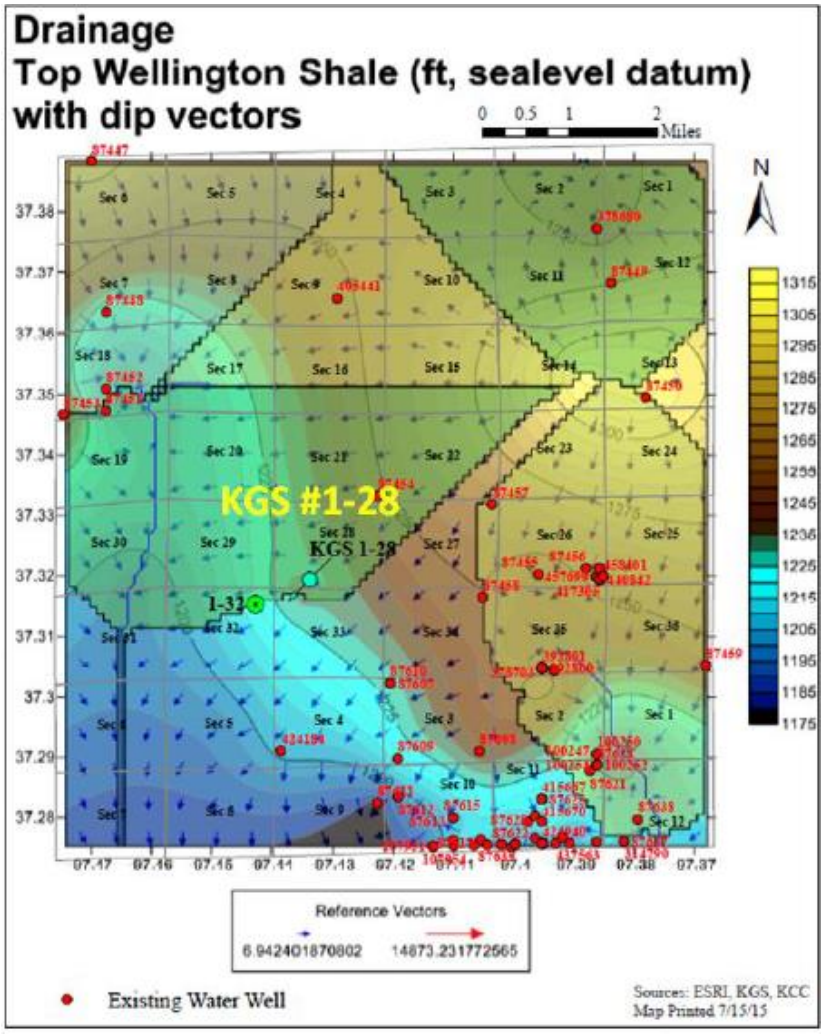

Figure 3.4 Elevation of unconsolidated-bedrock contact showing dip vectors (Watney et al., 2015). Arrows indicate dip direction and assumed water flow direction. Elevations are grouped to divide changes in dip direction and thus variations in drainage patterns.

3.3 Stratigraphic Sequence

At the base of the stratigraphic succession, Wellington is underlain by a Precambrian mesozonal granitic basement pluton; the character of this pluton suggests it was exposed and eroded following the Nemaha faulting and prior to late Cambrian sedimentation (Figure 3.5, Denison et al., 1984).

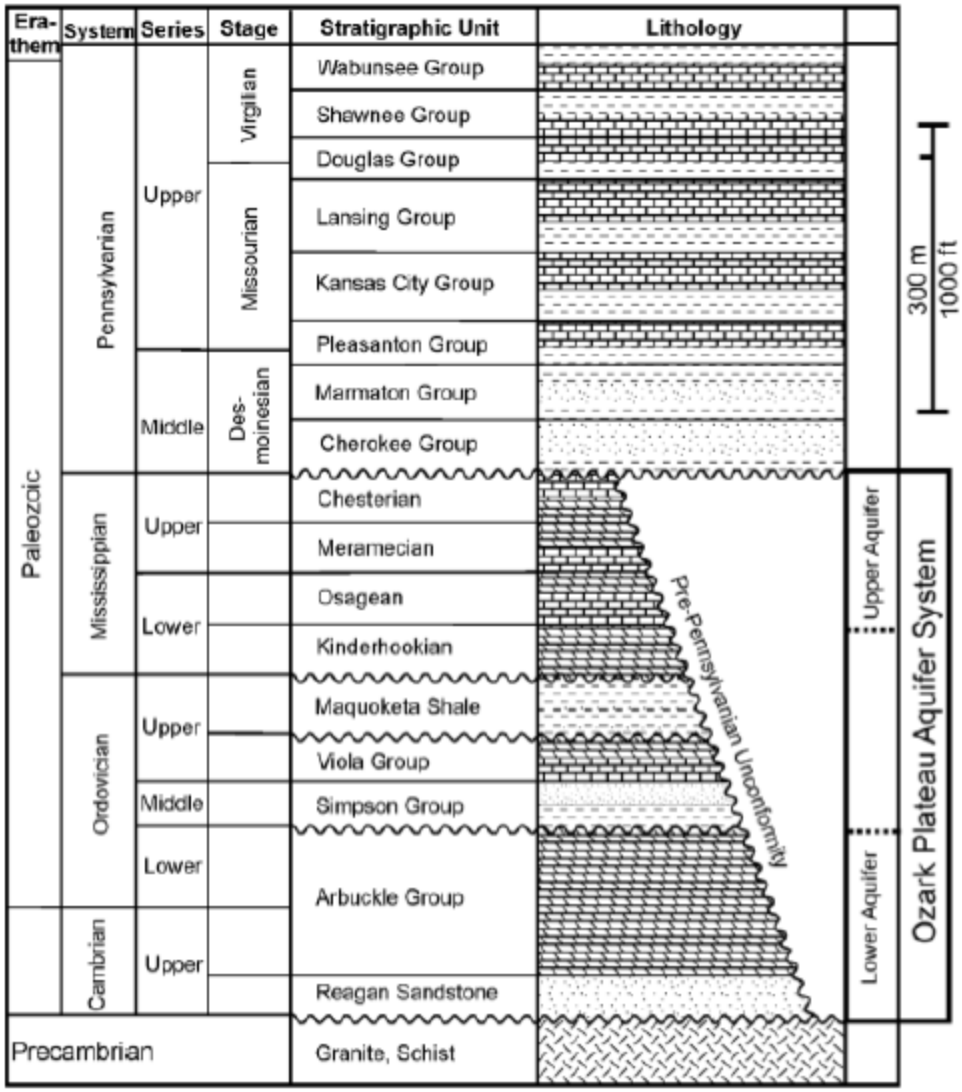

Figure 3.5 Stratigraphic succession of Kansas. Permian System is detailed in Figure 3.6 (Carr, 2005).

The weathered boundary at the top of the basement granite contains a permeable aquifer "granite wash" composed principally of arkosic sand material that is thought to yield appreciable quantities of groundwater throughout northern parts of Kansas and eastern Missouri (Jewett et al., 1968). Above this, nonconformable Paleozoic strata dip westward and vary in topography related to the NE-SW Nemaha uplift anticline complex ~18 mi east of the study site. In areas immediately adjacent to the Nemaha uplift at depth, eroded Cambrian-Ordovician strata expose

Silurian rocks with an east and westward thickening away from the central anticline axis. The Arbuckle group of Cambrian age is a major saline reservoir connected to the Ozark Plateau Aquifer System (OPAS), which is laterally extensive between southern Missouri and eastern Colorado (Macfarlane, 2000). Upper Arbuckle dolomite, a porous dolomitic carbonate with thin shaly beds (Merriam, 1963), is overlain by upper Devonian Chattanooga Shale and Mississippian Kinderhookian Carbonate, which together provide significant supplies of hydrocarbons throughout the region. The top of the Paleozoic succession is unconformably overlain by Mesozoic and Cenozoic strata that can be seen outcropping in the western two-thirds of Kansas; the lower Permian System marks the top of the stratigraphic succession in Wellington, Kansas, and eastward.

3.4 The Permian System

The Permian System, the main geologic focus of this research, can be divided into a lower Chase and Council Grove Group and an upper Sumner Group. The lower groups are defined as alternating beds of limestone and shale with disseminated flint deposits. The top of the lower Permian System is marked by the Nolans Formation, which forms the top of the Herington Limestone, a lithology similar in character to the Chase Group that underlies it. The Leonardian Series above consists of the Sumner Group with the base at the top of the Nolans Formation with the total Permian System thickness spanning approximately 1,750’ (West et al., 2010). Figure 3.6 shows the stratigraphic sequence of the Permian System within Wellington, Kansas, with a focus on the Sumner Group portion of the Leonardian Series.

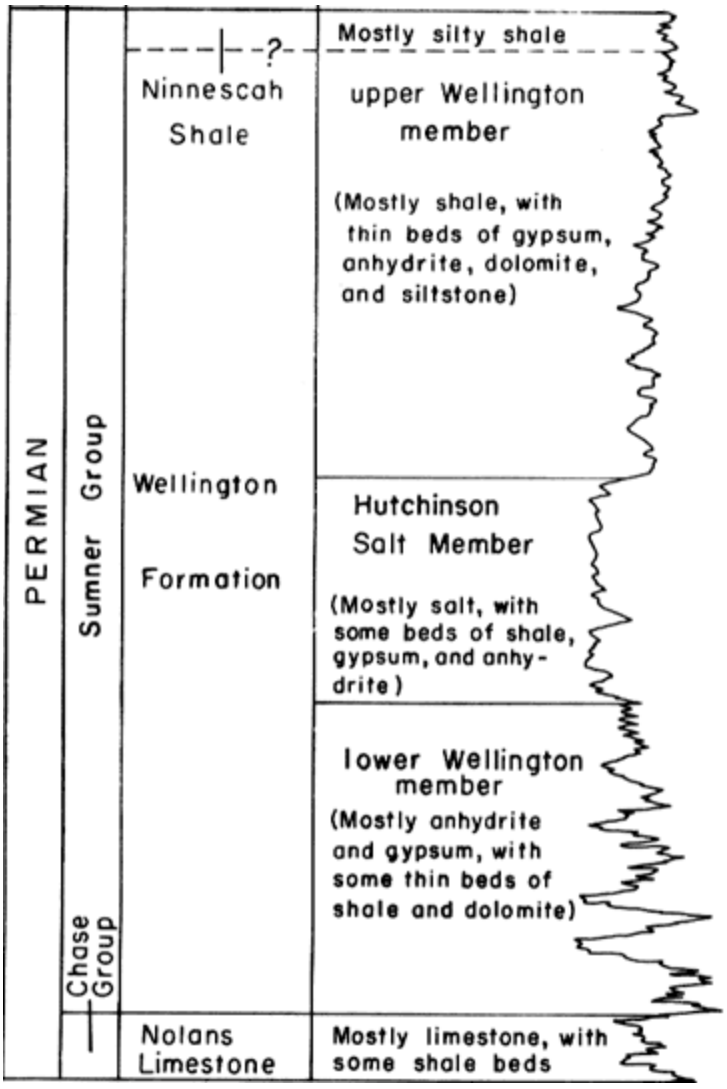

Figure 3.6 Stratigraphic sequence of the Permian System in Wellington, KS (Ver Wiebe, 1937)

All domestic and monitoring wells within the study site are screened within the Permian System, more specifically the upper Wellington Member. The upper portion of the Sumner Group is defined by the Wellington Formation which is divided into an upper Ninnescah Shale, a reddish-brown silty shale with thin veins of gypsum and alternating layers of limestone, and un-named Wellington Member, a gray, calcareous shale with localized gypsum/halite/anhydrite deposits and thin beds of argillaceous limestone. The lower portion of the Sumner Group

contains a lower Hutchinson Salt Member, an interbedded halite, anhydrite and shale sequence that thins to the northeast and a Wellington Member with mostly anhydrite and gypsum interbedded with thin layers of shale and dolomite (Miller et al., 1996; West et al., 2010). The interbedded marine cyclic deposits of the Hutchinson Salt Member accumulated as shelf carbonates as a result of evaporation and inundation of the Permian mid-continental seaway (Watney, 1980); its elevation is shallowest in Wellington, Kansas. Extensive dissolution occurred along the eastern updip edge at the boundary between the Hutchinson and Wellington members, yielding an interconnected hydrologic network (Macfarlane, 2000). The 200 to 300 ft thick Wellington Shale Member above extends from the top of the Hutchinson Salt to the ground surface in the study area and is overlain by the Ninnescah Shale in the western third of Sumner County. The depositional framework of the Wellington Formation is purportedly an arid tidal flat with evaporite deposits thickening with depth (Elrod, 1980). The high salinity of the brine groundwater within the Permian System is attributed to the presence of gypsum crystals ($CaSO_4 \cdot 2H_2O$ – var. selenite & satin spar) and halite that were deposited during burial (top at ~20-40' BGS) and is believed to have developed from secondary mineralization within shrinkage cracks following deposition (Watney et al., 2015). The shales were deposited as muds, primarily composed of illite clays, within a closing and opening seaway. Intermittent wet and dry seasonal changes suggest active dissolution and precipitation of the selenite crystals associated with recurrent over/under saturated conditions of the pore spaces within the shale. This process led to an increase in salinity for groundwater with prolonged exposure to water-rock interaction. Further reports indicate prominent copper sulfide mineralization within the upper Wellington Shale developed mostly by secondary solution and replacement mineralization processes within

vugs (Lambert et al., 1981). Predominant minerals include covellite, azurite, chalcocite and chalcopyrite as identified by petrographical studies (Elrod, 1980; Lambert et al., 1981).

3.5 Structural Geology

Beds dip to the SW owing to NE-ward ramping of the Nemaha complex east of the study site. Figure 3.7 shows the depth to bedrock variations throughout the study area, which roughly follows the surface topography.

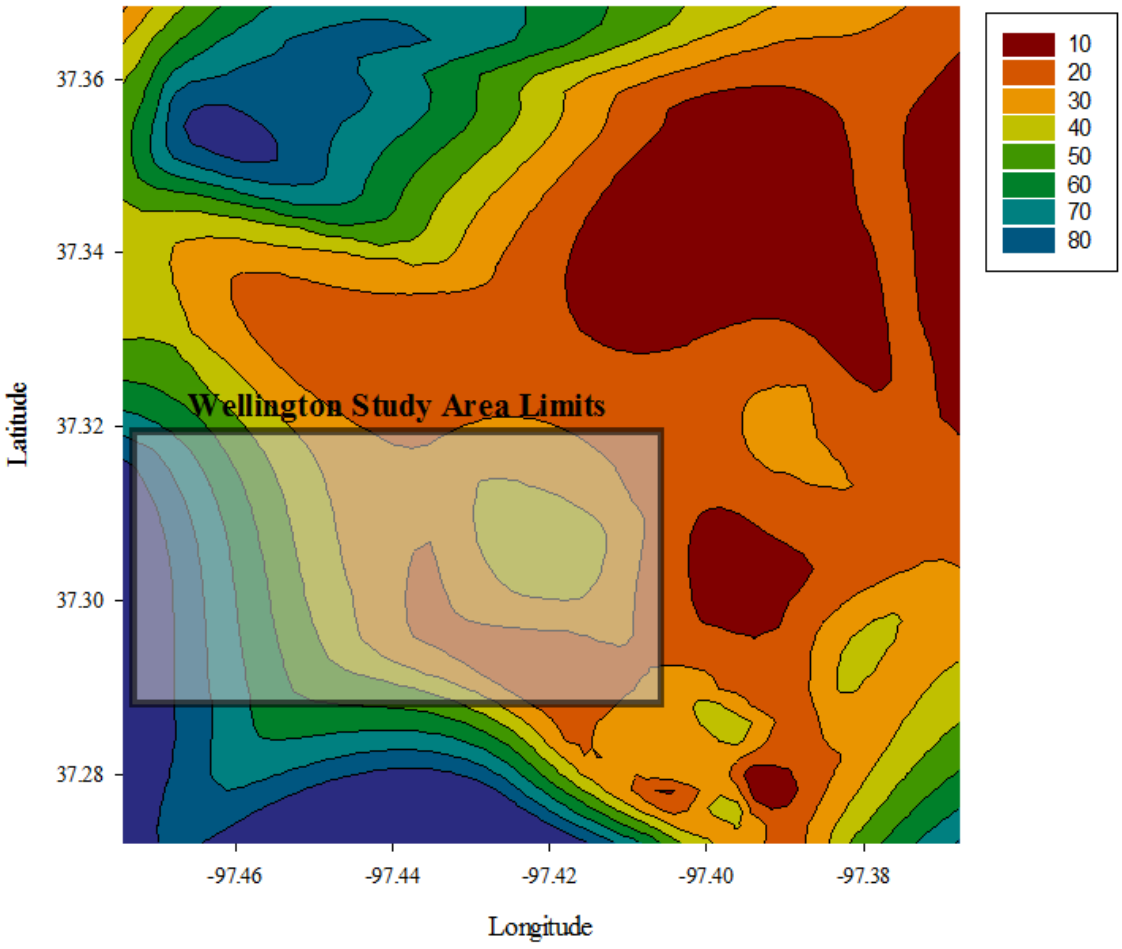

Figure 3.7 Depth to top of the Permian Wellington Shale (feet) at the regolith-bedrock contact as generated in SigmaPlot® using bedrock elevations provided by the KGS.

Former evaluations of the local Wellington area indicate development of an erosional paleoterrace feature sloping southwest to an incised paleovalley lowland (Watney et al., 2015). Overburden sediments on the paleoterrace are composed principally of fine silts and clays with minor sand lenses of loess origin, whereas deposits overlying the paleovalley contain coarser sand and silt resulting from modern drainage (Watney et al., 2015).

Geological structure assessment of the Arbuckle and Mississippian reservoirs suggests a CO_2 leakage event is unlikely. An absence of critical transmissive faults within the Wellington study area locale, as shown by seismic data, indicates hydraulic communication between the Mississippian and Arbuckle systems is not well established. Elevated chloride concentrations within the Mississippian, relative to the upper Arbuckle, and geochemical/mineralogical evidence for a competent confining baffle zone between the two horizons (Barker, 2012; Holubnyak et al., 2016) support the idea that transmission of any formation fluid is unlikely to occur from the repository.

However between April 2016 and March 2017, the KGS has documented 59 shallow earthquakes that range in magnitude of 2.0-3.5; the earthquakes are attributed to induced seismicity from saltwater injections into deep formations including the Arbuckle and Mississippian via Class II disposal wells (KGS, 2015). Recent geophysical advances have linked the increased seismic activity within these repositories to minor pore-pressure changes that are hydraulically connected to faults; they may also be related to re-pressurization of the injection reservoir and resulting change in shear or normal stress on associated faults. Seismicity in the Wellington area has been identified as nucleating from the basement contact, which has implications for re-activation of fault systems that extend from the basement into horizons just above the Mississippian (Bidgoli, personal communication, 2017). Despite the presence of a

small fault east of injection well KGS 2-32, it has been found that saltwater injections may continue to take place without the risk of re-activating larger faults in the region; an earthquake larger than magnitude 5.8 would trigger fault movement (Bidgoli, personal communication, 2017).

Predicting a CO_2 leakage event on the basis of pressure data collected from drill stem tests of the Mississippian injection intervals has proven to be a complex task. As a result, this thesis will not identify the probability of CO_2 migration through the fault/fracture network due to a lack of data and complexity between sub-hydrostatic and hydrostatic head. The small fault located eastward of KGS 2-32 is not likely to present a challenge to CO_2 security due to short propagation and failure to connect unrelated layers (Bidgoli, personal communication, 2017).

3.6 Mississippian Pay/Injection Zone Mineralogy

The Mississippian reservoir pay zone is mineralogically characterized as a cherty dolomite mudstone with abundant tripolite chert and minor anhydrite(?) deposits (Barker, 2012; Watney et al., 2001). The fine-grained and well-connected intercrystalline porosity of the Mississippian differs from the lower dolomitic intergrowth matrix porosity of the Arbuckle injection zone (Barker, 2012). Figure 3.8 shows euhedral quartz crystals and fibrous chert that occur near the middle of the Mississippian injection zone (3,686’); chert nodules in this interval range between 0.25-200 mm in size. It is thought that anhydrite occupying the pore spaces between quartz and dolomite grains is undergoing silicification, as shown through SEM imaging (Barker, 2012).

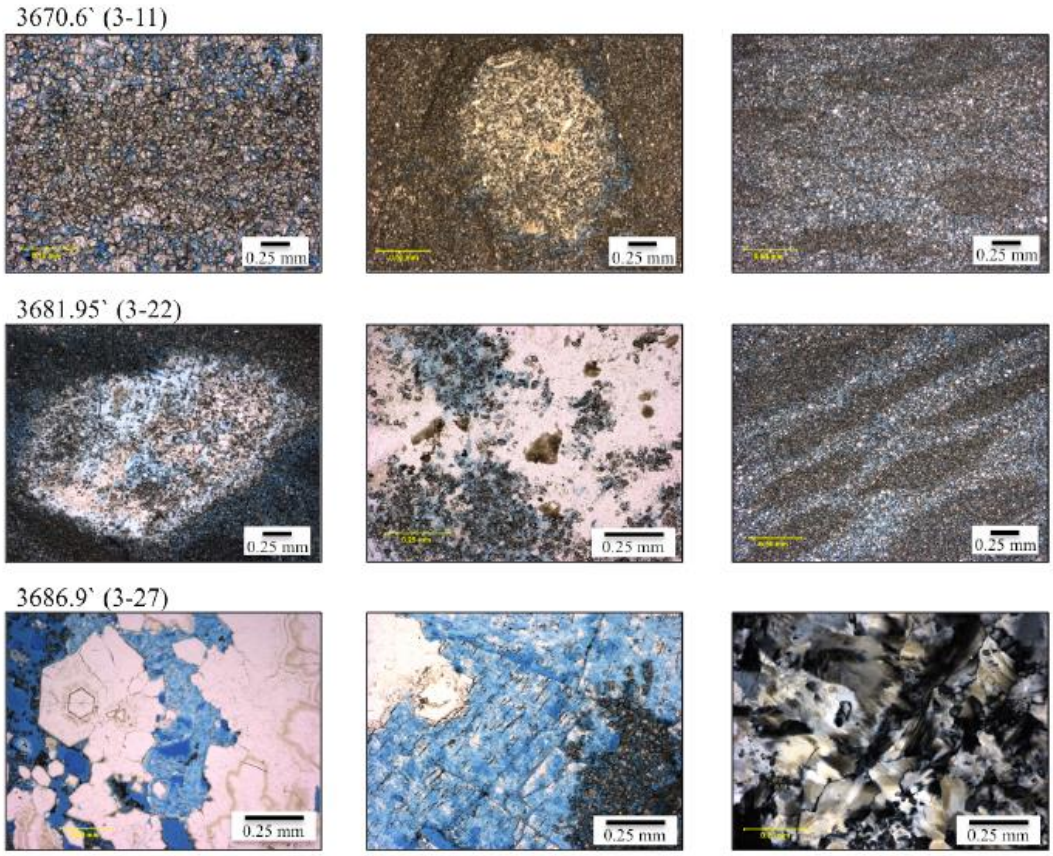

Figure 3.8 Thin sections of notable Mississippian injection zone intervals showing porous cherty dolomite with interstitial quartz crystals (Barker, 2012).

Chapter 4 - Methods and Materials

4.1 Sampling

Since initial sampling activities were led by the Kansas Geological Survey, it was required that sampling protocol was in accordance with the Environmental Protection Agency (EPA) guidance ASTM D6452-99 (ASTM, 2012). This set of standards was agreed upon between the members of the region-specific EPA and site-specific KGS team in a QASP designed specifically to address the Wellington Oil Field Small Scale Carbon Capture and Storage Project; by extension these protocols apply to monitoring of the shallow aquifer. As such, the chosen groundwater sampling methodology described below follows a specific ASTM regulation to ensure sampling is conducted in the correct manner and sample quality is of the highest degree. For well construction information please see Appendix A.

4.1.1 Sample Containers and Treatments

Volume	Container Type	Preservation*	Analysis
125-mL	HDPE	F/A	Major cations, trace elements, DOC
125-mL	HDPE	F/UA	Major anions
125-mL	HDPE	F/A	REE - dissolved
250-mL	HDPE	UF/A	REE - dissolved + particulate
500-mL	HDPE	UF/UA	Extra water
120-mL	Glass	UF/UA	δ^2H, $\delta^{18}O$
60-mL	Glass	F/UA	Dissolved CO_2

*UF,F/UA,A - Un-filtered, Filtered / Un-acidified, Acidified

Table 4.1 Sample containers and their respective analyses that were used in sampling.

4.1.2 Pre-collection Sample Container Cleaning

All sample containers (with exception of REE containers) were pre-cleaned according to rigorous guidelines stipulated by the EPA prior to sample collection to ensure supreme sample quality. For REE container preparation, see section 4.4. High-density polyethylene (HDPE)

containers were subjected to an acid bath following a thorough pre-rinse with ultra-pure (18.2 Ω at 25°C) de-ionized water (hereafter, DIW) – all DIW used in container preparation was ultra-pure and will be referenced simply as DIW. A >5% HNO_3 and >5% HCl (reagent-grade, ACS-certified) solution was prepared in a large HDPE container and properly stored in a low traffic area of the lab for the bottles to soak in overnight; all bottles were fully inundated to allow for complete surface area coverage during decontamination. Following the 24-hour period, acid-cleaned containers were removed and rinsed with DIW and allowed to dry upside down on clean paper towels. Each container was inspected to ensure no residue was left in the containers. Sample containers were then tightly capped, labeled and immediately secured in clean Ziploc® bags for temporary storage. Glass sample containers were not washed prior to sample collection as their intended analyses did not require any pre-cleaning procedures.

4.1.3 Equipment Cleaning and Calibration Checks

Prior to operation of any equipment in the field, cleaning and calibration checks were instituted to ensure optimal performance and sample quality preservation. The submersible groundwater pump and interface-probe were cleaned with DIW and Alconox® solutions to ensure organic/inorganic gross particle removal. After sampling at each location, instruments that contacted sample water were subjected to decontamination using DIW. A detergent solution was not required in the field, as sample locations did not contain any dissolved organics in the way of hydrocarbons.

A Hach® HQ40d meter was utilized with pH and specific conductance probes (CDC401) as well as oxidation-reduction potential (ORP, MTC101) probes; the probes were calibrated in the field each day prior to operation. Three sets of readings within manufactory calibration range were achieved using the calibration solution before calibration was considered complete.

Turbidity was recorded by an Extech® TB400 turbidity meter and was manually calibrated each day using the provided 0-100 NTU solution. In addition, the Horiba® U-51 multi-parameter water quality meter that was utilized during the second round of sampling to collect water quality readings was manually pre-calibrated by the rental servicer and auto-calibrated again each day using the provided solution.

4.1.4 Sample Filtration

Analyses requiring filtration of sample water necessitated the use of a vacuum filtration system and was performed in accordance with ASTM D6564-00. The glass filtration apparatus was comprised of a steel clamp, glass Buchner funnel, glass sand core filter head, 0.45 μm Millipore® membrane filter and a glass 1000-mL filter flask with attached outlet port. Quarter-inch flexi-tubing was secured to the outlet port and either a hand pump or peristaltic pump was used to de-pressurize the flask allowing for increased efficiency for sample filtration through the filter membrane. The apparatus was pre-cleaned (see section 4.1.2) and stored in an acid bath in between sample locations to ensure preservation of pristine condition. Additionally, to expedite filtration, Henke-Sass Wolf® sterile polypropylene 24-mL syringes were used with Millipore® Millex-HP Hydrophilic PES 0.45 μm filter attachments.

4.2 Purging of Wells

Purging is a standard groundwater sampling practice employed to remove stagnant water from the well casing prior to sampling to ensure the sample is representative of the screened aquifer. This research employed conventional purging principles as per ASTM D6452-99 (ASTM, 2012) by lowering the submersible pump to within 3-5 feet of the top of the water column and slowly lowering throughout the purge to accommodate water column depletion for wells with a recovery rate that does not exceed the pumping rate (SW-1, 2, 3). Purge rate for low

yielding wells was carefully monitored so as to prevent over-stressing the aquifer. Purge completion was based on volume of water removed and stabilization of water parameters. Volume of water to be removed from the well was calculated [Equation 1] based on diameter of casing, depth to water (DTW) and depth to bottom (DTB) of the well; the diameters of the monitoring well casings ranged between 3-4" which corresponded with a "gallons of water per foot" factor of 0.367 and 0.653, respectively.

Equation 1 (3" casing): $V = 0.367*(DTB-DTW)$

Due to the poor hydraulic conductivity of the formation screening the two deepest monitoring wells of the study area, purge rate was restricted at these sample locations to 1-1.25 gallons per minute (GPM). All potable wells and the shallowest monitoring well allowed for faster pumping rates at an average of 2.5-4 GPM. Normally, three well volumes of water is required to be purged from the well casing to ensure the entirety of stagnant water has been removed. However, only monitoring well SW-3 (potable wells exempt) was able to evacuate three volumes of water during purge due to its higher yield; monitoring wells SW-1 and SW-2 were only capable of evacuating, at most, a single casing of water. As a result, monitoring wells SW-1 and SW-2 had to allow the maximum 24-hour recharge period for fresh aquifer water to infiltrate the well casing. For further information of well purging see Appendix B. Since potable water volume could not be calculated due to the specific design of these wells, volume of water removed during purge was noted, but completion of purge was based on stabilization of water parameters alone as per EPA guidance.

The oil well (oil well 61, hereafter 61) that was sampled in the study area was selected based on its proximity to injection well KGS 2-32 and high CO_2 (injectate) charge. Using practices obtained from Berexco LLC personnel, brine samples from 61 were extracted via a barrel test at the discharge line. A pre-cleaned (see section 4.1.2) HDPE 5-gallon bucket was

used to collect a sample at the discharge line of 61. When the line was engaged, oil and brine were purged from the reservoir at an uncontrolled rate, until the bucket was sufficiently filled. In this case, there was no purge requirement before sampling; the sample was immediately collected as per procedures outlined in section 4.2.2.

4.2.1 Water Quality/Chemistry Parameter Measurements

During a well purge, various water parameters such as pH (SU), specific conductance (ms/cm), turbidity (NTU), ORP (mV), dissolved oxygen (DO, mg/L) and temperature (°C) are monitored every five minutes until stabilization within a pre-set percentage range. Under these guidelines, stabilization occurs when, for at least three consecutive measurements, the pH remains constant within 0.2 Standard Units (SU), specific conductance varies no more than approximately 3 percent of reading in µs/cm, DO is within 0.3 mg/L or 10% saturation, whichever is greater and turbidity is below 10 Nephelometric Turbidity Units (NTU). Temperature and ORP are less reliable indicators of purge end due to their sensitivity to changing ambient conditions as the sample is raised to ground surface; however ASTM guidance stipulates temperature stabilizes within 1°C and ORP within 10 mV.

A Hach® HQ40d, Extech® TB400 and CHEMetrics® V-2000 were utilized during the first round of groundwater sampling whereas a Horiba® U-51 and Extech® TB400 were utilized for the second round.

For each of the following water quality instruments and in accordance with their specific factory specifications, accuracy and repeatability are outlined for each parameter (Table 4.2). Accuracy is measured by calibrating four points for turbidity and electrical conductivity and two points for all other measurements against a standard solution. Repeatability is measured by the ability to reproduce the results against the standard solution at 25 °C and 1 atm.

Horiba U-51		
Parameter	**Accuracy**	**Repeatability**
pH	±0.1	±0.05
ORP (mV)	±15	±5
DO (0 to 20 mg/L)	±0.2	±0.1
COND (% from std.)	±1	±0.05
TEMP (°C)	±0.3	±0.10
Hach HQ40d		
pH	±0.002	0.001 - 0.1
ORP (mV)	±0.1	±0.1
COND (% from std.)	±0.5 %	±0.01
TEMP (°C)	±0.3	±0.10
Extech TB400		
TURB (NTU)	±0.5	±0.01
CHEMetrics V-2000		
DO (2 mg/L)	±0.6	--
DO (4 mg/L)	±0.8	--
DO (11 mg/L)	±1.1	--

Table 4.2 Water quality instrument accuracy and repeatability.

A CHEMetrics® V-2000 and Hach® 1900 photometer used for quantification of alkalinity, arsenic, sulfate, manganese, silica, chloride, ammonium, iron (ferrous/total), nitrate, nitrite and sulfide was calibrated using each individual kit's provided calibration solution. In addition, some parameters were identified by CHEMetrics® kits that did not require a photometer. Each of these parameters required immediate analysis in the field due to the expiration of their true values over time. Further details on field kits can be found in section 4.3.1.

4.2.2 Sample Collection Procedures

Samples collected from monitoring wells were retrieved using a clean 36"x 1.5" Teflon® bailer. Bailing required careful handling so as to not agitate the sample. Bailers were carefully

lowered into the well casing and gravity allowed the bailer to slowly sink about 4-5 feet before the bailer was hauled back to the surface. Samples collected from potable wells not requiring preservation or filtration were retrieved directly from the discharge line at the dispenser. Clean, non-powdered, new pairs of nitrile gloves were worn at each sample location. First sample water was poured directly into the appropriate containers purposed for un-preserved and un-filtered stable isotopes and dissolved CO_2 analyses. Next sample water was emptied into the 500-mL Buchner funnel to be filtered through the filtration apparatus (see section 4.1.4). All sample bottles, except those used for stable isotope analysis, were subjected to conditioning and preservation as per ASTM D6517-00 (ASTM, 2005). Upon three conditions of the sample container, sample water was filled to the top of the bottle and preserved at a rate of 2 mL per 1000 mL using Fisherbrand® optima grade HNO_3 (67-70%) via pipette to achieve a pH < 2 for acidified samples. Bottles were tightly capped and wrapped with electric tape to prevent leakage during storage and transport.

4.2.3 Sampling of Potable Wells

For the residential (potable) water to be qualified for analysis, it must be untreated and sampled by an above-ground dispenser. The pumping rate at the hand pump is adjusted using the attached lever. The groundwater is then purged into a 5-gallon bucket and water parameter readings were collected every five minutes and evaluated by Hach® probes or a Horiba® flow-through cell (see section 4.1.3). Purge rate was sustained at a constant rate, typically between 2-4 GPM, and purge water was disposed of at the behest of the property owner. Since potable/residential wells are not constructed similarly to monitoring/observation wells, volume of standing water cannot be calculated and, as a result, time of sample is dictated entirely by

stabilization of water parameters. If stabilization has not been achieved after 45 minutes, the sample can be collected in accordance with the QASP (2015).

4.2.4 Sampling of Monitoring Wells

Upon arrival at each well, a Solinst® (Model 122) interface probe was used to measure the water level. For the two deeper monitoring wells (SW-1, SW-2), purge adequacy was not dependent on volume of water removed (ASTM, 2012). Instead, water parameters were collected until a sufficient amount of water had been purged from the casing at the discretion of the project leader. Following purge, the well was monitored until a water volume, equivalent to the amount needed to fill all of sample containers, had recharged into the well casing. Low-yielding wells such as SW-1 and SW-2 did not purge a full casing of water in fear of re-introducing soil fines within the sand pack or water column during well dryness.

Clear 3/8" polyvinyl chloride (PVC) tubing was connected to a Geotech® SS geosub pump and submerged to two feet below the top of the water column. Pumping rate was controlled with associated controller and DC-AC inverter powered by a car battery to yield an average pumping rate of 1-2 GPM. Once the top of the water column was drawn down to base of the pump, ensuring all floating material was removed from casing, the pump was then lowered concomitantly with water table depletion. Purge water was collected and stored in 55-gallon drums for proper disposal by Berexco LLC. Water quality readings were collected at the beginning of the purge and every 5 minutes after until parameters stabilized (see section 4.2.1). Teflon® bailers were used to obtain the water sample following purge and sufficient recharge. Due to the absence of oil or pollutants, these bailers were re-used upon decontamination with DIW.

4.3 Analysis Methods

4.3.1 Field Kits

In-field analysis of quickly degrading ionic/elemental constituents required the use of a CHEMetrics® V-2000 and Hach® 1900 photometer as outlined in section 4.2.1 along with several field kits for identification. The field kits and associated accuracies as stated by the manufacturer are shown in Table 4.3.

Field Kit Brand	Cat. No.	Analyte	Accuracy
Hach	24443-00	Alkalinity (as $CaCO_3$)	*
Hach	20635-00	Chloride (Cl^-)	*
Hach TNT 865	--	Sulfate (SO_4^{2-})	*
Hach TNT 839	--	Nitrite (NO_2^-)	*
Hach EZ Arsenic	28228-00	Total arsenic	*
CHEMetrics Vacu-vials	K-9010	Silica (SiO_2)	$\pm$0.13 (0 mg/L), $\pm$0.15 (0.5 mg/L), $\pm$0.6 (3 mg/L), $\pm$0.75 (7.5 mg/L)
CHEMetrics Vacu-vials	K-9523	Sulfide (S^-)	*
CHEMetrics Vacu-vials	K-6933	Nitrate (NO_3^-)	$\pm$2.5 (0 mg/L), $\pm$1.5 (5 mg/L), $\pm$3.8 (12 mg/L)
CHEMetrics Vacu-vials	K-6210D	Ferrous and total iron	Comparator match method
CHEMetrics Vacu-vials	K-1403	Ammonia (NH_3)	*

* Available in literature or upon request to manufacturer

Table 4.3 Field kits used with their stated accuracies. Most statement of accuracies were absent or required a separate method to manually calculate which was not completed.

4.3.2 Major Ions

Major cation and anion analysis via ion chromatography formed the basis for the water chemistry characterization. The Ion Chromatograph (Thermo® Dionex ICS-1100) equipment at KSU utilized Chromeleon® software for data processing. Anions were analyzed by an AS22 analytical column using carbonate eluent and an AERS suppressor whereas the cation system used a CS12 column and CERS suppressor with sulfuric acid eluent (Kirk et al., 2015). Column and system integrity requires samples to be diluted to less than ~4 ms/cm specific conductivity, necessitating dilution for high-salt containing samples. Samples analyzed for cations are filtered

(0.45 μm) and acidified (0.2% HNO_3); samples for anions are filtered (0.45 μm) only. Samples are arranged on the program which corresponds to their position on the Dionex® AS-DV autosampler to delineate cationic and anionic samples. A set of four standards (1R through 4R) is used for each cation and anion analysis to set the calibration range. A random standard is placed equally throughout the analysis to serve as an intermittent quality control while blanks containing DIW are evenly distributed. Once samples are diluted to the appropriate range, the sample is then transferred to a 500-μL capsule and placed into the 50-position carousel where an auto-injector begins the analysis. After injections, the user will then visually inspect peak areas that were auto-fitted by the software and manually correct poorly fitted peaks.

4.3.3 Stable Isotopes

All water samples were analyzed for δ^2H and $\delta^{18}O$ by a Picarro® L1102-i cavity ring-down spectrometer at Isotech Laboratories, Inc. in Champaign, Illinois. Additional water samples were analyzed for $\delta^{13}C$ DIC by a Thermo® Finnigan Gas Bench II isotope-ratio mass spectrometer with Thermo® Delta V Plus at Isotech. Water samples were unpreserved, unfiltered and collected watertight in 120-mL glass bottles sealed shut with the cap and electric tape and refrigerated at 4° C until analysis (see section 4.2.2). These samples were the first to be collected upon sampling at each location in an effort to reduce atmospheric contamination. All methods of analysis were completed by trained professional laboratory technicians following a rigid quality assurance plan and standard operating procedures guideline.

4.3.3.1 Isotope-Ratio Mass Spectrometry

A sample volume of 1.0-mL is injected into a helium flushed 12-mL Exetainer® containing 0.1-mL of 85% phosphoric acid and a magnetic spin bar. Sample size is determined based on alkalinity, which is measured by titration with 0.1 N HCl. The sample is stirred for a

minimum of one hour and then allowed to equilibrate for 24 hours. At time of analysis, the sample vials are placed in the GasBench tray. The CO_2 generated is flushed out of the vial through a two-port needle. Water is removed by two Nafion® traps and pure CO_2 is separated using a gas chromatograph column. The CO_2/helium mixture then enters the mass spectrometer and is compared against a reference standard a total of six times. To ensure quality control, a check standard and replicate is analyzed every ten samples.

4.3.3.2 Cavity Ring-Down Spectrometry

Water samples are individually filtered into 2.0-mL vials with 0.2 μm syringe filters. High salinity brine samples require vacuum distillation before proceeding. The vials are then loaded onto trays attached to the autosampler. Samples are analyzed by the cavity ring-down spectrometer in replicate in accordance with the manufacturer's recommendation. To ensure quality control, two reference water samples are used to verify accuracy and reproducibility. The system is calibrated by analysis of primary reference standards obtained from IAEA or NIST. This reference standard and a replicate are analyzed every ten samples.

4.3.4 Dissolved Carbon

Samples Shepherd, SW-3 and 61 were submitted to ALSMV Environmental in Simi Valley, CA, for analysis of dissolved CO_2 and hydrocarbons. These samples were collected unpreserved and unfiltered in 60-mL glass bottles, watertight with zero headspace and sealed tight with electric tape. EPA-certified, SOP VOA-DISGAS method RSK 175 was employed during the analysis, as described by the procedures below.

4.3.4.1 Dissolved CO_2

CO_2 gas was extracted from the samples using a HP® 5890 gas chromatograph equipped with a thermal conductivity detector. A volume of 8.0-mL of helium was injected into a calculated volume for each sample and agitated with a sonic disrupter for 15 minutes before equilibrating for four hours. A volume of the headspace was withdrawn with a gas-tight syringe and analyzed using a manual injection technique. Henry's Law was used to calculate the amount of dissolved CO_2 in the original sample.

4.3.4.2 Dissolved Hydrocarbons

Dissolved hydrocarbons such as methane, ethene, ethane, propylene and propane were quantified using a HP® 5890 GC equipped with a flame ionization detector (FID). These samples were preserved in the same manner as the dissolved CO_2 analysis, cited in the above description. EPA-certified guidance method RSK 175 was cited to complete this analysis. The sample was injected with 8.0-mL of helium and agitated using a sonic disrupter before allowing to equilibrate for two hours. A volume of the headspace was withdrawn using a gas-tight syringe and analyzed using a manual injection technique. Henry's Law was used to calculate the amount of dissolved organic gases in the original sample.

4.3.5 Dissolved Organic Carbon

Samples reserved for DOC analysis required in-field filtration (0.45 μm) as well as acidification. However, due to late consideration of this analysis to be included in this research, samples were not immediately acidified using the correct acid (0.2% HCl). Instead, acidification by HCl took place immediately prior to analysis using Fisherbrand® optima grade HCl (32-35%) at a rate of 2-mL per 1000-mL to a pH < 2.

Water samples were analyzed for non-purgeable organic carbon (NPOC) within the Department of Engineering at KSU using a Shimadzu® TOC-L TNM CSH E100 analyzer coupled with an ASI-L autosampler fitted with 24-mL glass vials. The TOC utilizes the 680^{o}C combustion catalytic oxidation method allowing for detection of soluble and insoluble organic compounds. A calibration and standard were created on 7/3/16 and again on 4/4/17 with an R^2 value of 0.88 for both.

4.3.6 Trace Elements

All samples were analyzed for trace elements via inductively-coupled plasma mass spectrometry (ICP-MS) at the Beadle Center within the University of Nebraska – Lincoln Spectroscopy and Biophysics Core. Trace elements such as As, Al, B, Ba, Co, Cd, Cr, Cu, Hg, Li, Mo, Pb, Ni, Rb, Sb, Sr, Ti, U, W, Zn as well as major elements Na, K, Mg and Fe were analyzed. Samples were filtered (0.45 μm) and acidified (0.2% HNO_3) in the field and refrigerated at 4°C until analysis. The samples were then transferred to pre-cleaned (DIW) polypropylene centrifuge tubes (Fisherbrand® 50-mL polypropylene - Cat. No. 05-539-9) and transported with ice packs to the laboratory. An ICP-MS (Agilent® 7500 cx) coupled with an HPLC/diode array detector (Agilent® LC1200) was used to analyze the water samples. The samples were auto-diluted 10-fold and 100-fold, with 50 ppb of gallium used as a quality control. Analysis of each sample was performed in triplicate to achieve reproducibility and precision.

4.4 REE Pre-concentration

A pre-concentration procedure was required for quantification of REEs in high salinity samples. Since total dissolved solids of the monitoring well samples (parts-per-thousand) far exceeded the concentration of REEs (parts-per-trillion), each saline water sample (SW-1, SW-2 & SW-3) needed to be stripped of major and minor interfering ions in solution for an accurate

measurement. In this procedure, a ferric chloride ($FeCl_3$) reagent was created and added to the samples to scavenge and precipitate out the trace elements from the water matrix, leaving the major ions in solution behind. This research analyzed both the dissolved (filtered by 0.45 μm Millipore® filter) and particulate + dissolved (un-filtered) fractions of REE in water samples to get the total amount contributed by both fractions. The procedure outlined below is provided by methods found in literature (Shannon & Wood, 2005; Chevis et al., 2015). Domestic and surface water samples were not subjected to the iron co-precipitation procedure as they were not saline enough. Instead, these samples only received the cation exchange chromatography treatment to ensure barium and iron was eluted prior to analysis.

4.4.1 Lab Space

All REE extractions and fluid transfers were performed in a low-traffic portion of a laboratory inside of a cleaned perchloric acid Labconco® 1000 fume hood. The fume hood was cleaned with a clean cloth and DIW followed by a thorough decontamination with acetone.

4.4.2 De-ionized Water

All water used in bottle cleaning and laboratory preparation procedures was collected from a certified ultra-clean de-ionized water dispenser utilizing type 1 ultra-pure 18.2 MΩ.cm (at 25°C) de-ionized water with TOC < 5 ppb generated from a Millipore® Milli-Q Element A10 equipped with a 0.22 μm Millipore® Millipak Express 40 filter. The system processes tap water through a series of filtration membranes that incur reverse osmosis. A dual wavelength ultra-violet lamp purges organic molecules through photo-oxidation before water is processed through a cartridge to remove remaining trace ionic and inorganic contaminants. The ultra-pure water is then re-circulated through to the dispenser where a Quantum® application ICP cartridge removes ionic and inorganic constituents down to the trace level.

4.4.3 Acid Bath

Teflon® and glass beakers as well as polypropylene centrifuge tubes that were used during the REE pre-concentration procedure were ultra-cleaned according to the procedure outlined by Shannon & Wood (2005) and Chevis et al. (2015). Following a thorough DIW rinse, containers were subjected to a 24-hour 20% Fisherbrand® A200S-212 reagent-grade HNO_3 acid bath. Fisherbrand® polypropylene 50-mL centrifuge tubes were filled with the acid solution and secured tightly with the threaded cap while 100-mL Teflon® containers were stored in previously cleaned 1000-mL glass beakers with aluminum foil covering the open top. All containers were stored overnight in the fume hood. Following the 24-hour period, containers were again rinsed with the DIW and subjected to another acid bath containing 20% Fisherbrand® optima grade HNO_3 (67-70%). Containers were again rinsed with DIW following the second acid bath and allowed to dry in a previously cleaned (DIW, acetone) Thermo® Scientific Heratherm oven for 1 hour up to 60°C. Centrifuge tubes were sealed tightly upon dryness and Teflon® containers were laid on their side and temporarily stored there at ambient temperatures until needed.

4.4.4 Ferric Chloride Reagent

Puratronic® iron powder (-22 mesh, 99.998% metals basis) was selected as the pure valent iron reagent for the $FeCl_3$ solution. About 0.558 g (mole-equivalent) of this iron was weighed using a Denver Instrument® timberline balance. The iron was then directly transferred into the Teflon® beaker using clean Fisherbrand® weigh paper. Next, 4.0-mL of Fisherbrand® optima grade HCl (32-35%) was added to the Teflon® beaker and placed on a Fisher Scientific® Isotemp hotplate set to 100°C. After approximately one minute, 2.0-mL of Fisherbrand® optima grade HNO_3 (67-70%) was added incrementally (drop-by-drop) to expedite oxidation to $FeCl_2$. Once the reaction slowed, 2-6 μL of Fisher Scientific® reagent-grade ACS-certified H_2O_2 (30%)

was added to oxidize the reaction to $FeCl_3$. The solution was then removed from the heat source and allowed to cool in the fume hood. Upon cooling, 4.0-mL of DIW was added to the solution to obtain a 1 M $FeCl_3$ solution.

4.4.5 Iron Co-Precipitation Method

Dried centrifuge tubes were removed from the Thermo® Heratherm oven and weighed. A sample volume of 50-mL was added to the centrifuge tube and weighed again to ensure the exact volume of sample could be calculated. Next, 0.200-mL of the $FeCl_3$ reagent was added to the water sample. To facilitate precipitation of $FeCl_3$, 0.5-1.5 mL of Fisherbrand® optima grade NH_4OH (20-22% as NH_3) was incrementally added (drop-by-drop) and shaken before further addition to ensure permanent flocculation of iron precipitate. The addition of NH_4OH raised the pH of the solution to approximately 8-8.5, allowing the $FeCl_3$ to precipitate, however care was taken to avoid raising pH beyond 8.5 in fear of enhancing calcium recovery and impairing separation ability of REE from barium (Greaves et al., 1989). A limit of 3.0-mL of NH_4OH was dictated by D. Chevis (Tulane University) to ensure pH was under 8.5 (Chevis et al., 2015). Upon visual confirmation of permanent flocculation, the centrifuge tube was placed in the centrifuge (Eppendorf® Centrifuge 5430) for three to four minutes at 5000 revolutions-per-minute (RPM). Upon completion of sample centrifuge and confirmation that the flocculate adhered to the bottom of the container, the sample was then allowed to stand upright allowing the residual flocculate to settle. Following this, the supernatant was decanted via pipette and the precipitate was rinsed with DIW before re-entering into centrifuge. This process was repeated three times before the solid precipitate was re-dissolved in 5.0-mL of Fisherbrand® optima grade 2 M HCl. Greaves et al. (1989) concluded that preservation by HCl is ideal for keeping iron in solution and prevented from column adsorption.

4.4.6 Cation Exchange Chromatography

Poly-Prep® (AG® 50W-X8 resin; 200-400 mesh – 63-150 μm hydrogen ionic form; 1.7 meq·mL^{-1} capacity; Cat. No. 731-6214) BioRad® pre-packed cation exchange columns were used for the second part of the REE pre-concentration procedure for elution of iron and barium and to eliminate residual major ions in dissolved precipitate. The need for barium to be isolated from the REE fraction comes from the analytical interference of barium's oxide isotopes with both isotopes of Eu^{3+}; this signal distortion can cause a spike or positive anomaly in observed Eu concentration which can misconstrue result interpretation. In addition, the low ionization potential of barium reduces the ionization efficiency of the REEs being analyzed. Initial separation of barium is achieved from the precipitation of hydrated ferric iron reagent during the co-precipitation portion of the procedure.

The base of the columns were cut with a new acetone-cleaned blade to induce drainage of the factory preservative fluid before passing through 1-2 mL of optima grade 6 M HNO_3 to elute residual trace elements adhered to the resin from the manufactory process. Following a slight retraction of the resin, about 0.5-1.0 mL of DIW was used to "reset" the position of the resin before addition of another acid of different ionic form; 1.0-mL of optima grade 2 M HCl was then passed through to "prime" the column for the 2 M HCl dissolved sample precipitate. Following fluid drainage, the dissolved sample is then loaded onto the column. When the sample passes through the resin, the negatively-charged hydrogen form adsorbs ions with a net positive surface charge, while the 2 M HCl keeps iron in solution, allowing this ion and all other major ions to pass through into the waste beaker. The resin is then prepared again with 0.5-1.0 mL of DIW before passing through 3-5 mL of optima grade 2 M HNO_3 to elute the barium off of the column and isolate the REE fraction. At this point, the trace elements have been successfully

isolated from interfering ions and a significant proportion of major ions in the solution. Optima grade 8 M HNO_3 is used to strip the REE fraction from the column and collected in a pre-cleaned Teflon® beaker. The beaker is then placed on a hot plate at 100°C for three to four hours and the user is left with a small concentrated aliquot of sample which is re-dissolved in 10-mL of optima grade 1-2% HNO_3. A centrifuge tube is cleaned and weighed before storing the sample. Analysis was completed by a Finnigan® Element 2 high resolution ICP-MS. All sample preparation procedures were completed at KSU and analysis of the samples were performed at Tulane University.

Following analysis, the RAW REE data was modified by a concentration factor that is dependent on the mass of the sample used in the pre-concentration procedure and the resulting mass of the sample in the 1% HNO_3 solution following the pre-concentration procedure and before analysis. Information on pre-concentration factors can be found in Appendix G.

Chapter 5 - Results

All samples collected and results obtained refer to the following sample descriptions in Table 5.1. An aerial view of the sample site is shown for reference in Figure 5.1. For further information regarding well construction information see Appendix A.

Domestic	**Screen Interval**	**Well. Shale start depth**	**Well Purpose**	**Dates Collected**
Ast	26-46'	13'	Lawn & Garden	7/19/16
Becker	23-55'	50'	Lawn & Garden	7/20/16
Shepherd	23-47'	38'	Household	10/6/15 & 7/19/16
Zehr	20-60'	19'	General	10/6/15 & 7/19/16
Observation	**Screen Interval**	**Well. Shale start depth**	**Well Purpose**	**Dates Collected**
SW-1	50-100'	14-15'	Monitoring	10/6/15 & 7/20/16
SW-2	100-200'	20'	Monitoring	10/6/15 & 7/20/16
SW-3	25-50'	30'	Monitoring	2/11/15[1], 3/17/15[1], 10/7/15 & 7/19/16
Surface Waters	**Screen Interval**	**Well. Shale start depth**	**Well Purpose**	**Dates Collected**
Slate Creek 1	N/A	N/A	N/A	10/6/15 & 7/18/16
Slate Creek 2	N/A	N/A	N/A	7/18/16
Other	**Screen Interval**	**Well. Shale start depth**	**Well Purpose**	**Dates Collected**
MIZ	3,664-3,706'	--	Monitoring - CO_2	1/10/11[2], 6/11/15[1], 1/19/16[1], 3/9/16[1], 7/20/16 & 8/10/16[1]
Arbuckle[2]	N/A	--	--	1/23/11 - 3/7/11

[1]Samples were collected and analyzed by the KGS

[2]Samples were collected via drill-stem tests during well installation and analyzed by Barker (2012)

Table 5.1 Well identification descriptions including dates the samples were collected. A pre-injection sample is one that was collected before January 2016.

The 2011-dated MIZ (Mississippian Injection Zone or Miss. Inj. Zone) (1) and Arbuckle samples (8) were collected and analyzed by Barker (2012) whereas the 2/11/15 (1), as well as 3/17/15 (1) samples, were collected and analyzed by the KGS. Arbuckle samples are considered pre-injection in relation to the start of CO_2-EOR operations. Original samples collected from this work include everything else in Table 5.1. The MIZ sample collected by Barker (2012) was retrieved from inactive injection well KGS 1-32 whereas the 7/20/16 sample was collected at Oil Well 61 (Figure 5.1). Furthermore, the Arbuckle samples collected by Barker (2012) at 4,175-

4,575 ft. were from KGS 1-32, whereas the samples collected from the 4,866-5,250 ft. interval were from KGS 1-28. The depths of each sample for the wells were chosen to be the middle of the screen. Samples dated before and after 1/9/16 are categorized as pre- and post-injection, respectively.

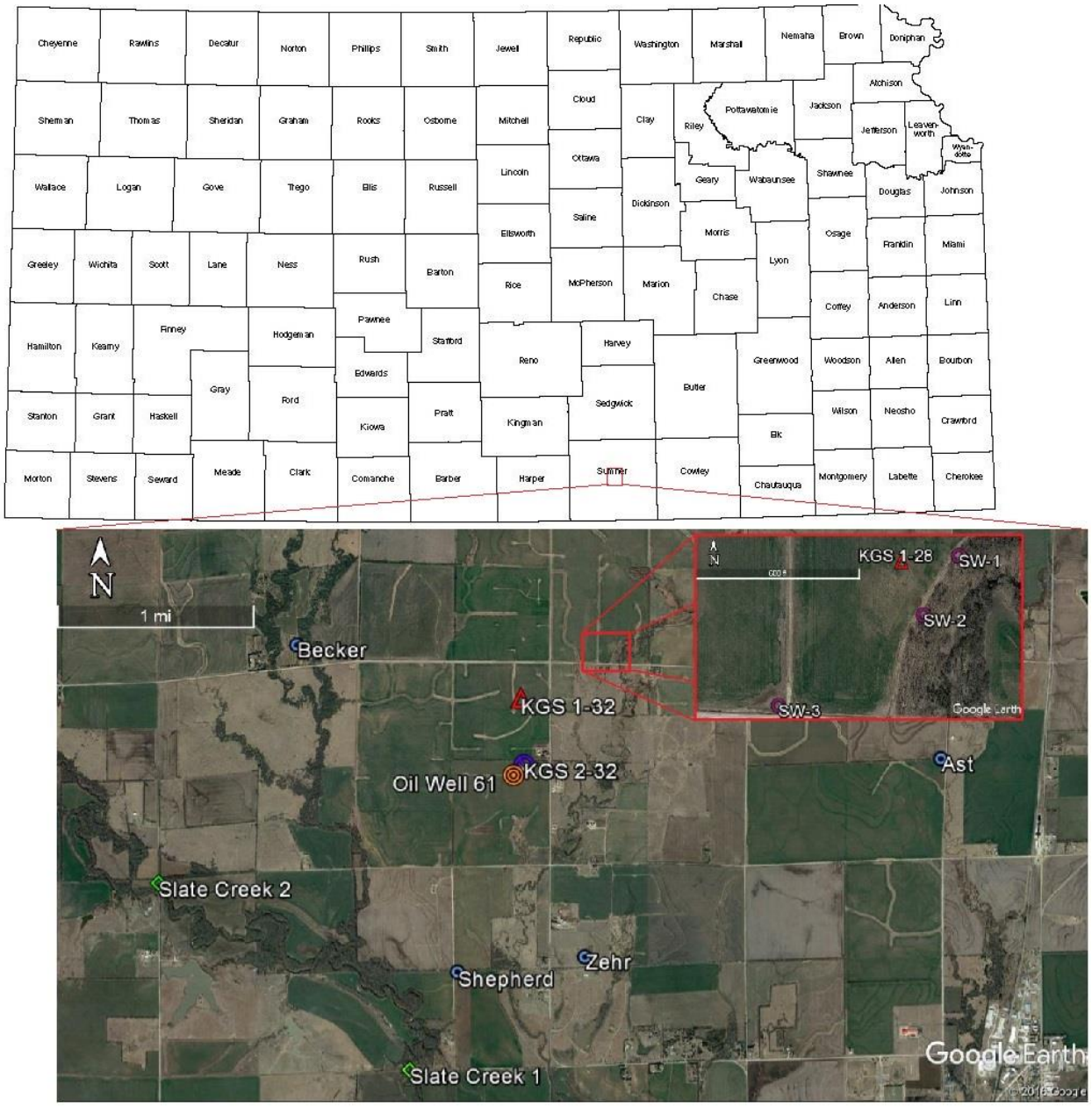

Figure 5.1 Aerial map view of the sample locations in Wellington, Kansas.

5.1 Water Quality

Initial water quality parameters such as DO, pH, turbidity, ORP, temperature and specific conductivity were collected in the field prior to and during sampling. Figure 5.2 details average water quality values as a function of depth for all samples collected during the pre- and post-injection sampling events. For a complete tabulation of water quality parameters, see Appendix B.

Specific conductivity, an indirect measure of TDS measured in ms/cm, shows a wide variation at the 20-60 ft. depth interval, particularly between the shallow monitoring well and the domestic wells. According to Figure 3.4 as shown by Watney et al. (2015), 20-60 ft. samples SW-3 and Ast are located on the paleoterrace (NE quadrant) whereas samples Shepherd, Zehr and Becker are located within the incised paleovalley (SW quadrant) of the study area. There also appears to be a general positive correlation with depth among the samples and although not shown, sample SW-2 exceeded the detection range of the instrument with a reading >100 ms/cm.

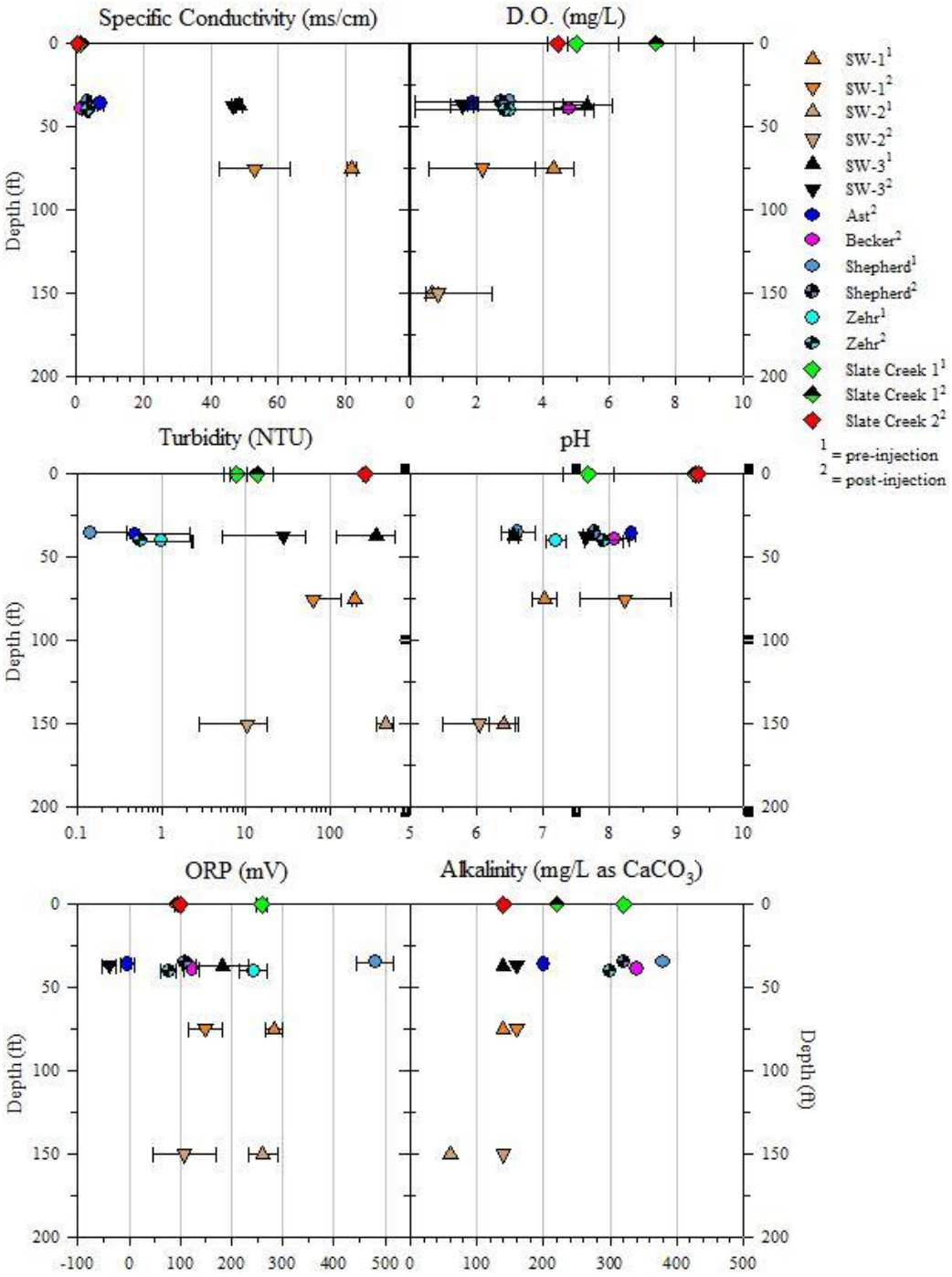

Figure 5.2 Water quality variation with depth. Specific conductivity of sample SW-2 was above detection range and Becker turbidity was zero; both are not displayed. Error bars indicate standard deviation of repeated measurements during sample collection.

Dissolved oxygen values generally decrease with increasing depth. It is interesting to note, however, that the 50-100 ft. SW-1 concentration is elevated relative to the shallower 25-50 ft. SW-3 and 23-46 ft. Ast samples.

Turbidity, a measure of the 'murkiness' of the water, quantifies the translucency based on light blockage from suspended particulates within the sample. Proper well construction and drilling practices are important for accurate turbidity readings, as an improperly developed well may lead to a higher accumulation of fines at the bottom of the screen, leading to perturbation during pumping and a poor reflection of true aquifer water. In addition, if the borehole and well casing diameter, as well as screen slot and gravel size, are not properly matched, there may be insufficient filter space for the gravel pack to remove fines before infiltrating into the well casing. Higher sample quality is reflected in lower turbidity readings, as shown by proper pumping practices, although this is not always achievable and does not apply to samples that do not require pumping e.g. surface water or oil brine samples.

The elevated turbidity reading in sample Slate Creek 2 was anticipated, as sampling unintentionally occurred following a rain event; however, pre-injection samples SW-2 & SW-3 are yet higher. In contrast to DO or specific conductivity, turbidity does not appear to have a correlation with depth. Additionally, the turbidity differences among both rounds of SW-1, SW-2 and SW-3 samples may be explained by the pumping method differences from Oct. 2015 and Jul. 2016; an auto-bailer was used to pump water at high rates (2-4 GPM) near the base of the water column for all SW wells in Oct. 2015 whereas a geosub pump was used to pump water near the top of the column at 1-2 GPM in Jul. 2016—the difference is the fines tend to settle near the base of the water column. With exception of the slightly more basic SW-1 samples, there is a general decrease in pH with increasing depth; the most basic samples were collected at the

surface, whereas the most acidic samples were collected at the deepest interval. Moderate variability was detected among the 20-60 ft. depth interval with the range encompassing the surface water and underlying SW-1 sample. It is interesting to note the basification of samples Slate Creek 1, Shepherd, Zehr, SW-1 and SW-3 from the pre- to post-injection. In contrast, sample SW-2 shows acidification from pre- to post-injection. The most neutral pH observed among the sample set is that of pre-injection sample SW-1, with more basic values in the depth intervals above and acidic below, although post-injection shows a significant standard deviation from the average of 0.69.

ORP is a general measure of a solution's ability to oxidize or reduce a multi-valent ion. In general, the value of ORP can provide the relative extent of oxidation or reduction for specific half reactions; each reductant has an associated oxidant where the electrons originated. These values generally require a firm understanding of the pH and Cl concentration of the solution, as they are controls on the ORP. In addition, it is important to understand the governing half reactions that are occurring based on dominant ionic distribution. We observe two samples, Ast and SW-3, which display negative ORP values on the plot with emphasis towards reducing conditions. There is high variability among the 20-60 ft. interval with the lowest reducing values represented for post-injection SW-3 and highest oxidizing values for pre-injection sample Shepherd. Furthermore, every post-injection sample is reduced with respect to their post-injection counterparts to similar extents.

Alkalinity is a measure of the ability for a solution to buffer an acid. As such, the least alkaline samples would be expected to have the lowest pH. This trend is generally observed between the two plots, although sample Slate Creek 2 and pre-injection Shepherd show an inverse relationship. There does not, however, appear to be a consistent trend with depth. In fact,

samples Slate Creek 2, SW-1, SW-2 & SW-3 all show similar values despite different depth intervals.

Figure 5.3 illustrates calculated water quality parameters such as ionic strength, hardness and TDS vs specific conductivity; these diagrams are included to further resolve differences in salinity variation among the dataset. A logarithmic scale was used as the variability was extreme. Note the general correlation among the three graphs with depth. The hardness of the waters correlates with an increased presence of dissolved Mg and Ca. Total permanent hardness as calcium carbonate ($CaCO_3$) is calculated by taking the measured concentration of Ca and Mg in mg/L and multiplying by the molar mass ratio of $CaCO_3$ / Ca (2.497) and $CaCO_3$ / Mg (4.118), respectively, then summing the results together. Higher hardness effects in water are reflected in scales formed by precipitation of constituents combining with Mg and Ca, whereas softer water may promote corrosion. The accepted classification system is outlined in Table 5.2.

Mg/L	Classification
< 17.1	Soft
17.1 - 60	Slightly Hard
60 - 120	Moderately Hard
120 - 180	Hard
> 180	Very Hard

Table 5.2 Hardness classification of water as calcium carbonate.

According to these values, every sample, with exception of surface water sample Slate Creek 2 (moderately hard), is considered very hard at varying magnitudes. There is also a positive correlation with depth with exception of sample SW-3 which shows enrichment with respect to SW-2 & SW-3.

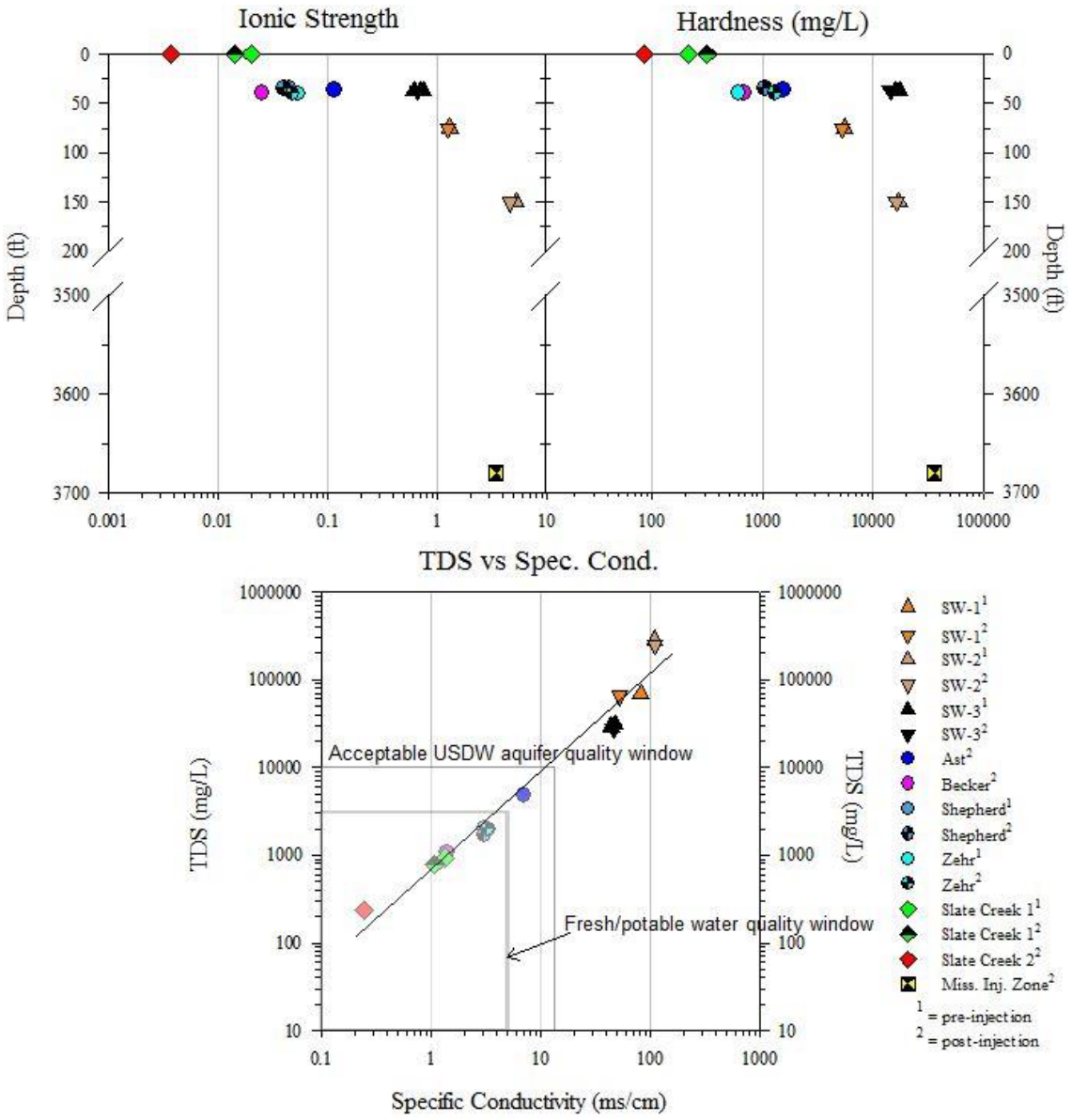

Figure 5.3 Calculated water quality parameters based on salinity and ionic composition. Acceptable USDW and fresh/potable water quality windows are set forth by underground injection control (UIC) guidance under the SDWA for regulatory USDW and potable water standard compliance. The fresh/potable water quality standard of 3,000 mg/L was dictated for Region V and no current standard exists for Kansas, Region VII, but is used instead as a reference.

Ionic strength is a parameter that is sensitive to the major ionic contributors of the total dissolved solids. As such, ionic strength is calculated by the following formula for major ions:

$$I = \frac{1}{2} \sum c_i * {Z_i}^2$$

Where I is ionic strength, C is concentration in mol/L and Z is valence. The major ions used for this calculation were Ca, Mg, Na, K, HCO_3, SO_4, Cl and NO_3. Furthermore, total dissolved solids versus specific conductivity was used to discern a line of best fit among the dataset to outline the limits of the acceptable USDW and fresh/potable water quality windows. The windows dictate acceptable standards for a USDW during injection activities and acceptable drinking water quality limits for human consumption (Region V). According to these outlines, all of the domestic wells have maintained the potable quality standard with the exception of domestic sample Ast. Furthermore, the domestic well and surface water samples follow the line of best fit more closely than do the shallow monitoring wells.

Further observations of shallow salinity variation are shown in Figure 5.4, which plots saline contours of the 20-60 ft. interval. Data gaps were interpolated by SigmaPlot®, the program used to generate this visual. A high salinity gradient is observed over the sampling area. With respect to SW-3, the following salinity gradients for the domestic wells were calculated: Ast - 2.39 ($mg \cdot L^{-1}ft^{-1}$); Becker – 3.35 ($mg \cdot L^{-1}ft^{-1}$); Shepherd – 2.84 ($mg \cdot L^{-1}ft^{-1}$); Zehr – 3.28 ($mg \cdot L^{-1}ft^{-1}$). Gradient is equal to the difference in average concentration of total dissolved solids (mg/L) for SW-3 (2-11-15, 3-17-15, 10-7-15 & 7-19-16) and each well divided by the distance in feet. The distance between SW-3 and each well ranged 1.5 – 1.8 miles.

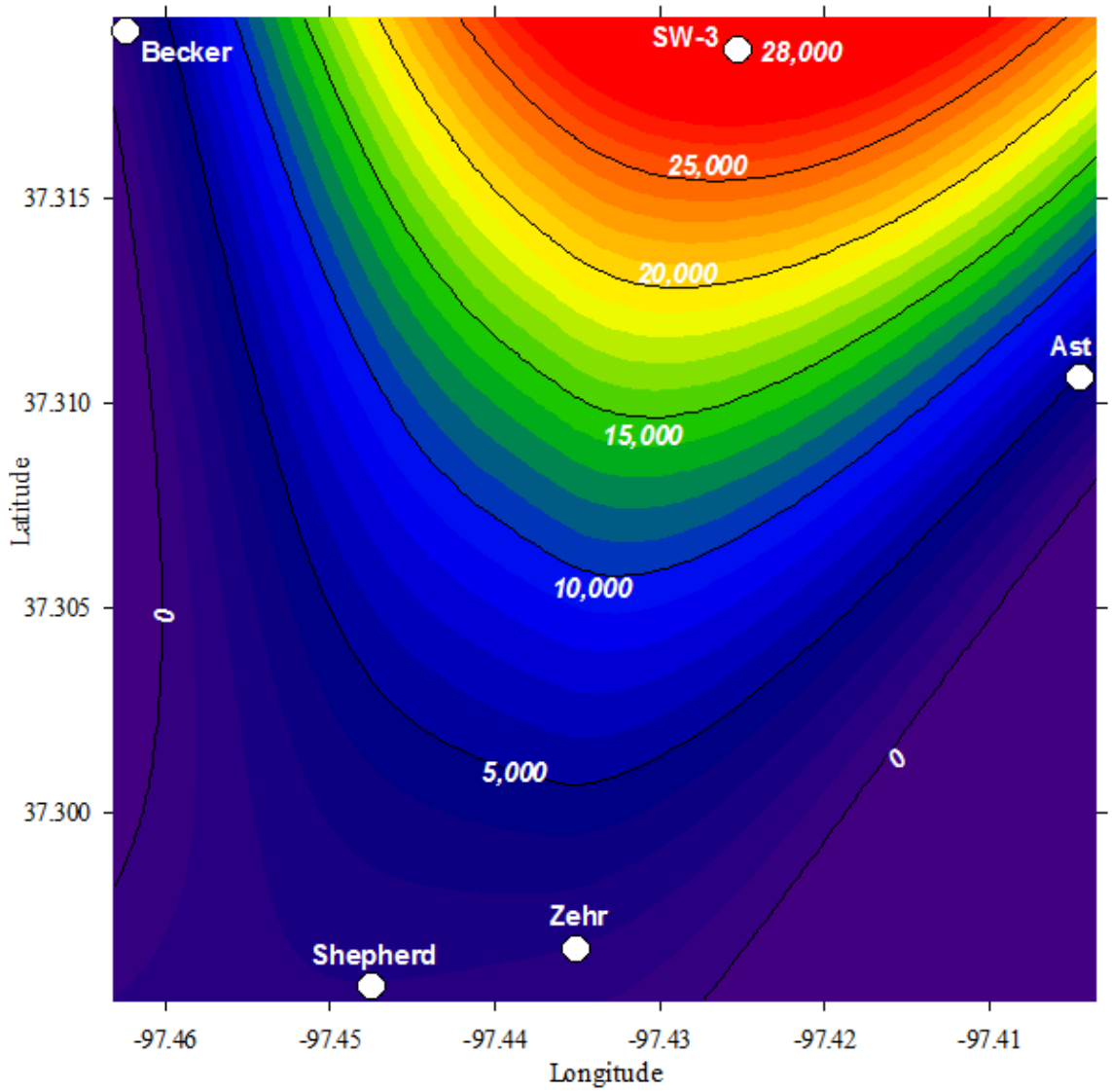

Figure 5.4 Isobath spatial salinity variation. Salinity is defined as TDS measured in mg/L calculated by adding all cations and anions in solution. The length between longitudinal tick marks is equal to 1 km distance (0.621 miles).

5.2 Major Ions

Results of samples requiring dilutions for ion chromatography were calculated by taking the difference of the final result for each individual ion of the diluted sample and the result of the DIW used in the dilution multiplied by the dilution factor. Results of DIW-corrected and DIW-uncorrected values are reported in Appendix D; however, only the DIW-corrected values are

shown on the graphs in this section for all samples except those of Barker (2012). Additionally, a single seawater sample that was referenced by Barker (2012) is used as comparison.

A piper diagram is shown in Figure 5.5 to illustrate water typing classification. According to the diagram, the water type of SW-3 changes from Ca-Cl to Na-Cl between Mar. 2015 and Oct. 2015 and Zehr changes from Mg-Cl to Ca-Cl. The change from Mg-Cl to Ca-Cl in sample Zehr may not be representative of actual conditions as Ca could not be quantified in the pre-injection sample. Samples SW-1, SW-2 and MIZ remain Na-Cl type while Ast, Becker, and Slate Creek 2 are reported as Na-SO_4, Mg-HCO_3 and Ca-HCO_3 type, respectively.

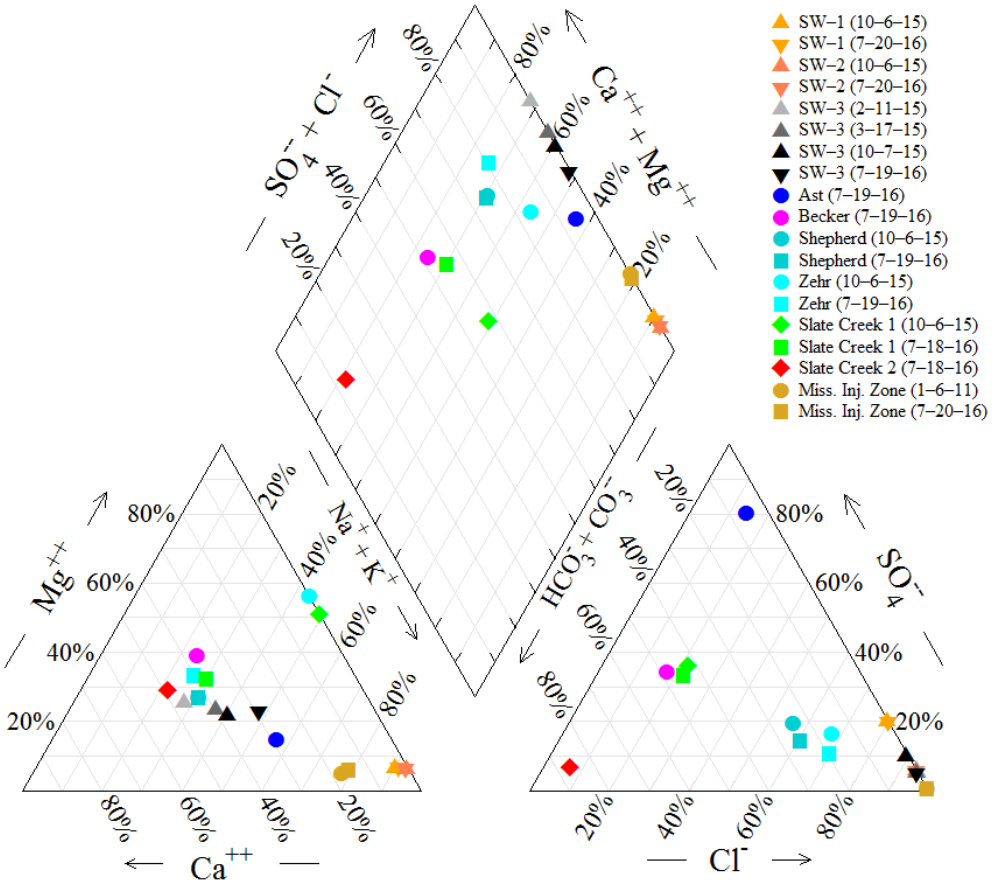

Figure 5.5 Piper diagram classification of hydrochemical facies of water samples collected in Wellington, Kansas. Samples SW-3 (2-11-15 & 3-17-15) were collected and analyzed by KGS. Sample MIZ (1-6-11) was collected and analyzed by Barker (2012).

All ions in Figure 5.6 show consistent enrichment-depletion patterns with the salinity variation graphs above indicating a positive correlation with depth. In particular, the 20-60 ft. interval displays high variability of K, Na and Ca among the domestic wells. The shallow monitoring wells show a progressive Mg, K and Na enrichment and Ca depletion with increasing depth. Surface water samples all show lower ionic concentrations relative to the rest of the dataset with the exception of K and SO_4. Additionally, sample SW-2 is enriched with respect to Cl, SO_4, Na and Mg relative to MIZ

A further look into major ionic relationships is shown in Figure 5.7, where Cl is used as a normalizing factor. (Ca + Mg) relative to Na is plotted against Cl to observe compositional variations intended to represent recent salinization events as shown in Whittemore (1995). According to this diagram, there is a general softening of water with respect to Na as a function of depth. Samples SW-2 and SW-3 represent exceptions to this trend as they have lower mass ratios than the deeper Arbuckle and Mississippian zones. The fingerprint of the salinity is shown in the Br/Cl graph. With the exception of sample Slate Creek 2, SW-1 and SW-2, Br/Cl values appear to be consistent among the surface, shallow and deep intervals with a mass ratio range of 13.7 – 48.7. The two deep intervals appear to be disconnected with Arbuckle and MIZ values ranging 17.3 – 26.1 and 39.0 – 44.0, respectively. However, shallow samples Shepherd, Becker, Zehr and SW-3 plot close to the mass ratio for the MIZ samples with a range of 33.7 – 48.7.

With respect to Na/Cl mass ratio values, MIZ samples range 0.48-0.62 while domestic and monitoring well samples range from 0.24 to 2.58, with an apparent gap in composition between about 0.4 and 0.7. In contrast, the oilfield brine compositions plot within the range of this gap. The high Na/Cl mass ratio in domestic sample Ast is unique within the dataset, with the next highest Na/Cl mass ratio value found to be 1.17 for domestic sample Becker. Mississippian

and Arbuckle mass ratio values of SO_4/Cl are consistently lower than shallower zones, with MIZ values ranging from 0.005 to 0.006, whereas shallow wells range from 0.067 to 7.55; sample SW-3 represents the low end of the range and sample Ast the high end.

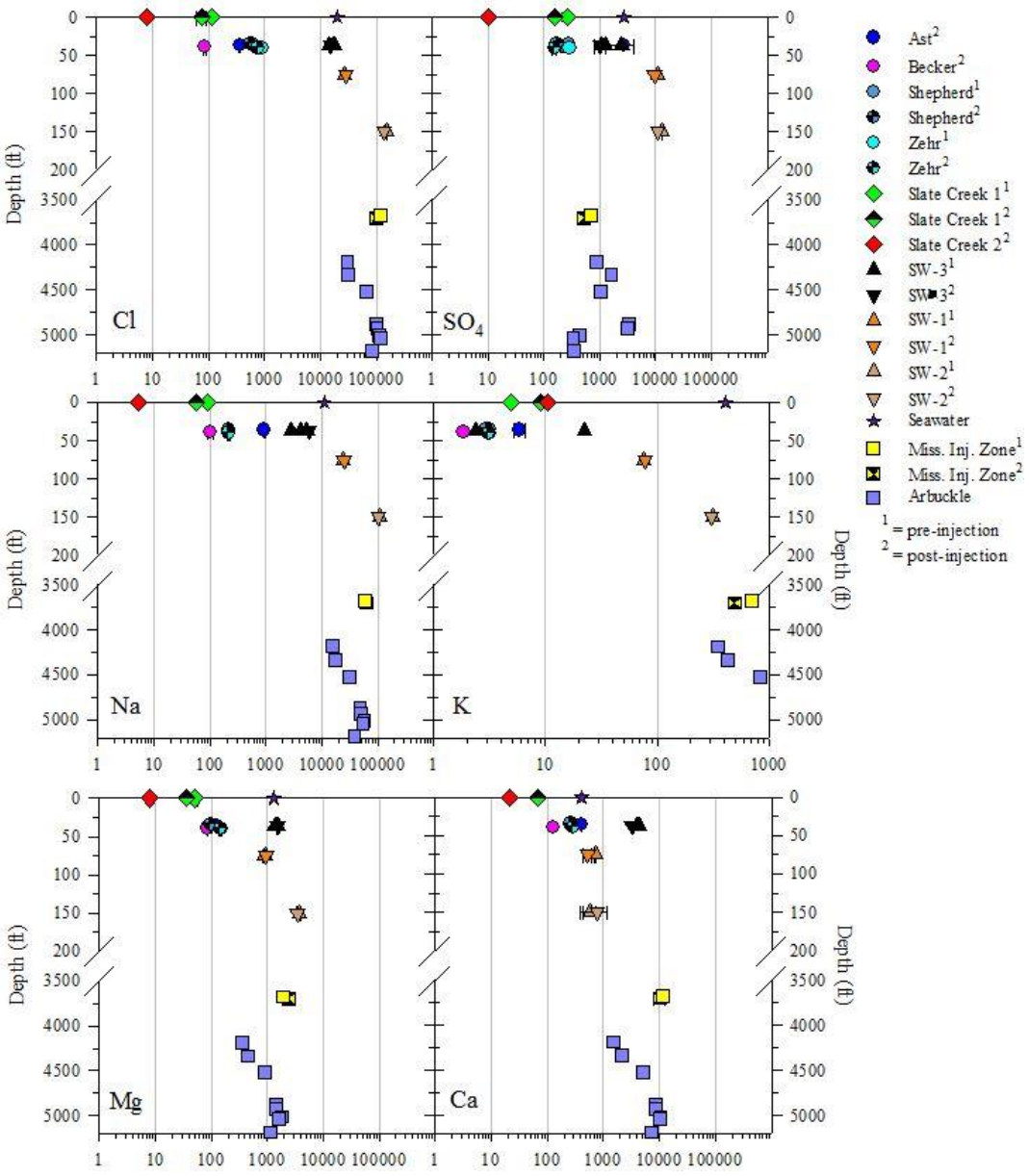

Figure 5.6 Major ions as a function of depth, all results are reported in mg/L.

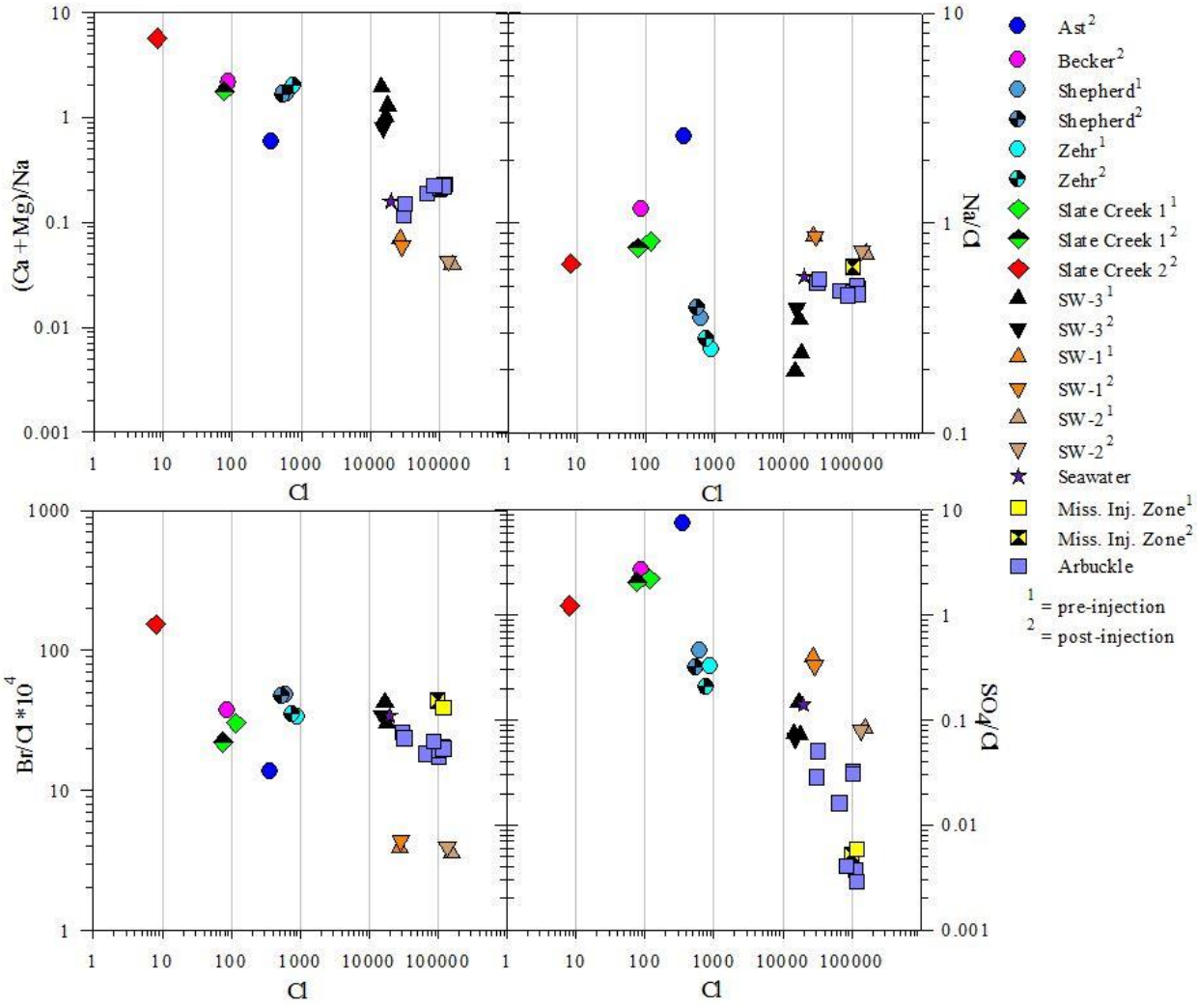

Figure 5.7 Conservative major ion relationships typically observed in saline systems, all results are reported in mg/L.

5.3 Stable Isotopes

This chapter reviews the results obtained from $\delta^{18}O$, $\delta^{2}H$ and $\delta^{13}C$ analysis of all surface water, groundwater and oil brine samples from the study site. Sample intervals include surface water, shallow zones spanning from 20-60 ft., 50-100 ft. and 100-200 ft. BGS and the deeper Mississippian injection interval at 3,664-3,706 ft. BGS (MIZ). Data are presented in depth profiles (Figure 5.8) and $\delta^{18}O$ vs $\delta^{2}H$ graphs (Figure 5.9). For a complete tabulation of stable isotope values, see Appendix E.

Global and local meteoric water lines are shown for reference. GMWL data are from Craig (1961b), whereas the LMWL information is from Dr. Jesse Nippert of KSU Department of Biology; the LMWL is based on over 500 rainfall samples for the Konza Prairie, KS area (Nippert, personal communication, 2017).

Figure 5.8 shows depth profiles of $\delta^{18}O$ and $\delta^{2}H$. The data show a steady decrease in isotopic ratio with depth for the shallow aquifer zone, although the deepest shallow well (SW-2) has a slightly less depleted ^{2}H value relative to the shallower SW-1 monitoring well. Deeper samples show an opposite trend: samples are increasingly enriched starting with the top of the baffle zone through the Arbuckle, although the shallower MIZ is enriched with respect to the deeper zones. Additionally, there is an observed ^{18}O and ^{2}H temporal depletion among the MIZ samples with the pre-injection sample representing the most enriched ^{18}O and ^{2}H values in the dataset aside from surface water sample Slate Creek 2.

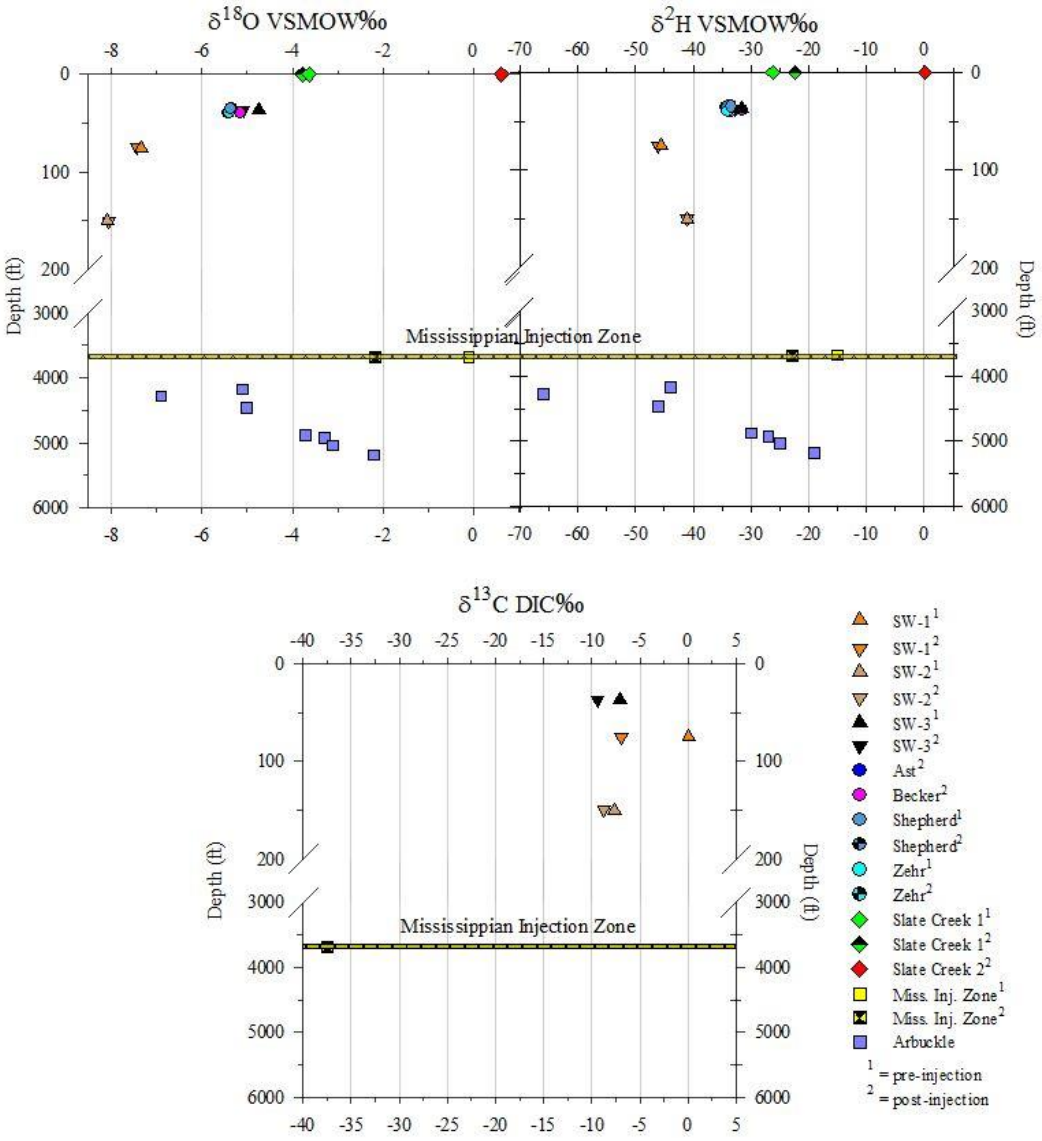

Figure 5.8. Variation of stable isotopes with depth represented as ‰ deviation from VSMOW.

δ^{13}C DIC values within SW-2 and SW-3 are relatively consistent for both sampling rounds. Sample SW-1, however is significantly depleted from pre- to post-injection from 0.065‰ to -6.9‰; these values are enriched relative to SW-2 and SW-3. Additionally, the MIZ is significantly depleted in relation to the shallower samples with a δ^{13}C DIC value of -37.5‰.

Figure 5.9 shows $\delta^{18}O$ vs $\delta^{2}H$ with reference to a GWML and LWML. Enrichment-depletion trends among samples of similar depths and geologic settings are shown. Similar to Figure 5.8, there appears to be a general depletion trend with depth until the MIZ is encountered which essentially restarts the trend. The 100 ft., 200 ft. and 4,280 ft. zones are the most depleted, whereas the surface and 3,677 ft. interval are the most enriched. Additionally, all samples spanning the depth interval 20-60 ft. are closely grouped, with mean $\delta^{18}O$ and $\delta^{2}H$ values of -5.23 (±0.232) and -33.1 (±1.10), respectively. Shallow well SW-3 shows a slightly different enrichment trend than the proximal shallow domestic samples with a regression slope similar in magnitude to that of the MIZ. Shallow domestic samples Shepherd, Zehr, Becker and Ast all fall along the GMWL showing depletion relative to the LMWL while deeper Arbuckle and Mississippian samples are all enriched with respect to the LMWL.

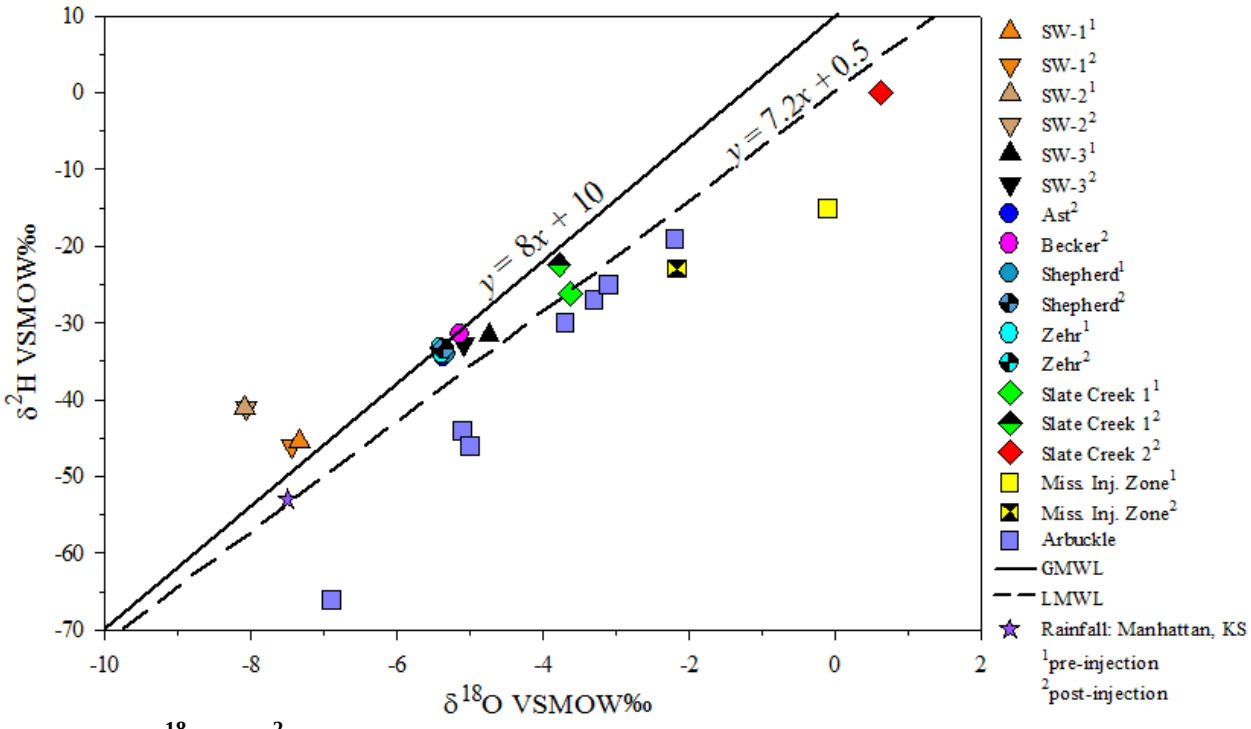

Figure 5.9 $\delta^{18}O$ vs $\delta^{2}H$ in comparison to a GMWL and LMWL. The equations used to generate each MWL are displayed above their respective regressions.

5.4 DOC/CO_2/Hydrocarbons

5.4.1 Dissolved CO_2/Hydrocarbons

Dissolved CO_2(aq) and a select suite of hydrocarbons are discussed in this section. Although DOC values were obtained for the entire sample repertoire, only a few key samples were analyzed for dissolved CO_2 and hydrocarbons. The set of targeted organic constituents is listed in section 2.3.6. Additionally, four pre- and post-injection MIZ samples were collected and analyzed by the KGS; only one MIZ sample displayed below was collected and analyzed by this research. For a complete tabulation of dissolved organics/inorganics, see Appendix F.

Figure 5.10 shows CO_2 and organic constituents that were detected in concentrations above detection limit as a function of depth. Samples analyzed included Shepherd, SW-3 and one MIZ sample. The shallow samples were selected based on their geographic proximity to the CO_2 injection well. The MIZ sample was analyzed for CO_2 to compare injection-zone-charged activities to the selected shallow samples.

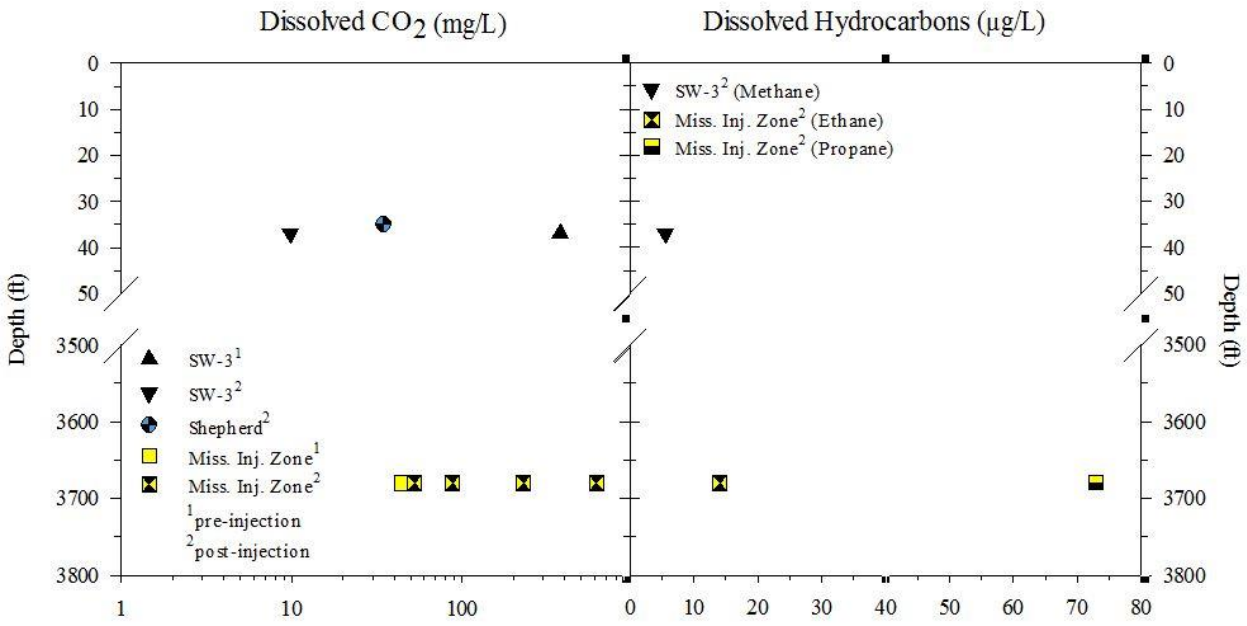

Figure 5.10 Dissolved organic/inorganic C species of a few key samples as a function of depth. Samples Shepherd, SW-3 and Miss. Inj. Zone represent key horizons that are critical to the investigation.

Oil well 61, which screens the Mississippian injection interval, shows an increase in CO_2 concentration from initial pre-injection (6/11/15) to final post-injection (8/10/16) sampling events, as to be expected. In contrast, the pre-injection sample SW-3 (2/11/15) collected by the KGS was detected at a significantly higher concentration (378 ppm) than post-injection (7/19/16 – 9.8 ppm). Shepherd organic concentrations fell below the detection limit, whereas SW-3 was detected at 5.5 µg/L for methane. The MIZ sample, however, detected unnatural petrochemical constituents such as ethane and propane and below detection for the other targeted organic constituents including methane.

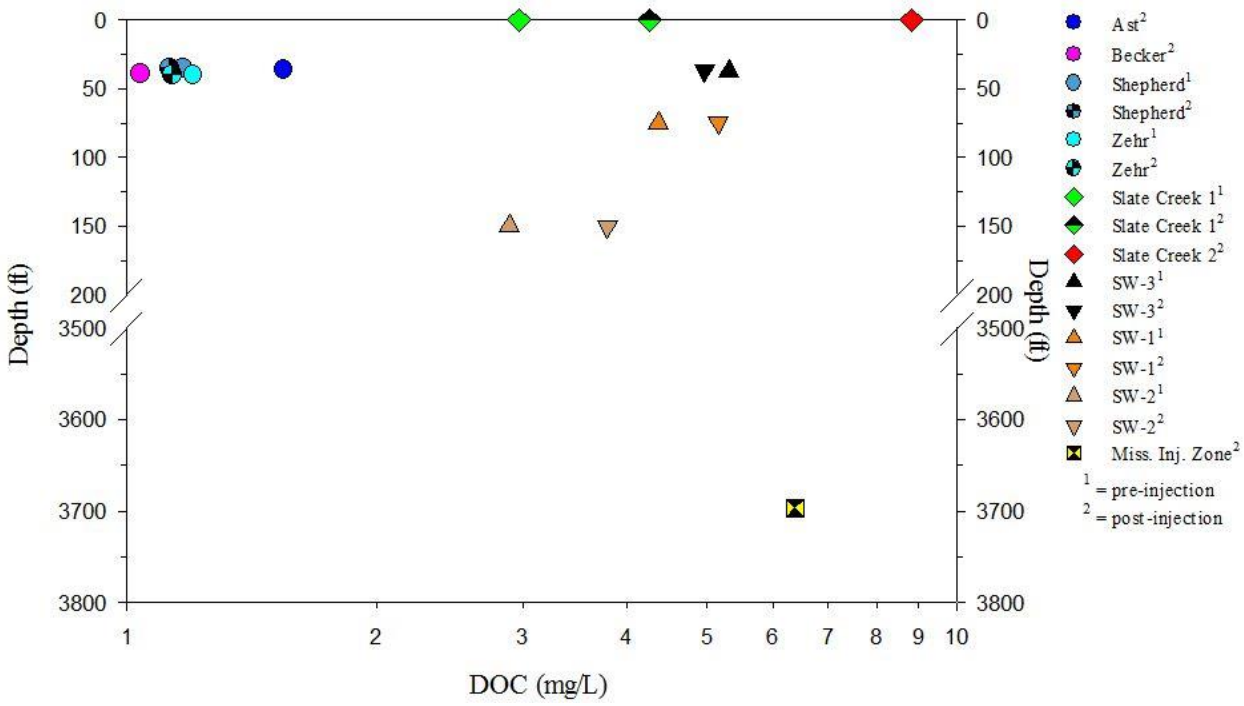

Figure 5.11 DOC concentrations as a function of depth

According to Figure 5.11, the domestic wells range from 1.0 to 1.5 mg/L DOC, whereas the shallow monitoring wells ranged 2.9 to 5.3 mg/L. Among the shallow monitoring wells there is a negative correlation with depth with concentrations that overlaps the surface water samples. The elevated DOC of the MIZ was anticipated due to the presence of dissolved hydrocarbons in the subsurface reservoir. The surface water samples ranged from 3.0 to 8.8 mg/L, with sample Slate Creek 2 containing the highest concentrations in the entire dataset.

5.5 Rare Earth Elements

All post-injection samples, with the exception of MIZ, were analyzed for REEs in the form of both the dissolved fraction (dREE) (< 0.45 μm) and particulate fraction (pREE) (unfiltered). Particulate concentrations were calculated to be the difference of the dissolved and unfiltered concentrations. Pre-injection samples were not analyzed for REEs, as their intended

purpose did not require a time series observation. The intended application of REEs in this work is principally to correlate the interrelation of lithologic signatures to biogeochemical processes driving trace metal cycles. Identification of enrichment-depletion patterns would help illustrate differences in water-rock interaction to supplement other geotracer data. The entire dataset was normalized to Post-Archaean Australian Shale (PAAS) of Taylor and McLennan (1985).

The domestic and surface water samples (low TDS) were analyzed in a different manner than that of the shallow monitoring well samples (high TDS). As discussed in section 4.4, the more saline samples required an iron co-precipitation procedure to remove major ions from the solution as they would interfere with the accuracy. Both low and high TDS samples were subjected to a cation chromatography column exchange procedure to elute barium and iron, however. The domestic and surface water samples were analyzed entirely by high resolution ICP-MS for only a single isotope of each REE whereas the shallow monitoring well samples were analyzed at a mix of medium and high resolution ICP-MS for multiple isotopes of specific elements, which were averaged before reporting of the final value (see Appendix G). For the majority of the REEs, RSD fell below 10%, with Eu reporting less precise values ranging 4.21 to 81.67 RSD% for the low TDS samples and 0.55 to 23.80 RSD% for the high TDS samples. For more details on instrument accuracy, see Appendix G. The raw dataset was calculated back to original concentrations using a concentration factor that is based on the mass of the sample before and after the pre-concentration procedure.

For the domestic wells, the raw dissolved ∑REE ranged 15.44 to 1,563.29 ng/L whereas raw particulate ∑REE ranged 425.54 to 261,558.22 ng/L. The PAAS-normalized dataset showed a clear enrichment of HREE relative to LREE for most dREE plots (Figure 5.12; Figure 5.13; Figure 5.14; Figure 5.15; Figure 5.16; Figure G.1).

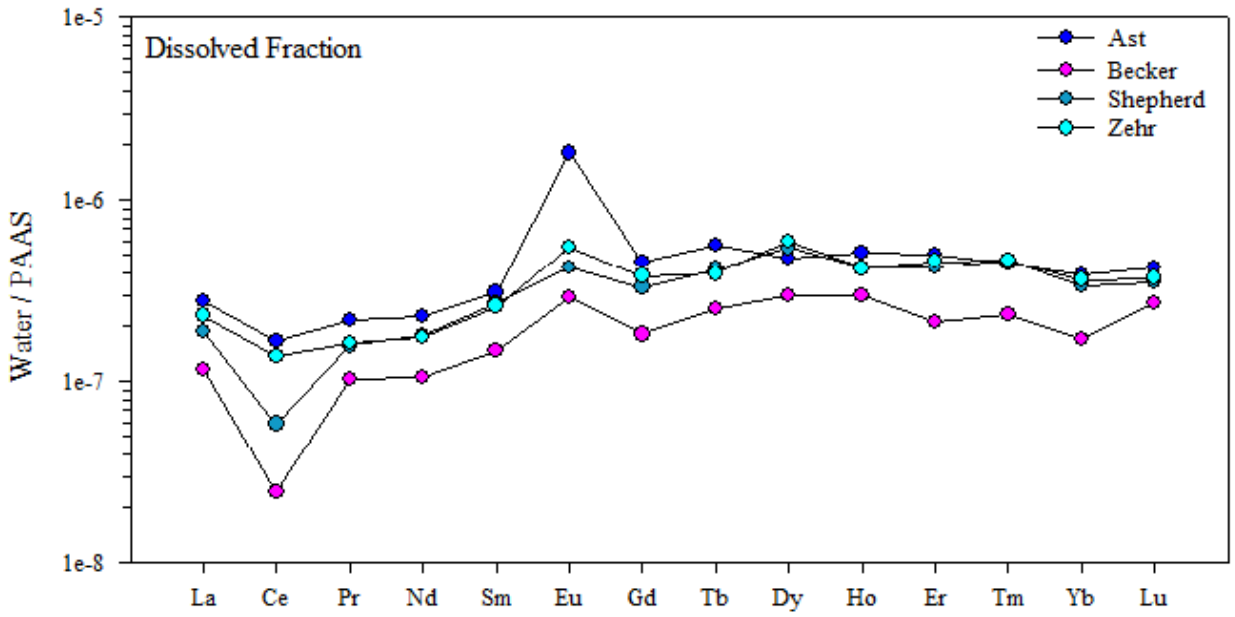

Figure 5.12 'Dissolved only' fraction of domestic well REEs normalized to PAAS (Taylor & McLennan, 1985).

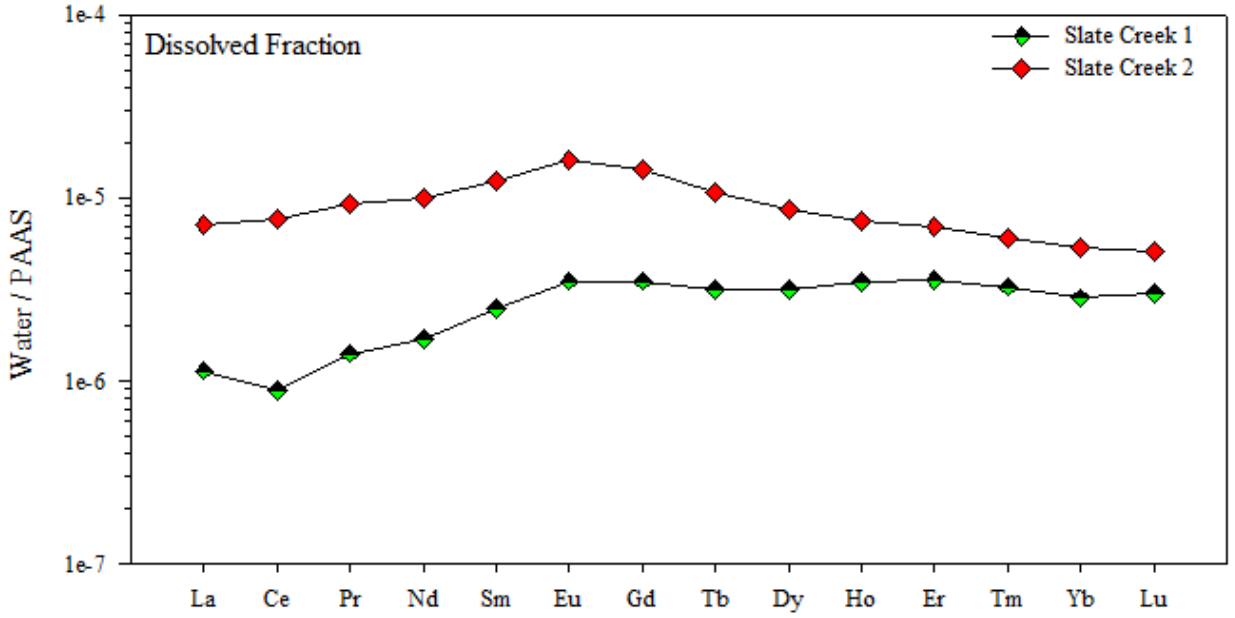

Figure 5.13 'Dissolved only' fraction of surface water REEs normalized to PAAS (Taylor & McLennan, 1985).

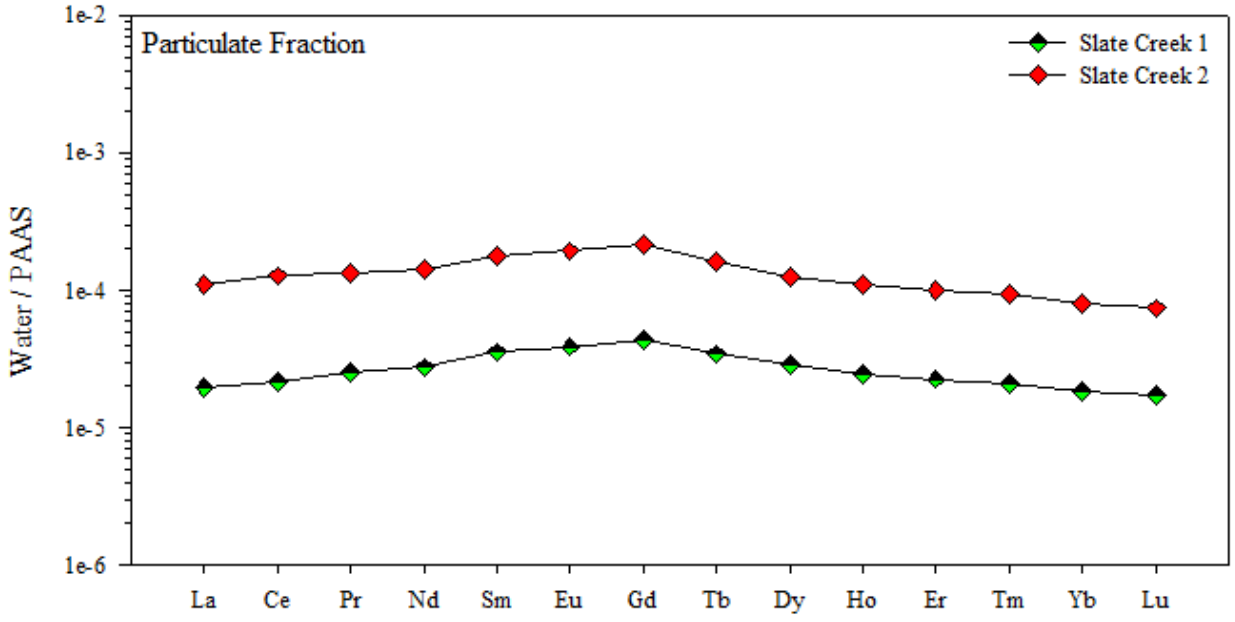

Figure 5.14 'Particulate only' fraction of surface water REEs normalized to PAAS (Taylor & McLennan, 1985).

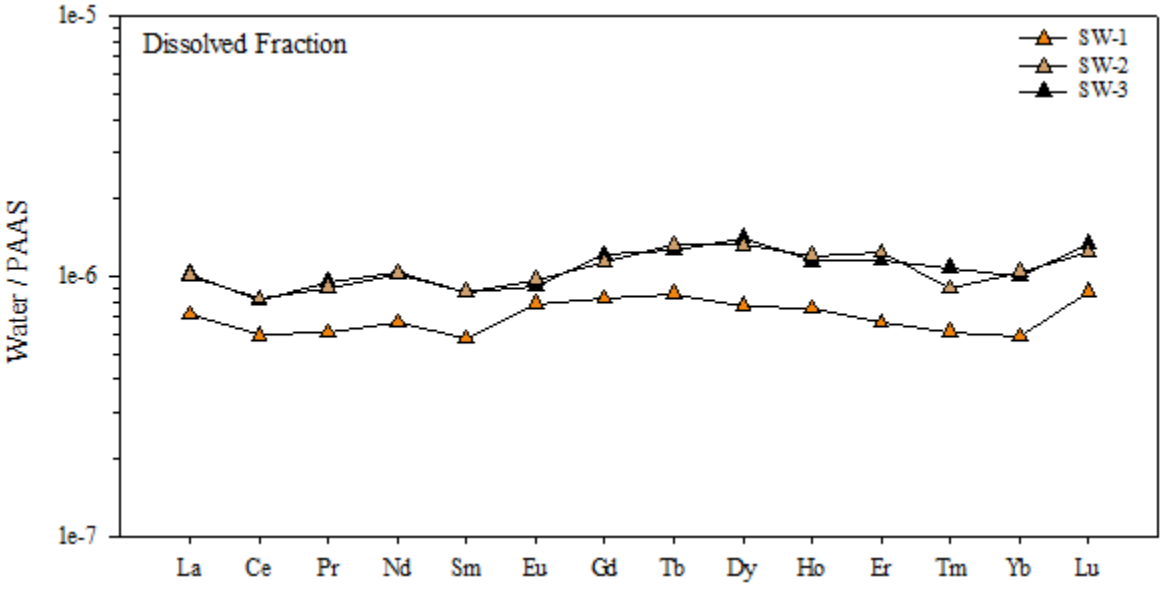

Figure 5.15 'Dissolved only' fraction of shallow monitoring well REEs normalized to PAAS (Taylor & McLennan, 1985).

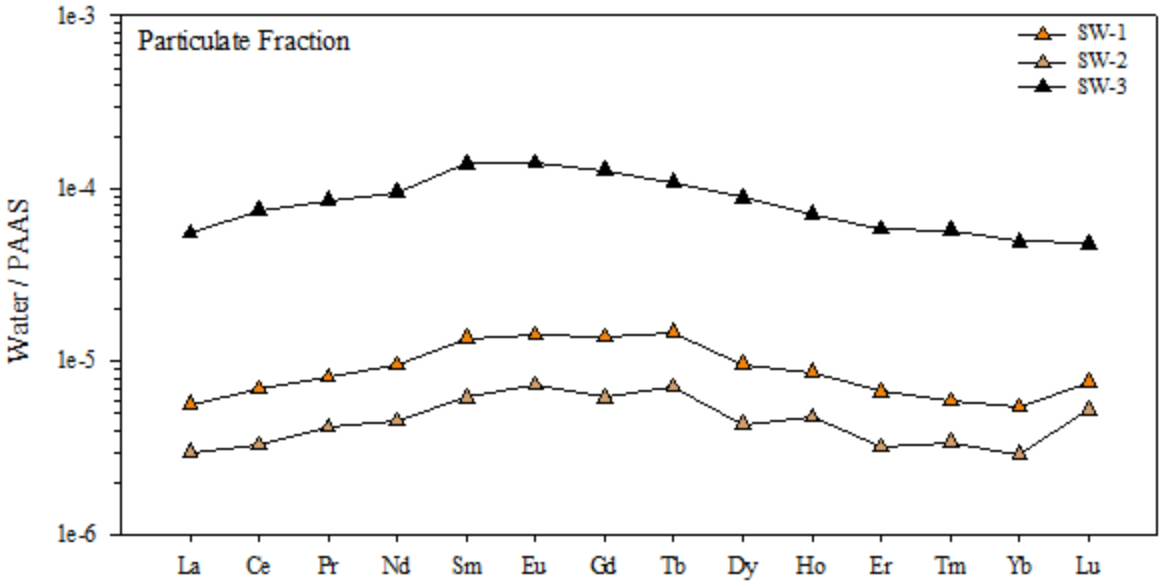

Figure 5.16 'Particulate only' fraction of shallow monitoring well REEs normalized to PAAS (Taylor & McLennan, 1985).

With the exception of Ho and Er, domestic wells Shepherd, Zehr and Becker show very similar dissolved HREE-enriched distribution patterns. The Eu anomalies for these three samples also appear to be similar in magnitude; however the Ce anomaly is negative to varying extents (Figure 5.12). Sample Ast shows a similar distribution pattern to that of the other domestic samples however with a more attenuated Ce anomaly and a greater positive Eu anomaly as well as a unique Dy depletion. Surface water samples Slate Creek 1 and Slate Creek 2 are located within the same tributary, with Slate Creek 1 downgradient from Slate Creek 2. In Figure 5.13, it is interesting to note differences between the two surface water dREE patterns, in particular the relatively-flat HREE-enriched pattern for Slate Creek 1 as opposed to the MREE-enriched pattern for Slate Creek 2. Furthermore, there is a prominent negative Ce anomaly within Slate Creek 1 whereas the Ce anomaly in Slate Creek 2 is almost nonexistent.

The saline shallow monitoring well samples showed distinct dREE distribution patterns relative to the lower TDS samples (Figure 5.15). The relatively-flat HREE distribution pattern is

a similar concept to that of the dREE Slate Creek 1 pattern. However, there is a notable negative Sm anomaly consistent across all shallow monitoring well samples with SW-2 showing a unique negative Tm anomaly. Furthermore, there appears to be no significant Ce or Eu anomaly, although SW-2 and SW-3 show slightly negative Ce anomalies. Relative abundances for the dREEs of the shallow monitoring wells also appear to be greater in magnitude than the domestic well samples but lower than that of the surface water samples.

The pREE fraction was analyzed for all samples to distinguish REE abundance differences that may be conducive to colloidal transport mechanisms. Certain REEs (Eu, Ho, Er) were detected at greater concentrations in the dissolved (filtered) phase than for the dissolved and particulate (unfiltered) phase for the domestic well samples (Figure G.1). This was primarily a result of the data nearing the instrument's detection limit. Therefore, the instrument was likely not capable of accurately quantifying these elements to such low concentrations. In general, the pREE distribution patterns for the domestic well samples are unique to one another (Figure G.1). The depletion-enrichment trends for samples Shepherd, Zehr and Becker are significantly prominent relative to sample Ast which shows a smoother REE pattern overall. The strong negative Pr and Yb anomalies in samples Becker and Zehr are likely a function of the data nearing the instrument's detection limit, therefore these patterns are not likely representative of actual conditions. The prominent La anomaly in Becker however is a valid unique occurrence. Surface water pREE patterns are different than that of the domestic water samples in that concentrations for both the filtered and unfiltered were high enough to where the detection limit issue is irrelevant. Therefore, the pREE surface water patterns are more complete and representative of actual conditions. Both Slate Creek 1 and Slate Creek 2 are similar in overall shape, showing strong enrichment in the MREE relative to the LREE and HREE, but significant

differences in absolute abundances, with Slate Creek 2 nearly an order of magnitude higher than Slate Creek 1. Both of the REE distribution patterns are relatively-flat with no prominent anomalies. Another notable observation is the complete dissimilarity of REE distribution patterns between the surface waters and domestic wells. With exception of sample Ast, the domestic wells appear to be significantly more influenced by mechanisms that control depletion-enrichment trends. In contrast, the shallow monitoring well REE distribution patterns are more similar to the surface water patterns than the domestic well samples. The pREE for SW-3 is nearly an order of magnitude greater than that of SW-1 and SW-2 which appears to be on the same order as Slate Creek 2. The shallow monitoring well samples also appear to have a Sm + MREE enrichment relative to LREE and HREE. Additionally, absolute REE abundances appear to decrease with depth.

5.6 Trace Elements

All samples, including Arbuckle and MIZ from Barker (2012), were analyzed for the same suite of trace elements via different analytical approaches (ICP-MS vs ICP-OES). Samples that are absent within a given graph were not plotted as a result of falling below the detection limit. Standard deviations relative to the mean of multiple analyses are represented as error bars and are shown where applicable; however, an absent standard deviation may imply either no duplicate was analyzed or the duplicate reproduced the first analysis within the sensitivity of the approach. Figure 5.17 and Figure 5.18 illustrate sample depth variation of 18 trace elements. Results of specific elements that are absent on the plots are not shown as they fell below the method detection limit and limit of quantitation. For a full numerical listing of trace metal values, see Appendix F.

The following elements were chosen for this research for the reason that they could be preferentially mobilized following water acidification. The large surface area of the clays within the aquifer sediments provides the means for significant trace element sorption to occur. Very few of the plots in Figure 5.17 show a trend with depth, the most notable exceptions being Rb, U and Li; Pb and Ba also show a slight correlation with depth, although not as prominent as the aforementioned elements. The increase in Rb concentration with depth is reminiscent of a similar trend with Ca (Figure 5.6). Li also increases with depth for the shallow domestic wells, but the pre-injection MIZ and the Arbuckle samples have significantly lower concentrations. Ba concentrations appear to be more evenly distributed within the 50-200 ft. interval than the shallower 25-50 ft. interval however at lower concentrations. Additionally, the presence of Al in the shallow wells versus the domestic and surface water samples does not seem to correlate well with any of the other trace elements. Arsenic appears higher in concentration in the surface water samples relative to shallow domestic and monitoring wells. However for post-injection MIZ, due to high error and poor standard deviation it is uncertain whether this portion of the Mississippian represents the high or low end of arsenic concentrations in the dataset.

Figure 5.18, similar to Figure 5.17, is arranged such that vertically adjacent elements bear some semblance of chemical similarities. The apparent flushing of Cu from pre- to post-injection samples SW-2, SW-3 and MIZ with a ubiquitous absence of Cu in all domestic and surface water samples is worth noting for an area high in agricultural activity. Within the domestic wells, Fe varies from 0 to 60.7 µg/L and 66.4 to 2594 µg/L for the shallow wells. Additionally, W and Mo are present in domestic well Ast at 1.5 and 12 µg/L, respectively. For more information on data accuracy, see Appendix F.

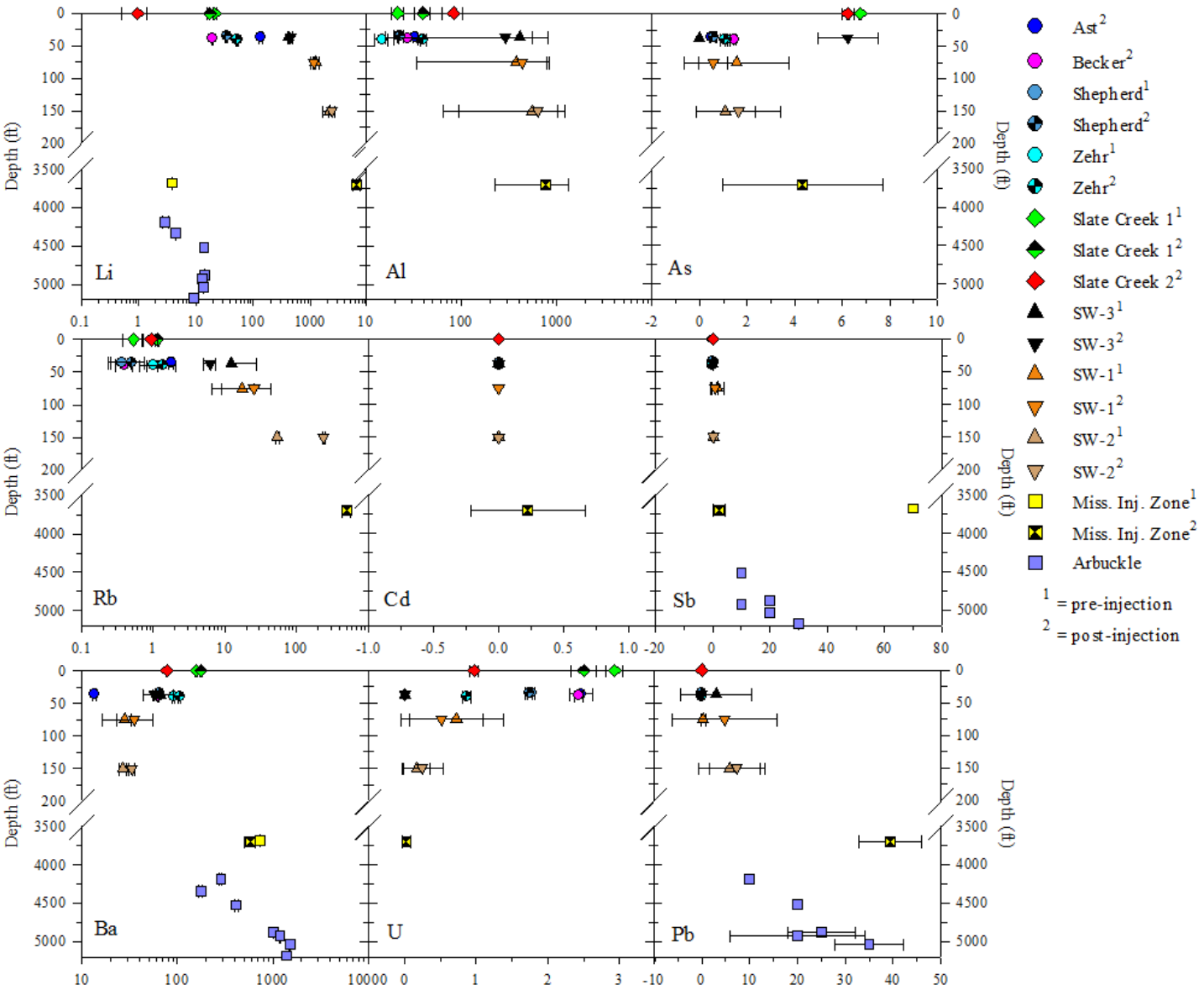

Figure 5.17 Trace metal variation as a function of depth in µg/L. Arbuckle values absent on graphs indicate they fell below detection limit. Zero values that could not be graphed due to a logarithmic scale are absent. All numerical values can be found in Appendix F.

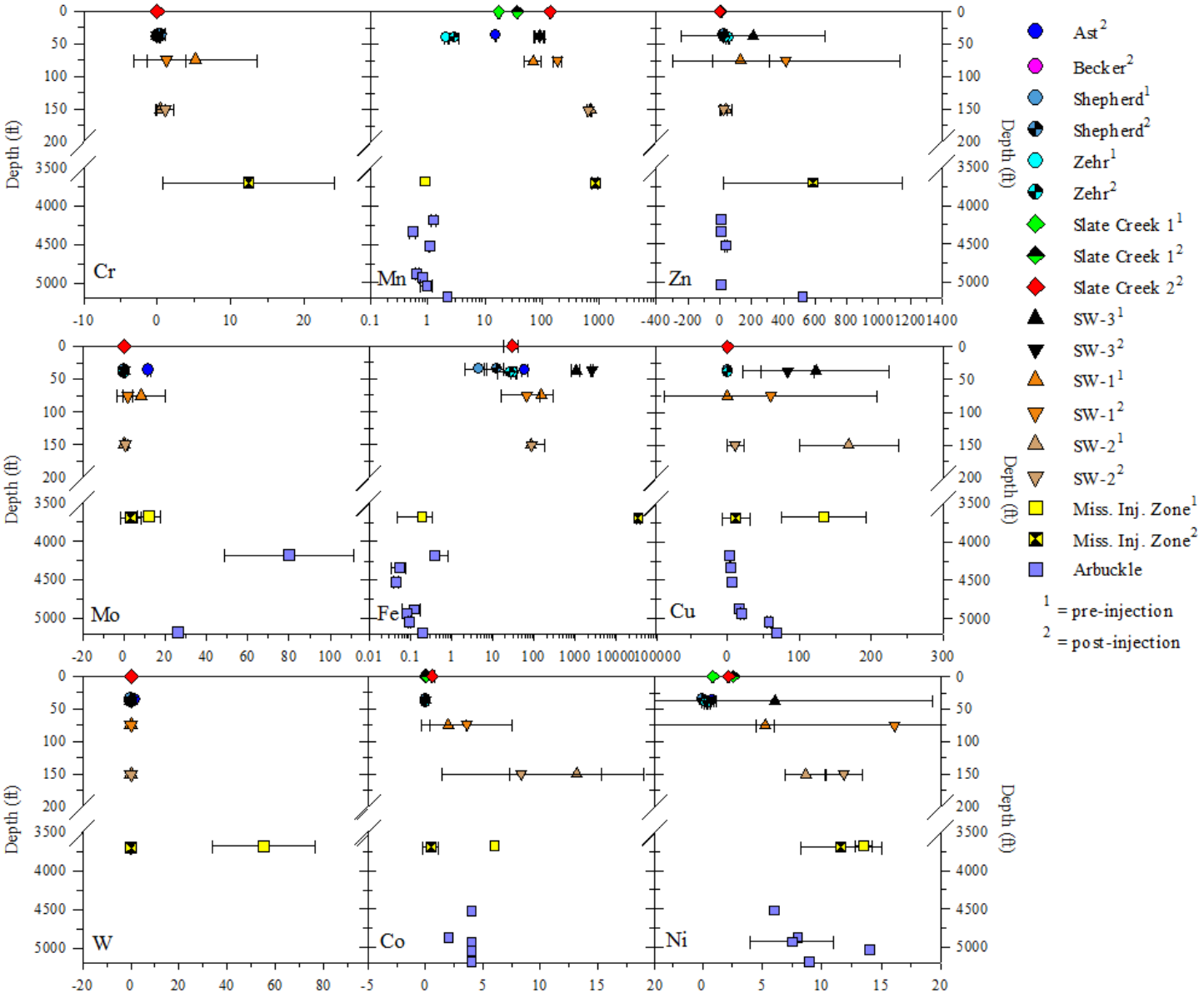

Figure 5.18 Trace metal variation as a function of depth in µg/L. Arbuckle values absent on graphs indicate they fell below detection limit. Zero values that could not be graphed due to a logarithmic scale are absent. All numerical values can be found in Appendix F

5.7 Geochemical Modeling

5.7.1 Speciation

Comprehensive geochemical investigation required the use of speciation to resolve dissolution/precipitation reactions that are occurring at each sample location at the time of sample collection. The program used for this model was Geochemist's Workbench (GWB) SpecE8 application. Major ions used in the reaction basis for all samples include Br, Cl, SO_4, HCO_3, K, Mg, Na, Sr with an assumed 1 free kg of water as the solvent. In addition to major ion chemistry, the model considered water quality conditions such as pH and specific conductivity at an assumed temperature of 25° C. Additionally, a thermodynamic dataset "thermo_minteq.tdat" was used to calculate the activity coefficients based on the method pursuant to Visual MINTEQ release 2.40.

For the following table and figures, a log Q/K value greater than zero indicates oversaturation or that formation of products is thermodynamically favorable, whereas a value less than zero indicates undersaturation or that product dissolution is favorable. The minerals that were most positive in magnitude (oversaturation) and common evaporite minerals in the speciation output were chosen to be represented. Samples were divided into three separate graphs according to their categorical representation (domestic wells, shallow monitoring wells, oil wells & surface waters) to improve resolution of each plot.

According to Table 5.3, the mineral that is most prominently oversaturated within the dataset is dolomite with a log Q/K range of 0.07 (SW-1) to 3.18 (Slate Creek 1). Coincidentally, sample Slate Creek 1 is also oversaturated to the greatest extent with respect to calcite, aragonite and magnesite. Additionally, it is interesting to note the absence of mineral oversaturation within

the pre-injection sample Shepherd while the post-injection sample precipitate dolomite, calcite, aragonite and magnesite. Evaporite minerals such as gypsum, anhydrite, halite and epsomite are all dissolving to varying extents within each water system. Pre-injection sample SW-3 appears to be oversaturated with respect to gypsum and anhydrite, while SW-1, SW-2, Ast and MIZ are close to oversaturation of evaporite minerals relative to the domestic wells. Plots of samples separated into their respective categories are shown in Figure 5.19, Figure 5.20 and Figure 5.21.

	Log Q/K							
[1]pre-injection [2]post-injection	Dolomite	Calcite	Aragonite	Magnesite	Gypsum	Anhydrite	Halite	Epsomite
Ast[2]	2.52	1.25	1.06	0.43	-0.11	-0.33	-5.19	-3.06
Becker[2]	2.49	1.10	0.91	0.55	-1.18	-1.40	-6.68	-3.85
Shepherd[1]	-0.34	-0.21	-0.39	-0.98	-0.93	-1.14	-5.52	-3.83
Shepherd[2]	2.09	1.01	0.83	0.24	-1.13	-1.35	-5.58	-4.04
Zehr[1]	--	--	--	-0.22	--	--	-5.35	-3.57
Zehr[2]	2.50	1.16	0.97	0.50	-1.19	-1.40	-5.45	-3.97
Slate Creek 1[1]	--	--	--	-0.04	--	--	-6.57	-3.89
Slate Creek 1[2]	3.18	1.74	1.55	1.13	-1.56	-1.78	-6.95	-4.29
Slate Creek 2[2]	2.59	1.26	1.07	0.49	-3.03	-3.25	-8.93	-5.93
SW-1[1]	0.07	-0.29	-0.47	-0.48	-0.07	-0.26	-1.98	-2.47
SW-1[2]	2.38	0.79	0.60	0.75	-0.27	-0.46	-2.00	-2.51
SW-2[1]	-0.22	-0.86	-1.05	-0.20	-0.09	-0.10	-0.19	-2.07
SW-2[2]	-0.54	-0.92	-1.11	-0.46	-0.10	-0.14	-0.37	-2.21
SW-3[1]	--	--	--	--	-0.10	-0.31	-3.20	-3.06
SW-3[1]	1.36	0.64	0.46	-0.13	-0.06	-0.26	-2.94	-2.98
SW-3[1]	0.17	0.05	-0.13	-0.72	0.22	0.01	-2.87	-2.72
SW-3[2]	2.54	1.18	0.99	0.52	-0.23	-0.44	-2.85	-3.05
MIZ[1]	--	--	--	--	-0.15	-0.25	-0.77	-3.58
MIZ[2]	--	--	--	--	-0.41	-0.51	-0.85	-3.69

Table 5.3 Log Q/K values from GWB speciation calculations of major ions. Green values indicate oversaturation of specified mineral whereas red values indicate undersaturation. Dashes indicate those minerals were not detected in the system due to an absence of specific ions that could not be analyzed for that sample. The first two SW-3[1] samples were collected and analyzed by the KGS whereas the MIZ[1] was collected and analyzed by Barker (2012).

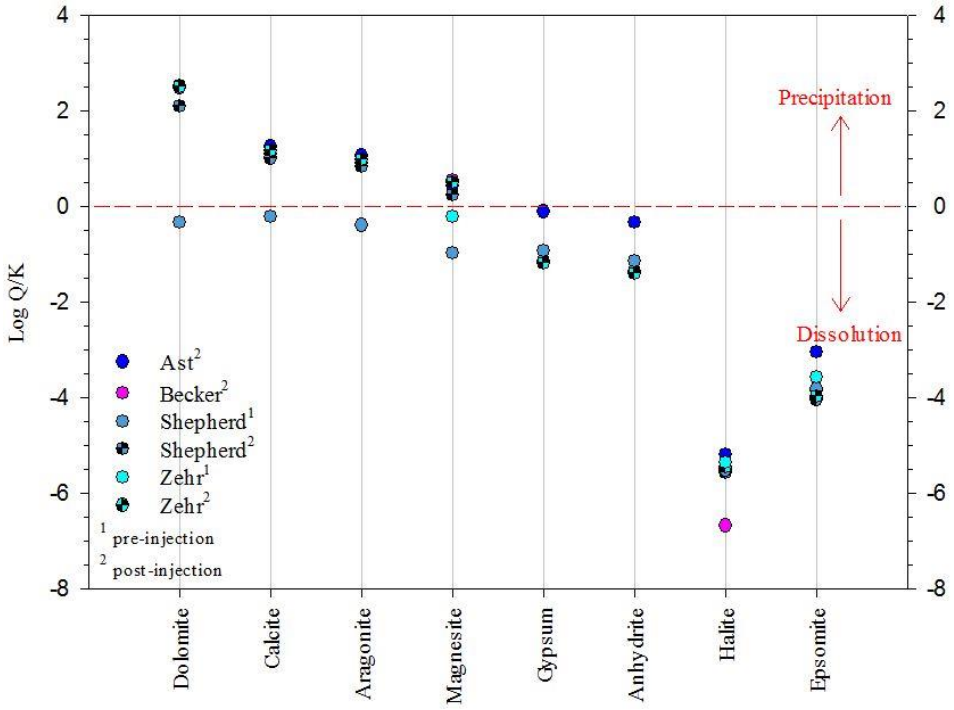

Figure 5.19 Scatter plot of log Q/K values for domestic wells in relation to prevalent minerals found throughout the entire system as speciated by GWB.

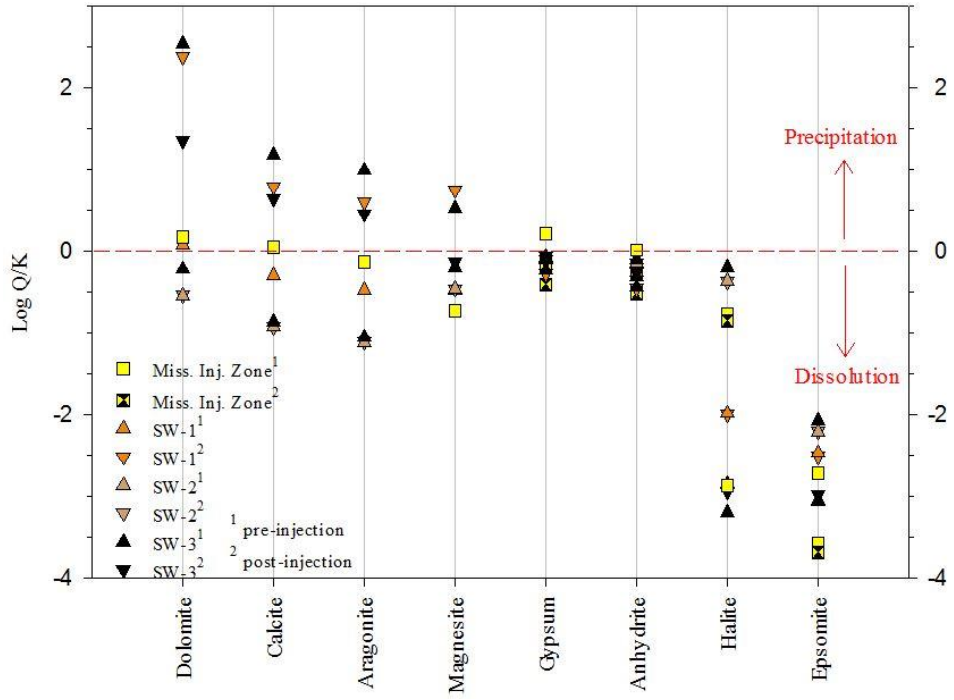

Figure 5.20 Scatter plot of log Q/K values for shallow monitoring wells in relation to prevalent minerals found throughout the entire system as speciated by GWB.

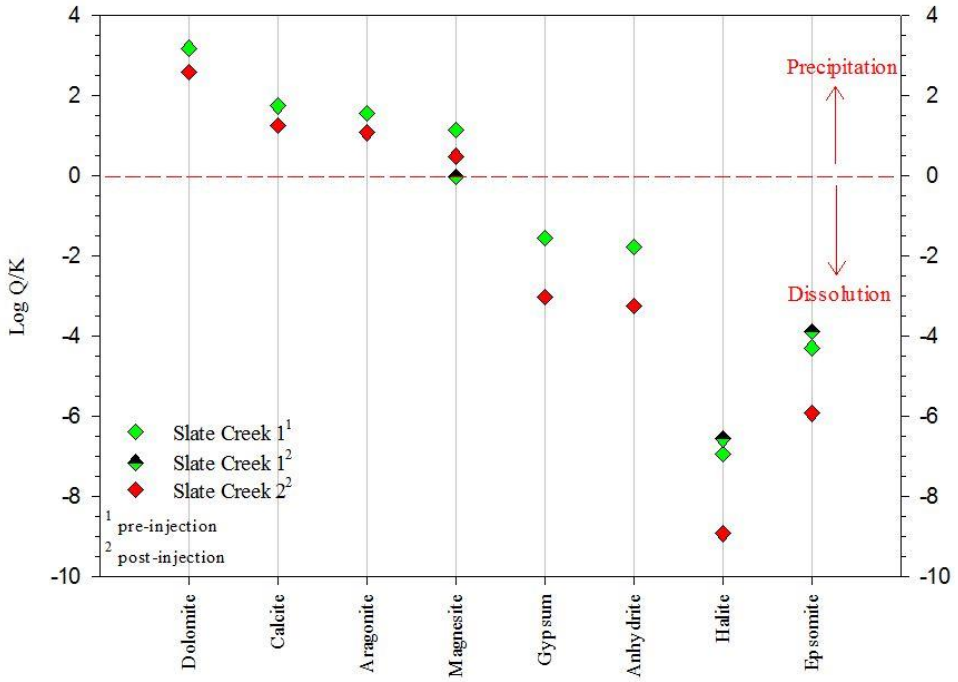

Figure 5.21 Scatter plot of log Q/K values for surface water samples in relation to prevalent minerals found throughout the entire system as speciated by GWB.

Chapter 6 - Discussion

6.1 Water-Rock Interaction

This study collected and analyzed a number of water samples of varying depths for a variety of geochemical parameters in an attempt to use conservative ions as proxies for water tracing. Major ion chemistry within the study site is mostly impacted by the presence of evaporite deposits and other mechanisms of Cl release. Shallow samples Shepherd, Becker, Zehr, Ast, SW-1, SW-2 & SW-3 are all screened within the Permian Wellington Shale Formation. However, saltwater intrusion from natural and anthropogenic sources has produced a large salinity gradient that increases NE with depth and inversely with bedrock elevation (Figure 3.7 and Figure 5.4).

Hydrochemical facies vary throughout the shallow aquifer, with all shallow monitoring wells on the paleoterrace showing a consistent Na-Cl type indicating significant influence from localized halite dissolution of evaporite deposits (Figure 5.5). Shepherd shows a consistent Ca-Cl composition and Zehr shows a shift from Mg-Cl to Ca-Cl, whereas samples Ast and Becker are a Na-SO_4 and Mg-HCO_3 type, respectively. The significantly lower concentrations of Na and Cl in Shepherd and Zehr indicate that halite has less of a control on shallow aquifer geochemistry in the paleovalley than on the paleoterrace. The predominance of Ca and Mg over Na in these chemistries suggests that minerals containing these ions are exchanging/weathering and/or present to a greater extent than halite. Speciation models seem to suggest that carbonates represent a major control on post-injection Shepherd and Zehr compositions which vindicates the origin of Ca and Mg from carbonate deposits. However, the simultaneous dominance of the Cl ion may indicate the Mg and Ca ion are related to an associated Cl deposit such as apatite or

bischofite, but this is not supported by the speciation model as these minerals would be closer to equilibrium in the output.

As previously established by Watney et al. (2015), concomitant changes in overburden sediments and bedrock elevation appear to have developed an elevated platform (paleoterrace) overlooking a channelized paleovalley within the study site. This interpretation may explain some of the observations of this study in terms of water yields from various wells (see Appendix A). For example, the relatively high groundwater yields from SW-3, Zehr and Shepherd do not correlate well with water yields typical of shale in Kansas, e.g. 0.5-5 GPM (O'Connor, 1971). Becker is screened almost entirely within the Quaternary sandy sediments, yet still has a lower yield than Zehr, which is screened entirely within the Permian Shale. This suggests that there could be secondary porosity contributing to faster recharge within this area. The erosion of the bedrock during formation of the paleovalley in the Quaternary could have led to bedrock scouring and subsequent development of bedrock channels as a result of extensive dissolution of preexisting evaporite deposits; this, in turn, could have produced secondary porosity and the observed yield differences (Richardson & Carling, 2007).

Monitoring well SW-3 has a higher yield than SW-1 and SW-2, with lower TDS, suggesting that recharge may be infiltrating through a sandy portion of the paleoterrace, such as the sediments just above SW-1. The flow could then proceed along bedrock planes into SW-3 at a rate similar to that of the domestic wells. Wells screened within the paleoterrace, namely SW-1, SW-2, SW-3 and Ast, may not have developed secondary porosity from erosion similar to wells screened within the paleovalley which led to greater TDS from higher pore-space water residence time and prolonged water-rock interaction.

The abnormally elevated presence of SO_4 in Ast may be due to oxidation of sulfur possibly from local pyrite deposits, as shown by high Fe (60 µg/L) and DOC (1.5 mg/L) as well as lower DO and nitrate values with respect to the other shallow groundwater wells. However, the prominence of evaporite deposits within the region provides an alternative argument for the dissolution of sulfate-bearing minerals such as gypsum, anhydrite or mirabilite. Furthermore, the possibility of contamination via oilfield brine intrusion is possible, as hydrogen sulfide oxidation could produce similarly substantial sulfate concentrations that may have migrated from the release site. It is also possible that weathering of gypsum deposits led to an increase in SO_4 values but Ca was precipitated or exchanged, therefore fractionating the dissolved chemistry. Becker contains the lowest TDS of all samples (1,070 mg/L; Cl < 100 mg/L), and is unique relative to the other wells in the study area as it screens 27 feet of sand and silt in the paleovalley with only 5 feet of screen into the Permian Shale. Therefore, this well likely contains almost exclusively groundwater contained within the Quaternary USDW.

Over saturation of dolomite, calcite, aragonite and magnesite within speciation models of all samples—with the exception of SW-2, MIZ and pre-injection Shepherd—foretell a ubiquity of carbonate precipitation. This is likely due to the strong presence of bicarbonate and associated major ions relative to other ions. The systematic increase in Mg/Ca ratios from the shallowest to deepest paleoterrace monitoring well may indicate increasing dedolomitization with depth (Szramek et al., 2007; Meister et al., 2011). Diagenetic effects of dedolomitization and replacement by calcite has been shown to reduce porosity (Shearman et al., 1961; Selley, 2000). This would enhance water-rock interaction of the deeper monitoring wells through a reduction in effective porosity.

Carbonate influence on geochemistry is also evidenced by $\delta^{13}C$ DIC values among shallow samples SW-1, SW-2 & SW-3 as well as the MIZ. ^{13}C-depleted values of SW-3 (-7.06 to -9.4 ‰) and SW-2 (-7.63 to -8.7‰) relative to SW-1 (0.065 to -6.9‰) may potentially highlight the importance of diagenetic effects on DIC and geochemistry. According to Kendall et al. (1995), $\delta^{13}C$ DIC in subsurface waters typically range -5 to -25‰ and are mostly affected by weathering of silicate and carbonate minerals and CO_2 dissolution. The negative ^{13}C excursion observed within the shallow paleoterrace monitoring well samples may be explained by carbonate precipitation or oxidation of biogenically-derived methane (van Breugel et al., 2006; Kendall et al., 1995). Carbonate speciation from HCO_3 to CO_3, as well as a concomitant increase in pH, also serve as isotopologues for $\delta^{13}C$ DIC, resulting in a decreasing value but favoring carbonate precipitation. The systematic negative excursion observed for all monitoring wells is an indication that carbonate precipitation may have increased between sampling events. These interpretations are supported by the apparent closed-system dynamics within the deeper monitoring wells as shown by poor hydraulic conductivity and relative $\delta^{18}O$-$\delta^{2}H$ plot placement. A low-flowing and vertically restrictive hydraulic system would eliminate the ambiguity of other contributing sources more so than samples from wells with higher yields. It is speculated that diagenetic factors as well as C-speciation between CO_2 and HCO_3 are the main influence on Ca-Mg and $\delta^{13}C$ DIC variation.

6.2 Isotopic Tracing

Stable isotopes of $\delta^{2}H$ and $\delta^{18}O$ were employed to investigate their potential for tracing water movement. Unfortunately, there are limited stable isotope data available in the literature against which to compare our data for ground and surface water from south-central Kansas. Nonetheless, our data for $\delta^{2}H$ v $\delta^{18}O$ reveal a shifting LMWL over time as shown by deviations

of deeper Arbuckle and Mississippian as well as shallower Permian values from the current LMWL. This shift may be explained by changes to climate or geographic position, particularly depending on the sample's proximity to large bodies of water at time of deposition (Sharp, 2007; Kendall et al., 1995). Typically, continental $\delta^{2}H$ and $\delta^{18}O$ will be isotopically lighter than coastal values due to progressive fractionation of the heavier counterparts during air mass movement (Kendall et al., 1995; Jouzel et al., 1994). The ^{18}O-enriched and ^{2}H-depleted values of sample SW-1 (50-100 ft.) relative to SW-2 (100-200 ft.) may indicate hydraulic separation between these zones. Pre- and post-injection values of SW-1 (50-100 ft.) and SW-2 (100-200 ft.) are precise and distinct from one another, indicating very little, if any, mixing is occurring between these zones. This apparent isolation establishes the impermeability of the shale at this depth. The ^{18}O and ^{2}H enrichment of SW-3 (25-50 ft.), relative to SW-1 and SW-2, and its overlap with the domestic wells within proximity of the LMWL and surface water samples is evidence that similarly fractionated water is recharging the shallow aquifer (20-60 ft.). In other words, isotopically fractionated water of similar composition to that of the domestic wells in the paleovalley permeated through the paleoterrace sediments to SW-3 and Ast at the time of sampling. The isotopic time series change of sample SW-3 also shows a trend that is similar to that of the MIZ, both of which plot along a similar regression line suggesting a geochemical connection between the two samples. The change to more depleted isotopic compositions for the post-injection relative to pre-injection MIZ samples may not be due to a temporal change however, given that the two samples are from different locations. The pre-injection MIZ sample was collected from KGS 1-32, 0.34 mi. northwest of KGS 2-32 where the post-injection MIZ sample was collected. Deeper Arbuckle samples span a wide range, e.g. -7 to -2 for $\delta^{18}O$ (Figure 5.9). As discussed by Barker (2012), this suggests little vertical communication between sample

zones. It is possible that during inundation of the interior seaway, these waters were trapped in the pore spaces and retained a historic LMWL. To this effect and following deposition in the late Permian, impermeable sediments precluded recharge within the vicinity of samples SW-1 and SW-2 thereby retaining connate water in the pore spaces and also preserving a historic LMWL. Groundwater flow throughout this portion of the formation is likely reduced relative to other sample locations, possibly due to tighter lithology and progressive secondary mineralization. The result is retention and prolonged water-rock interaction with nearby evaporite deposits owing to higher TDS in these wells in relation to shallower wells.

The shallow (20-60 ft.) interval isotopic deviation from the LMWL may also be a function of normal atmospheric locality differences where LMWL samples were collected. It is possible that the isotopic composition of meteoric water in Wellington is different than that of Konza Prairie which would have an effect on recharge interpretations. Notably, samples Zehr and Ast are screened entirely within the Permian Shale, whereas samples Shepherd and Becker are screened 15-27 ft. within the Quaternary deposits and seated 5-9 ft. into the Permian Shale. Regardless of LMWL position, the $\delta^{18}O$-$\delta^{2}H$ positioning suggests good hydraulic communication between the two geologic layers, as previously expressed could be due to solution veining or bedrock channeling from erosional processes (Whittemore, 1993).

There is also the possibility that CO_2-EOR activities have influenced the stable isotopic composition for the MIZ, yielding isotopically lighter fluid. Based on stable isotopic data, there is little evidence to suggest mixing is occurring between deep and shallow samples, other than for sample SW-3.

6.3 Major Ion Tracing

Major ionic mixing relationships among Br/Cl, SO_4/Cl, Na/Cl and (Ca+Mg)/Na serve as some of the most informative proxies for identification and differentiation of salinity sources (Whittemore, 1995; Whittemore, 1993; Freeman, 2007). In this section, we use methods outlined in Whittemore (1995; 2007) to show freshwater-evaporite-oilfield brine mixing trends in an effort to elucidate migration pathways. Chloride and bromide are typically used as conservative tracers in water mixing studies due to their high solubility and resistance to oxidation-reduction reactions (Whittemore, 1995). As seawater evaporates and NaCl crystals begin to form, Br is preferably enriched in the residual brine, although small amounts are admitted into precipitating phases; Br does not form independent minerals in evaporite environments, so it remains greatly enriched in the brine (Whittemore, 1995; Freeman, 2007). Differences in Br-brine enrichment within different saline sources allows for the use of Br/Cl ratios as a means for differentiating these sources.

Figure 2.3 was originally published in Whittemore (1995). It identifies an evaporite dissolution mixing zone through mass balance calculations of low and high Cl relative to Br/Cl from a network of 52 observation well nests screened in Quaternary sediments and the Permian bedrock of south-central Kansas. Whittemore (1995) found that the majority of the wells fell within the extents of the halite-dissolution mixing zone however points that plotted above the mixing zone were interpreted to be mixing with other salinity sources. Endpoint mixing curves between oilfield and freshwater-halite dissolution brine signatures intercepted the points to reveal potential variations in endmember composition. This study borrowed previously calculated halite-dissolution mixing zone delineations from Whittemore (1995) and imposed our data for comparison (Figure 6.1). Dashed lines in the following figure were not calculated, but

rather estimated based on endpoint location of the MIZ samples, curve for freshwater-halite dissolution mixing and the samples in between.

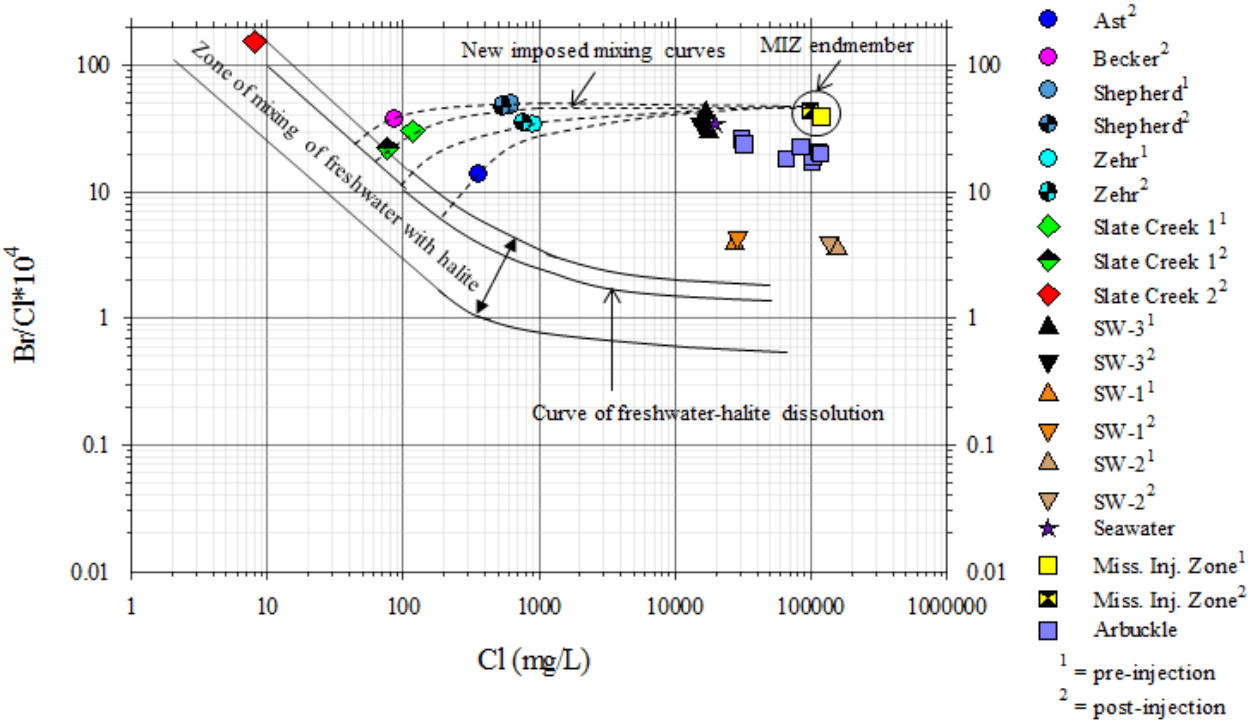

Figure 6.1 Br/Cl diagram constituting the limits of the freshwater-halite dissolution mixing zone as calculated by Whittemore (1995) juxtaposed with samples collected from this study of similar depths and location from the aforementioned publication. Imposed mixing curves were interpolated based on location of MIZ endmembers, points above the mixing zone extents and the curve for freshwater-halite dissolution.

Based on the relative location of our samples and the mixing curves from Whittemore (1995), all samples with exception of post-injection Slate Creek 1 and Slate Creek 2, plot outside of the freshwater-halite zone of mixing. Chloride additions to these samples may possibly be a function of agricultural cross contamination. Typical background nitrate values within shallow aquifer and bedrock settings are below 2 mg/L (Whittemore, 1993). Nitrate values from our study, as indicated by major ion chromatography, for all domestic wells with exception of Ast ranged 9.9 to 26.7 mg/L for both pre- and post-injection indicating higher than normal

concentrations. Furthermore, ammonium concentrations (see Appendix C), which typically are elevated in reducing settings particularly within bedrock, was found to range below detection (< 0.015 mg/L) to 0.033 mg/L within the domestic wells. Supported by this evidence, there is currently the possibility for elevated chloride levels to be related to agricultural influence from either concentrated irrigation water and/or presence of evapotranspiration concentration deposits within the shallow soil profile. However, nitrate values within SW-3 fell below detection with higher ammonium concentrations in the range of 0.41 to 0.63 mg/L. The Br/Cl diagram with imposed mixing curves struggles to differentiate elevated chloride levels as a function of irrigation activity and oilfield brine mixing. It is possible that the location of the freshwater-halite dissolution mixing curve on the Br/Cl diagram may be more site-specific and that the geographic difference between sample locations from original publication to our study results in different boundary extents. It is also possible that differences in analytical techniques and uncertainty as well as sample collection procedures between studies may also contribute to curve shift on the diagram. To further this, there currently appears to be development of a curve similar in slope to that of Whittemore (1995) that is composed of samples collected from this study just above the freshwater-halite dissolution mixing zone extents (Figure 6.2).

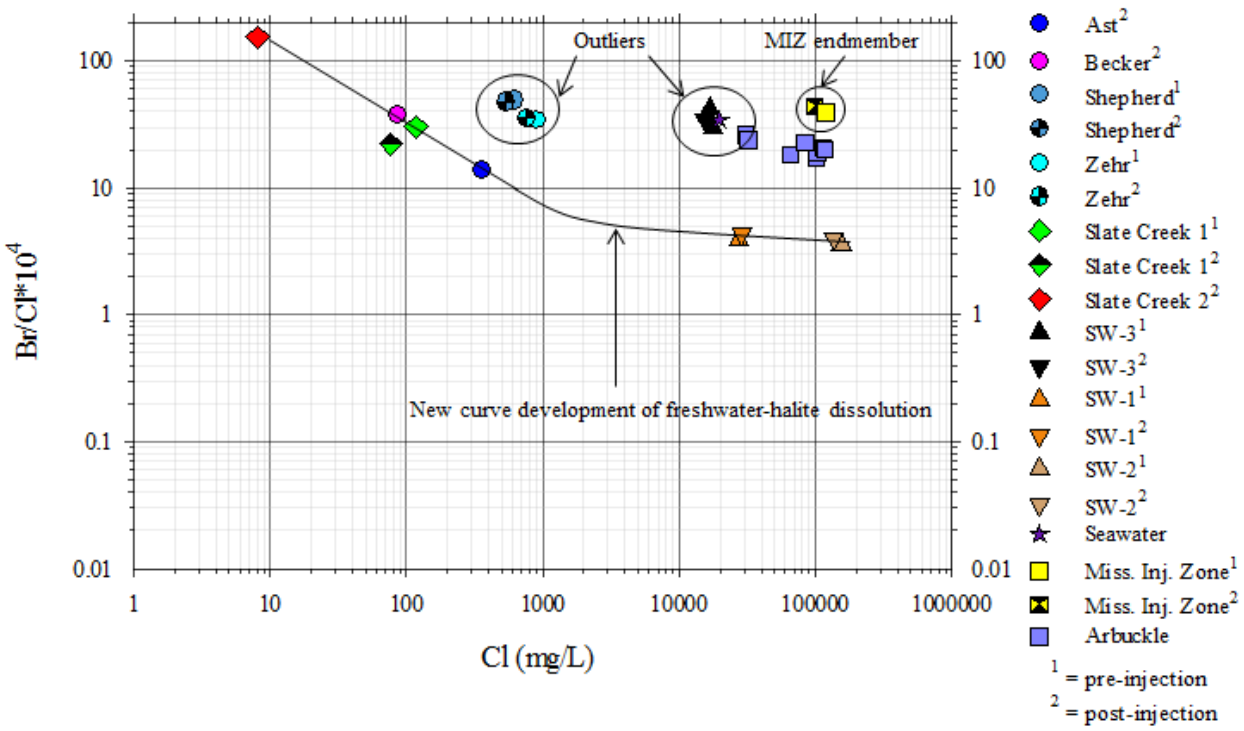

Figure 6.2 Suggested freshwater-halite dissolution curve shift for our Wellington samples. This curve was not calculated, but rather estimated and assumes chloride contributions within all shallow samples with exception of Shepherd, Zehr and SW-3 are a result of natural evaporite dissolution.

Figure 6.2 suggests a curve shift which would encompass all samples with the exception of apparent outliers Shepherd, Zehr and SW-3. This development is supported by SO_4/Cl, (Ca+Mg)/Na and Na/Cl values which shows that SW-2 and SW-1, in particular, appear to be purely influenced by evaporite, more specifically, halite deposits. Additionally, stable isotope signatures from the deeper monitoring wells in the paleoterrace show preclusion to hydraulic influence from shallower intervals indicating near-surface salinity releases would not likely impact these wells. The origin of sulfate in sample Ast also suggests local equilibrium with evaporite deposits and/or oxidation of sulfur; coupled with low evidence of outside chloride additions, it is not indicated that Ast geochemistry is influenced by irrigation or oilfield mixing. The higher than expected nitrate concentrations within Ast may simply be fortuitous through

bedrock oxidation of ammonium to nitrate (Whittemore, 1993). This suggested curve shift would be more suitable to address salinity source differentiation as supported by other geochemical evidence although further work is required in the form of further sample collection and mass balance calculation.

Major ionic evidence supported by SO_4/Cl plots show that oilfield brine-mixed samples tend to fall along a general mixing trend projected from the target oilfield brine signature (Figure 6.3) (Whittemore, 1995). SO_4/Cl ratios for typical oilfield brines fall below 0.01, whereas evaporite dissolution brines from Permian Shales in Kansas are higher for a given Cl concentration, ranging from 0.1 to 0.2 (Whittemore, 1995).

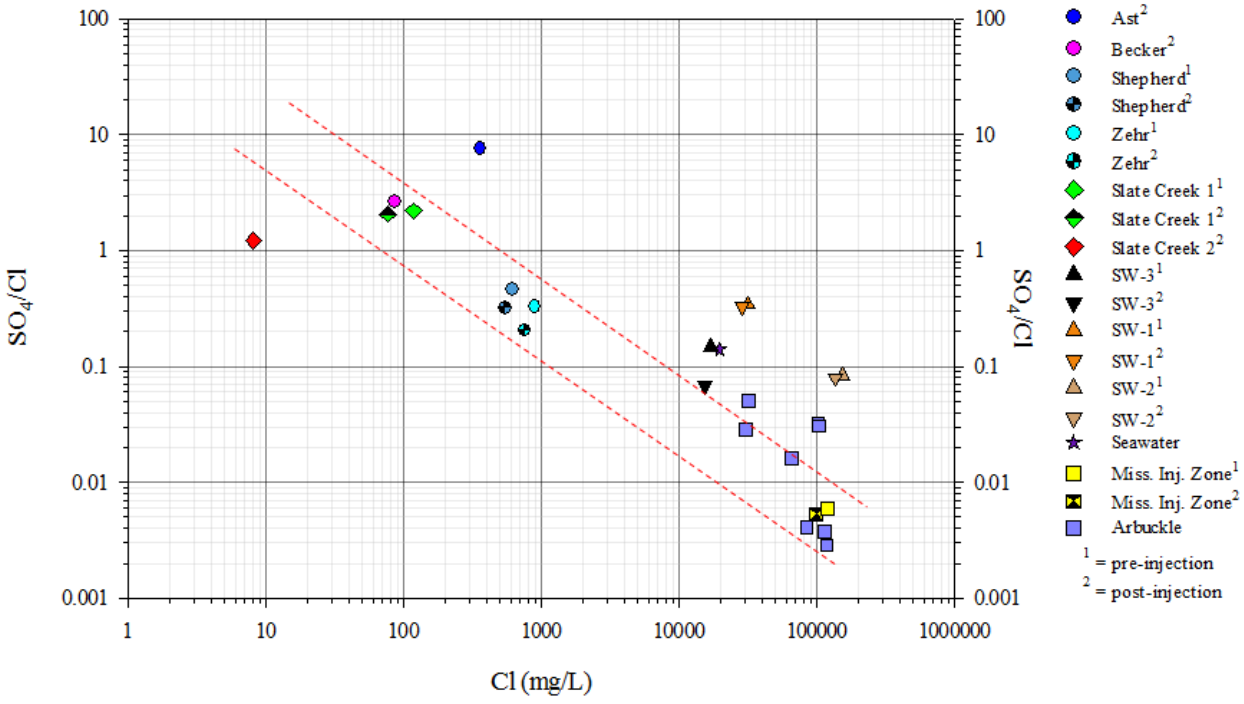

Figure 6.3 Possible zone of influence as inferred from Whittemore (1995) to show salinity contamination on the basis of SO_4-Cl mass ratios where MIZ samples are used as the source.

The result is an inclusion of samples Shepherd, Zehr, Slate Creek 1 with a progressive deviation within shallow monitoring well samples. Ratios such as Na/Cl and (Ca+Mg)/Na also

have implications for oilfield brine mixing, due to the general hardening of water from desorption of ion exchange sites on freshwater aquifer surfaces during plume sweeps (Whittemore, 1995). Typical Na/Cl ratios of oilfield brines in Kansas range from 0.4 to 0.6 and about 0.65 for halite solutions in the upper portions of the Wellington Shale (Whittemore & Hathaway, 1983). Na/Cl evidence suggests there may be oilfield brine mixing with these waters based on lower than normal values (0.24 to 0.62); however, sample Na/Cl mass ratios with potentially high residence time can be difficult to decipher due to possible equilibration with secondary minerals; the ratio can also be depressed due to adsorption onto clay sites in freshwater portions of the aquifer (Beaucaire et al., 1999; Whittemore & Hathaway, 1983). Mass ratios of (Ca+Mg)/Na are cited as being influenced by oilfield brine if they are elevated with respect to the signature of the source. In this case, the MIZ was detected to have a signature of 0.20, whereas samples Ast, Becker, Shepherd, Zehr, Slate Creek 1, Slate Creek 2 and SW-3 had higher ratios (Figure 5.7). Samples SW-1 and SW-2 had considerably lower (Ca+Mg)/Na and higher Na/Cl ratio values, indicating there has been no recent brine plume migration through this portion of the bedrock that contained a signature similar to that of the MIZ. Samples Shepherd, Zehr, and SW-3 however contain elevated (Ca+Mg)/Na mass ratios and lower Na/Cl ratios relative to the MIZ, which may suggest recent salt plume activity. Sample Becker has the lowest (Ca+Mg)/Na of the domestic wells accompanied by the lowest TDS which is speculated to be the result of its location within the arkosic paleovalley.

Based on groundwater flow direction, position of the affected wells and the above geochemical evidence, there may be hydraulic connection between the paleovalley and the paleoterrace linking SW-3 and Shepherd/Zehr sample intervals. This would be true if the salinity signal is confirmed to be oilfield brine from the Mississippian among these three samples.

However, the obscurity between elevated chloride levels with respect to concentrated irrigation and oilfield brine within these samples prohibits confidence in this interpretation. The generally coarser sediments that overlie these wells in relation to the paleoterrace wells coupled with evidence for secondary porosity in the bedrock and decent hydraulic communication would allow for increased mobility of a downward-migrating plume. The origin of methane within SW-3 is still debated. However, due to correlation with Br/Cl, Na/Cl and (Ca+Mg)/Na, as well as stable isotopic signatures with Mississippian samples, it is possible that a surficial hydrocarbon release from a nearby oil well or preexisting salt pit leaked into the vicinity of SW-3 (Whittemore, personal communication, 2016). Arguments for methanogenesis within SW-3 are also valid, as shown through the abnormally high concentration of DOC in SW-3. Oxidation of C within various organic molecules in the absence of oxygen would result in the production of methane and CO_2 ($CH_3COOH^- \rightarrow CH_4 + CO_2$) (Thauer, 1998). However evidence of reducing ORP and normal range DO values indicate that oxygen would be the terminal electron acceptor and methanogens could not compete in an aerobic environment, as indicated by favorable free energies (Park et al., 2006). Further work tailored to this specific discussion would be required for a more in depth analysis of potential methanogenesis within water wells of the study site.

6.4 REE Tracing

To further investigate the use of geotracers as a proxy to interpreting groundwater flow and source relation, dREEs were employed to understand the differences in inherent fingerprints left by the water-rock interaction. The distribution patterns of normalized dREE can provide significant detail into lithologic source tracing (Verplanck et al., 1999). REE concentrations in shale and clayey sediments are often higher than in other sedimentary rocks due to the higher amount of sorption sites (Grauch & Mariano, 2008; Papangelakis & Moldoveanu, 2014; Aide &

Aide, 2012). It is therefore indicated that REE distribution patterns are heavily influenced through water-rock interaction of the shale bedrock. In the following discussion, LREE is referred to elements La-Eu whereas HREE are Gd-Lu (Aide & Aide, 2012).

Domestic well and surface water samples were analyzed for dissolved REEs (dREE) and particulate REEs (pREE) to understand REE abundance fractionation as a function of solution complexation. In general, the domestic wells Shepherd, Zehr and Becker exhibited similar patterns for the dREE indicating similar lithologic origins. The pREE patterns for Shepherd, Zehr and Becker are characterized by their excessive depletion-enrichment trends which may be a function of sensitivity of the analysis, as discussed in section 5.5. The dissolved fraction for Sample Ast is similar to the dissolved fractions for the other domestic wells, however with a significantly larger positive Eu anomaly, negative Dy anomaly and an attenuated negative Ce anomaly.

Shallow monitoring well dREE patterns are different from that of domestic and surface water samples as they are flatter and do not have obvious Eu anomalies. Furthermore, the magnitudes of the REE abundances of the shallow monitoring wells are greater than that of all of the domestic wells, but not appreciably. This may suggest that the ligand responsible for mobilizing the dREEs in this setting is not vastly higher in concentration therefore potentially precluding the Cl ion as a major transporting agent. In general, the dREEs of all the shallow monitoring wells are similar to one another with the exception of a few minor anomalies, specifically the Tm-depletion in SW-2 and Sm-depletion in SW-1. The distribution patterns seem to suggest lithologic similarities among these sample locations that are not present in the domestic or surface water sample locations. It is likely that the mechanism which is controlling the Eu anomaly that is present within the domestic dREEs is not present at the shallow

monitoring well sample intervals. The pREEs for the shallow monitoring wells are also different than that of the domestic samples, although there is a faint resemblance with the surface water samples particularly with the prominent MREE-enrichment. Grawunder et al. (2014) cites MREE-enrichment to possibly be a function of S oxidation products, namely through pyrite oxidation in acid mine drainage settings. This MREE-enrichment however only appears to be present in the pREE pattern and is virtually nonexistent in the dREE pattern which is not supportive of this interpretation.

Surface water samples Slate Creek 1 and Slate Creek 2 show similar pREE patterns, although Slate Creek 2 has nearly an order of magnitude higher REE abundances than Slate Creek 1. For the dREE, Slate Creek 2 also has significantly higher LREE relative to Slate Creek 1, but the HREE tend to converge for the two samples, so that Lu for Slate Creek 2 is only about a factor of 2 higher than Slate Creek 1. It is possible that stream conditions following the heavy rain event during Slate Creek 2 sample collection influenced the geochemistry such that runoff inflated the REEs. However Slate Creek 1 just downgradient from Slate Creek 2 was sampled at a similar time but did not exhibit similar results. It is therefore inconclusive whether dissolved phase Slate Creek 2 is naturally distinct from Slate Creek 1 without additional sampling. An influx of clay particles (< 0.45 μm in size) would certainly enhance REE abundance in the dissolved phase lending the potential for significant surface area charge. The surface water sample pREE distribution patterns do not appear to correlate well with that of the domestic samples, indicating pREE fractionation is sensitive to small locality and hydraulic setting changes. Additionally, pREE/dREE ratios of each sample (Table 6.1) show that Slate Creek 1, in contrast to Slate Creek 2, steadily declines in ratio from LREE-HREE indicating LREE-depletion in dREE in relation to pREE and HREE-depletion in pREE in relation to dREE.

However, surficial conditions controlling REE distribution differs from groundwater in that flora and their root network may have more of an impact on initial REE influence. The table below illustrates significant pREE/dREE differences in SW-1 relative to the other samples. This information indicates that some mechanism in the pREE geochemistry for SW-1 is responsible for major REE abundance contribution; in particular, Sm and Eu have very high ratios. Sample SW-3, in contrast, exhibit much lower consistent pREE/dREE abundances indicating particulates represent less of a control on this geochemistry.

ID	LREE						HREE								∑REE
	La	Ce	Pr	Nd	Sm	Eu	Gd	Tb	Dy	Ho	Er	Tm	Yb	Lu	
SW-1	54.52	92.98	89.80	91.73	161.47	153.24	105.53	86.30	62.85	61.92	51.04	53.62	49.88	36.11	79.17
SW-2	7.97	11.75	13.44	14.41	23.67	18.17	16.85	17.30	12.50	11.49	10.11	9.62	9.37	8.77	13.27
SW-3	2.98	4.03	4.62	4.42	7.09	7.53	5.43	5.40	3.28	3.97	2.60	3.83	2.80	4.27	4.387
Slate Creek 1	17.09	24.59	17.95	16.17	14.19	11.04	12.34	10.90	9.14	7.03	6.34	6.38	6.38	5.67	10.17
Slate Creek 2	15.17	16.58	14.13	14.32	14.15	11.86	14.95	14.71	14.69	14.65	14.39	15.38	14.85	14.59	14.39
Ast	2.09	4.22	3.01	3.25	3.10	-0.33	2.80	1.74	2.31	1.38	1.43	1.71	1.69	1.57	1.46
Becker	6.84	4.16	0.03	0.27	0.95	0.68	0.51	0.34	1.09	-0.29	0.14	0.17	0.09	-0.10	0.64
Shepherd	0.34	1.52	0.23	0.29	0.39	0.22	0.57	0.36	0.74	0.27	0.32	0.41	0.41	0.34	0.41
Zehr	0.47	0.74	0.75	0.93	1.21	1.33	0.58	0.75	0.60	-0.07	-0.10	0.06	0.00	-0.10	0.47

Table 6.1 Table of pREE/dREE values showing relative predominance of REEs as a function of filter size (0.45 µm). A ratio value greater than one indicates a higher presence of particulate REE (> 0.45 µm) relative to dissolved REE (< 0.45 µm) for that element. The ΣREE column represents ΣpREE/ΣdREE. All values are normalized to PAAS (Taylor & McLennan, 1985).

The HREE decrease in normalized abundance in the pREE but remain relatively flat for the dREE. This may potentially indicate the presence of a solution complexing ligand within the dissolved phase that is controlling this pattern but is absent in the particulate phase. Potential colloidal transport mechanisms present in this setting could be clay particles weathered from shale surfaces; their high amount of sorption sites provides the mechanism for significant surface/solution complexation (O'Driscoll, 1991; Papagelakis & Moldoveanu, 2014). Furthermore, Verplanck (2013) suggests that REEs tend to behave conservatively in waters of pH < 5 and partition with solid phases at circumneutral pH, provided the fluid has sufficient

colloids present. It is possible that complex fractionation effects take place between the dREE and pREE due to elevated pH levels which obfuscate water-rock interpretations.

Difference in anomalies throughout the study area may suggest minor differences in geology, in particular prominence of evaporite deposits within the Permian Shale. Jianfei et al. (2014) demonstrated that Eu anomalies are controlled by groundwater processes during water-rock interaction of preferentially-mobilized reduced Eu species. There is an inverse relationship observed between the extent of negative Ce-anomaly and the extent of positive Eu-anomaly within the domestic wells. In other words, the sample with the greatest Ce-anomaly accompanied the most attenuated Eu-anomaly (Becker) whereas the sample with the greatest Eu-anomaly contained the most attenuated Ce-anomaly (Ast). The mechanism controlling the Eu anomalies possibly lessens the effect of a Ce-anomaly and vis versa only if this pattern is a function of redox conditions. Furthermore, sample Ast contains dREE abundances similar to that of other domestic wells with nearly 10x the amount of SO_4 while other inorganic ligands such as Cl, PO_4 and NO_3 are greater in the other domestic wells. This indicates that SO_4 may not represent a large control on solution complexation. However the Eu-anomaly is significantly greater in Ast relative to the other domestic wells, indicating that water-rock interaction as well as SO_4 concentration could be mobilizing Eu to a greater extent. The difference in REE distribution curves for sample Ast represent a potential geological dissimilarity either implicating equilibrium with a different mineral set or hydraulic separation. It is thus uncertain as to whether sample Ast is hydraulically connected with the other domestic wells, or if minor differences in geology along the groundwater flowpath changes the fingerprint before it reaches the next sample location. Furthermore, the shallow monitoring wells have demonstrated that the Cl ligand may not be as strong of a solution complexing agent as other ligands. REE competition with the

Cl anion against other significant cations in solution may fail to represent Cl as a strong surface site. Instead, another ligand may be responsible for this trend; currently it is speculated to be phosphate, as this ion would be more influential on surface geochemistry.

6.5 CO_2-EOR Influence

Based on available pre-injection and post-injection water chemistry data, there has been no substantial or abnormal change in geochemistry. The effects of CO_2 dissolution has been demonstrated to lower pH through carbonic acid dissociation which subsequently enhances the solubility of the fluid allowing more heavy trace elements to partition into the dissolved phase (Lawter et al., 2016). Measurements of pH however showed a general increase from pre- to post-injection resulting in an overall basification. Although trace metal desorption from rock/sediment surfaces varies as a function of mineralogy and time throughout CO_2 exposure, as shown by batch experiments and field tests (Barker, 2012; Lu et al., 2010; Zheng et al., 2016), there are a number of major and trace ions that remain mobilized in the fluid phase. Laboratory experiments indicate the most notable trace elements to remain mobilized are Pb, Mn, Cd, Cu, and Cr (Lawter et al., 2016; Frye et al., 2012; Zheng et al., 2016). These elements did not show any appreciable increase from pre- to post-injection of samples Shepherd, Zehr or SW-3; values remained at or close to zero. The MIZ also did not show an increase in these trace elements through pre- and post-injection, which possibly shows the significance of buffer potential within the carbonate reservoir. Release of trace elements from shale surfaces and membrane filtration is expected to be elevated relative to other rock types due to the largely clayey mineral makeup of the rock (Paikaray et al., 2005; Long & Larson, 1983). In addition, the high presence of calcite, iron-bearing minerals and organic content typically present in shale formations increases the sorption capacity of trace elements, leaving a high fraction sensitive to mobilization following fluid

acidification (Koschinsky et al., 2003; Lee et al., 1998; Autier & White, 2004). It is therefore likely that a large release of trace elements would occur in a shale-dominated geologic setting following a sudden CO_2 intrusion. It is currently speculated that the clay within the shale constitutes a greater stability for trace metals than dissolved complexing ligands. Furthermore, relative permeability and hydraulic conductivity values of shale aquifers are typically very low relative to other rock types, providing the opportunity for water-rock interaction over a greater period of time without significant flushing (Lewis et al., 2006); detection of a sudden contaminant release, whether natural or anthropogenic, would be much more vulnerable to natural attenuation due to retarded groundwater flow.

The time series change of CO_2 concentrations within the MIZ illustrated an increase in concentration with time thus exhibiting the success of CO_2 dissolution within the repository. The dissolved CO_2 concentrations from pre- to post-injection in sample SW-3 decreased indicating there was likely no leakage into the system. Although HCO_3, Ca and Mg are observed in excess within samples Shepherd, Zehr and Ast, as shown by over saturation of dolomite and calcite in the speciation model (Table 5.3), there is little evidence to link CO_2 influence, whether natural or anthropogenically-related, as the driving factor for carbonate precipitation. If increased precipitation of calcite is due to increasing CO_2 dissolution, there would be a general acidification pattern shown, which is not observed unless the buffer capacity of bicarbonate in the system is precluding acidification.

Other mechanisms controlling water chemistry upon a CO_2 intrusion would be the uptake of brine which may contain dissolved hydrocarbons in addition to a foreign salinity fingerprint. Major ion chemistry did not detect any change to Na or Cl from pre- to post-injection in samples Shepherd, Zehr or SW-3. In point of fact, TDS decreased for Shepherd, SW-3, SW-2, SW-1 and

Slate Creek 1 from pre- to post-injection. However, methane was detected in SW-3; its provenance is disputed, but it is unlikely that it originates from subsurface oilfield brine migration due to the overwhelming evidence of CO_2 security at depth as stated above. Low profile surficial releases related to spills or pipe leaks of producing oil wells located in the vicinity of SW-3 may be the source of methane. To further support this argument, $\delta^{18}O$ v $\delta^{2}H$ regressions among repeated MIZ and SW-3 samples may possibly indicate a connection. This evidence, although weak, would need to be further supported by additional sampling of SW-3 and oil well 61 to confirm. It is uncertain if the methane may be lingering from traces of oilfield brine left by years of salt pit leaching prior to the 1940s or if there was a recent release. Further research into this particular issue would require identification of contamination within sediments screening SW-3 to confirm the identity of the signal.

Impact of a CO_2 intrusion into an aquifer can inhibit or accelerate certain mineralogical changes based on geochemistry of the fluid. As shown by speciation calculations, carbonate precipitation, particularly dolomite, is favored due to a general over saturation of Ca, Mg and HCO_3 species that makeup the stoichiometry. Two types of reactions may occur to create dolomite precipitation, one in which it is replacing calcite (dolomitization) and one in which it is forming a primary mineral (Banerjee, 2016). In general, inorganic dolomite precipitation is favored with higher aqueous Mg / Ca ratios, higher temperature, carbonate alkalinity and degree of supersaturation (Mackenzie et al., 1983; Banerjee, 2016). A microbially-mediated dolomite precipitation has been known to occur, although this subject area is understudied. A lack of historically successful laboratory experiments involving the intentional precipitation of dolomite has been unable to derive the exact reaction kinetics of dolomite versus calcite (Arvidson & Mackenzie, 1999). The problem is seen in seawater, which typically exhibits high Mg / Ca ratios

and supersaturation with respect to dolomite, but absence of dolomite precipitation. Temperature fluxes, carbonate alkalinity, salinity, supersaturation and competition with other carbonates are all responsible for the rate and longevity of dolomite stabilization, particularly in higher temperature regimes with lower calcite supersaturation (Szramek et al., 2007; Arvidson & Mackenzie, 1999).

Intrusion of CO_2 into the Permian Shale would induce reactions on the basis of exposed mineralogical surfaces of the aquifer as well as the pore-fluid chemistry. In general many factors control the reactions between CO_2-mineral-fluid. Some of which include the mineralogy, fluid composition, porosity, pCO_2, surface area of minerals, kinetic rate constants, permeability, temperature, etc. Since each mineral is assigned a different surface area and kinetic rate constant, the reactivity is heterogeneous similar to the heterogeneity of the lithology (Lai et al., 2015; Kampman et al., 2014). Based on the fluid chemistry, we would expect calcite-silicate dissolution to occur, which has been shown to further drive alkalinity and precipitate less soluble Fe-Mg-Ca carbonates (Kampman et al., 2014; Lagneau et al., 2005). Dissolution-precipitation reactions that are currently ongoing would likely change the reactivity between the water-rock-plume interactions upon intrusion. Initial alkalinity would buffer the acidification; however, further alkalinity created through dissolution of carbonate-silicate minerals would be required to stabilize neutral pH. Due to low porosity and permeability of the Wellington Shale, the CO_2 gas molecules would incur large residence times, which would encourage the prolonged CO_2-mineral-fluid reactions. As discussed above, dolomite precipitation would be suppressed within the 0-200 ft. interval due to lower temperatures and prevalence of calcite supersaturation despite high mass ratios of Mg / Ca.

Chapter 7 - Conclusions

Surface and shallow groundwater in south-central Kansas is impacted by several forms of natural and anthropogenic contamination. Sensitive receptors located in the area such as creeks and domestic and irrigation wells screened within the shallow USDW obligated the need for contaminant source tracing and water quality characterization. Previous studies have developed methods for salinity source differentiation and an understanding of salinity distribution in the general region. This research used a variety of geochemical tools to elucidate groundwater flow pathways for contaminant migration in the shallow subsurface and understand lithologic control on geochemistry.

Water-rock interaction occurred to a greater extent within the paleoterrace wells due to greater residence times and poor hydraulic conductivity leading to higher TDS relative to wells seated in the paleovalley. The Na-Cl-dominating water type of the shallow monitoring wells within the paleoterrace suggests halite evaporite deposits represent a large control on geochemistry while paleovalley wells contained much less TDS indicating an absence of exposure to similarly soluble deposits. The difference in yield between the paleovalley and paleoterrace, could perhaps suggest a lower residence time in the paleovalley. The elevated yield of wells seated in the bedrock of the paleovalley versus those in the coarser sediments above could suggest erosional processes following the Permian led to the development of bedrock channels and solution veins. This opening of secondary porosity is speculated to have created a pathway for better hydraulic communication between Quaternary sediments and the underlying Permian System. The paleoterrace, however was not targeted by as extreme erosional conditions; retention of finer sediments on the paleoterrace precluded frequent exposure to meteoric waters post-deposition which inhibited development of vertical hydraulic pathways.

High Mg/Ca ratios and low temperature (< 25° C) of collected waters from SW-1 and SW-2 indicate dedolomitization, and replacement by calcite, thereby reducing effective porosity and increasing pore-space water residence times. This process is thought to systematically increase with depth into the paleoterrace further increasing TDS. The ubiquity of carbonate oversaturation indices throughout most of the dataset within speciation models suggests that cations such as Ca and Mg may be originating from these deposits in the paleovalley. The significant presence of the Cl anion within Shepherd and Zehr may result from outside chloride additions and not a result of natural water-rock interaction.

Environmental and isotopic tracers were used to identify the hydraulic connection between sample locations. In general, there was an observed connection between samples Becker, Shepherd, Zehr, Ast and SW-3. It is shown through $\delta^{18}O$ v $\delta^{2}H$ that these samples are recharged at a similar rate and with a similar source of water. The isotopic isolation and ^{18}O-^{2}H-depletion of samples SW-1 and SW-2 appear to show a complete hydraulic separation from shallower intervals. $\delta^{18}O$ v $\delta^{2}H$ regression lines for sample SW-3 however retains a trend that is similar to that of the MIZ which may suggest a recent shallow impact by the latter. Salinity tracing through the use of Br/Cl, SO_4/Cl, Na/Cl and (Ca+Mg)/Na mass ratios suggest salinity contributions for samples Ast, Slate Creek 1, Slate Creek 2, Becker, SW-1 and SW-2 are from natural evaporite dissolution. Samples Shepherd, Zehr and SW-3 however appear to be influenced by outside chloride additions, either agriculturally derived or via oilfield brine. The source of oilfield brine is debated; however previous studies suggest historic salt pit leaching or small-profile surficial releases are likely scenarios. The presence of methane in shallow well SW-3 may vindicate the release from a nearby oil well due to the unlikelihood for methanogensis

claims based on DO and nitrate values. An absence thereof in the other domestic wells indicates the occurrence is unique and confined to a small locality.

Rare earth element results showed that all four of the domestic wells retained similar dREE distribution curves owing to similar water source origin. The shallow monitoring wells showed vastly different dREE and pREE patterns than that of both the domestic and surface water samples which seem to indicate a difference in water source. Major ligands for solution complexation are not thought to be SO_4 or Cl as samples that contain significant proportions of these ions are not in possession of greater REE abundances than those without. Surface waters contained the greatest REE abundances which suggest PO_4 is the dominant ligand. The dREE pattern for Slate Creek 1, however roughly correlates with the domestic wells indicating meteoric recharge is similarly sourced with no appreciable differences in fractionation patterns.

Pre- and post-injection observations indicate there has been no leakage through CO_2-EOR activities at the site. A general basification of water was noted across the time series with a general decline in trace elements and generally stable bicarbonate values. A future CO_2 leakage event may be impeded by a decrease in vertical conductivity from reducing effective porosity noted by increasing dedolomitization. This process indicates conditions are currently favorable for dolomite dissolution which further increases alkalinity leading to a less-porous form of calcite and magnesite precipitation. CO_2 plume migration would thus be inhibited by the reduction in vertical conductivity and changing reactive surface area of the lithology, potentially increasing residence time and extent of CO_2 dissolution.

References

Aide, M.T. & Aide, C. (2012). Rare earth elements: Their importance in understanding soil genesis. International Scholarly Research Network, 2012, 1-11.

Aiken, G. (2002). Organic matter in ground water *in* U.S. Geological Survey Artificial Recharge Workshop Proceedings: Sacramento, California, U.S. Geological Survey, Open-File Report 02-89, 21-22.

Allard, B. (1995). Groundwater *in* Trace elements in natural waters: Ann Arbor, Michigan, CRC Press, 1-302.

Anawar, H.M., Akai, J., Komaki, K., Terao, H., Yoshioka, T., Ishizuka, T., Safiullah, S. & Kato, K. (2003). Geochemical occurrence of arsenic in groundwater of Bangladesh: sources and mobilization processes. Journal of Geochemical Exploration, 77(2-3), 109-131.

Anderson, N.L., Hopkins, J., Martinez, A., Knapp, R.W., Macfarlane, P.A., Watney, L.W. & Black, R. (1994). Dissolution of bedded rock salt: A seismic profile across the active eastern margin of the Hutchinson Salt Member, Central Kansas. Computers & Geosciences, 20(5), 889-903.

Arvidson, R.S. & Mackenzie, F.T. (1999). The dolomite problem: Control of precipitation kinetics by temperature and saturation state. American Journal of Science, 299, 257-288.

Autier, V. & White, D. (2004). Examination of cadmium sorption characteristics for a boreal soil near Fairbanks, Alaska. Journal of Hazardous Materials, 106B, 149-155.

Baba, A. & Tayfur, G. (2010). Groundwater contamination and its effect on health in Turkey. Environmental Monitoring and Assessment, 183(2011), 77-94.

Banner, J.L., Wasserburg, G.J., Dobson, P.F., Carpenter, A.B. & Moore, C.H. (1988). Isotopic and trace element constraints on the origin and evolution of saline groundwaters from Central Missouri. Geochimica et Cosmochimica Acta, 53, 383-398.

Barker, R. (2012). Geochemical and mineralogical characterization of the Arbuckle Aquifer: Studying mineral reactions and its implications for CO_2 sequestration. K-State Research Exchange, 1-168.

Beaucaire, C., Gassama, N., Tresonne, N. & Louvat, D. (1999). Saline groundwaters in the hercynian granites (Chardon Mine, France): geochemical evidence for the salinity origin. Applied Geochemistry, 14, 67-84.

Bethke, C.M., Sanford, R.A., Kirk, M.F., Jin, Q. & Flynn, T.M. (2011). The thermodynamic ladder in geomicrobiology. American Journal of Science, 311(3), 183-210.

Brickler, O.P. & Jones, B.F. (1995). Main facts affecting the compositions of natural waters *in* Trace elements in natural waters: Ann Arbor, Michigan, CRC Press, 302.

Chang, K.W., Minkoff, S.E. & Bryant, S.L. (2008). Modeling leakage through faults of CO_2 stored in an aquifer. Society of Petroleum Engineers, SPE 115929.

Chevis, D.A., Johannesson, K.H., Burdige, D.J., Tang, J., Moran, S.B. & Kelly, R.P. (2015). Submarine groundwater discharge of rare earth elements to a tidally-mixed estuary in Southern Rhode Island. Chemical Geology, 397(2015), 128-142.

Craig, H. (1961a). Standard for reporting concentrations of deuterium and oxygen-18 in natural waters. Science 133, 1833-1834.

Craig, H. (1961b). Isotopic variations in meteoric waters. Science, 133(3465), 1702-1703.

Da Lio, C., Carol, E., Kruse, E., Teatini, P. & Tosi, L. (2015). Saltwater contamination in the managed low-lying farmland of the Venice coast, Italy: An assessment of vulnerability. Science of the Total Environment, 533, 356-369.

Datta, S., Neal, A.W., Mohajerin, T.J., Ocheltree, T., Rosenheim, B.E., White, C.D. & Johannesson, K.H. (2011). Perennial ponds are not an important source of water or dissolved organic matter to groundwaters with high arsenic concentrations in West Bengal, India. Geophysical Research Letters, 38(20), 1-5.

Denison, R.E., Lidiak, E.G., Bickford, M.E. & Kisvarsanyi, E.B. (1984). Geology and geochronology of Precambrian rocks in the central interior region of the United States. U. S. Geological Survey, 1241-C, 1-20.

Dixit, S. & Hering, J.G. (2003). Comparison of arsenic(V) and arsenic(III) sorption onto iron oxide minerals: Implications for arsenic mobility. Environmental Science & Technology, 37(18), 4182-4189.

Drever, J.I. (1988). Organic compounds in natural waters *in* the geochemistry of Natural Water, 2nd ed.: Prentice-Hall, Englewood Cliffs, NJ, 107-127.

Elrod, D.D. (1980). A geochemical and petrographic survey of the Wellington Formation, North-Central Oklahoma]unpublished M.S. thesis]. Oklahoma State University, 1-100.

Flynn, T.M, Sanford, R.A., Ryu, H., Bethke, C.M., Levine, A.D., Ashbolt, N.J. & Santo Domingo, J.W. (2013). Functional microbial diversity explains groundwater chemistry in a pristine aquifer. BMC Microbiology, 13(146), 1-15.

Freeman, J.T. (2007). The use of bromide and chloride mass ratios to differentiate salt-dissolution and formation brines in shallow groundwaters of the Western Canadian Sedimentary Basin. Hydrogeology Journal, 15, 1377-1385.

Frye, E., Bao, C., Li, L. & Blumsack, S. (2012). Environmental controls of cadmium desorption during CO_2 leakage. Environmental Science & Technology, 46(8), 4388-4395.

Gogel, T. (1981). Discharge of saltwater from Permian rocks to major stream-aquifer systems in Central Kansas. Kansas Geological Survey, Chemical Quality Series 9, 1-60.

Gosselin, D.C., Smith, M.R., Lepel, E.A. & Laul, J.C. (1992). Rare earth elements in chloride-rich groundwater, Palo Duro Basin, Texas, USA. Geochimica et Cosmochimica Acta, 56, 1495-1505.

Granato, G.E., DeSimone, L.A., Barbaro, J.R. & Jeznach, L.C. (2015). Methods for evaluating potential sources of chloride in surface waters and groundwater's of the conterminous United States. U.S. Geological Survey Open-File Report 2015-1080, 1-89.

Grattan, S.R. & Grieve, C.M. (1998). Salinity-mineral nutrient relations in horticultural crops. Scientia Horticulturae, 78(1-4), 127-157.

Grattan. S.R. (2002). Irrigation water salinity and crop production. Division of Agriculture and Natural Resources UC Davis, ISBN: 978-1-60107-244-3.

Grauch, R.I. & Mariano, A.N. (2008). Ion-adsorption type lanthanide deposits. Society of Mining, Metallurgy and Exploration Annual Meeting and Exhibit Preliminary Program, 1-40.

Grawunder, A., Merten, D. & Buchel, G. (2014). Origin of middle rare earth element enrichment in acid mine drainage-impacted areas. Environmental Science of Pollution Research, 21, 6812-6823.

Greaves, M.J., Elderfield, H. & Klinkhammer, G.P. (1989). Determination of the rare earth elements in natural waters by isotope-dilution mass spectrometry. Analytica Chimica Acta, 218(1989), 265-280.

Hanson, G.N. (1980). Rare earth elements in petrogenetic studies of igneous systems. Annual Review of Earth and Planetary Sciences, 8, 371-406.

Hem, J.D. (1985). Study and interpretation of the chemical characteristics of natural water, 3rd ed.: Washington D.C. U.S. Geological Survey Water-Supply Paper 2254, 1-263.

Hem, J.D. (1989). Study and interpretation of the chemical characteristics of natural water, 3rd ed.: Washington D.C. U.S. Geological Survey Water-Supply Paper 2254, 1-263.

Hem, J.D. (1992). Study and interpretation of the chemical characteristics of natural water, 3rd ed.: Washington D.C. U.S. Geological Survey Water-Supply Paper 2254, 1-263.

Holubnyak, Y., Watney, W.L., Birdie, T., Rush, J. & Fazelalavi, M. (2016). Reservoir modeling of CO_2 injection in Arbuckle saline aquifer at Wellington Field, Sumner County, Kansas. KGS Open-File Report 2016-29, 1-150.

Ivshina, I.B., Kuyukina, M.S., Krivoruchko, A.V., Elkin, A.A., Makarov, S.O., Cunningham, C.J, Peshkur, T.A., Atlas, R.M. & Philip, J.C. (2015). Oil spill problems and sustainable response strategies through new technologies. Environmental Science Processes and Impacts, 17, 1201-1219.

Jackson, R.B, Vengosh, A., Darrah, T.H., Warner, N.R., Down, A., Poreda, R.J., Osborn, S.G., Zhao, K.G. & Karr, J.D. (2013). Increased stray gas abundance in a subset of drinking water wells near Marcellus Shale gas extraction. PNAS, 110(28), 11250-11255.

Jessop, P.G. & Subramaniam, B. (2007). Gas-Expanded Liquids. Chemical Reviews, 107(6), 2666-2694.

Jewett, J.M., Bayne, C.K., Goebel, E.D., O'Connor, H.G., Swineford, A. & Zeller, D.E. (1968). Precambrian Rocks *in* Stratigraphic Succession in Kansas. Kansas Geological Survey Bulletin 189.

Jianfei, Y., Xumei, M., Yanxin, W., Zhide, D. & Leihui, H. (2014). Geochemistry of rare-earth elements in shallow groundwater, northeastern Guangdong Province, China. Chinese Journal of Geochemistry, 33, 53-64.

Johannesson, K.H., Stetzenbach, K.J. & Hodge, V. (1997). Rare earth elements as geochemical tracers of regional groundwater mixing. Geochimica et Cosmochimica Acta, 61(17), 3605-3618.

Johannesson, K.H., Farnham, I.M., Guo, C. & Stetzenbach, K.J. (1999). Rare earth element fractionation and concentration variations along a groundwater flow path within a shallow, basin-fill aquifer, southern Nevada, USA. Geochimica et Cosmochimica Acta, 63(18), 2697-2708.

Johannesson, K.H., Cortes, A., Alfredo, J, Leal, R., Ramirez, A.G. & Durazo, J. (2005). Geochemistry of rare earth elements in groundwaters from a rhyolite aquifer, central Mexico *in* Rare earth elements in groundwater flow systems. Water Science and Technology, 51, 187-222.

Johannesson, K.H., Palmore, C.D., Fackrell, J., Prouty, N.G., Swarzenski, P.W., Chevis, D.A., Telfeyan, K., White, C.D. & Burdige, D.J. (2017). Rare earth element behavior during groundwater-seawater mixing along the Kona Coast of Hawaii. Geochimica et Cosmochimica Acta, 198(2017), 229-258.

John, D.A. & Leventhal, J.S. (1995). Bioavailability of metals *in* Preliminary compilation of descriptive geoenvironmental mineral deposit models. U.S. Geological Survey, 10-18.

Jones, O.S. (1950). Fresh water protection from pollution arising in the oil fields. University of Kansas Publications, Lawrence, KS.

Jorgensen, D. G. & Signor, D. C. (1981). Plan of study for the Central Midwest Regional Aquifer System Analysis in parts of Arkansas, Colorado, Kansas, Missouri, Nebraska, New Mexico, Oklahoma, South Dakota, and Texas. U.S. Geological Survey, Water-resources Investigations, Open-file Report 81-206, 1-28.

Jouzel, J., Koster, R.D., Suozzo, R.J. & Russell, G.L. (1994). Stable water isotope behavior during the last glacial maximum: A general circulation model analysis. Journal of Geophysical Research, 99, 25791-25802.

Kampman, N., Bickle, M., Wigley, M. & Dubacq, B. (2014). Fluid flow and CO_2-fluid-mineral interactions during CO_2-storage in sedimentary basins. Chemical Geology, 369, 22-50.

Kendall, C., Sklash, M.G. & Bullen, T.D. (1995). Isotope tracers of water and solute sources in catchments *in* Solute modeling in catchment systems. Wiley, New York, 261-303.

KGS. (2015). Kansas seismic action plan. KDHE corporation commission geological survey, 1-7.

KGS. (2016). Small scale field test demonstrating CO_2 sequestration in Arbuckle saline aquifer and by CO_2-EOR at Wellington, Field, Sumner County, Kansas. Q20 DUNS Number: 076248616.

Kirk, M.F., Wilson, B.H., Marquart, K.A., Zeglin, L.H., Vinson, D.S. & Flynn, T.M. (2015). Solute concentrations influence microbial methanogenesis in coal-bearing strata of the Cherokee Basin, USA. Frontiers in Microbiology, 6(1287), 1-14.

Koschinsky, A., Winkler, A. & Fritsche, U. (2003). Importance of different types of marine particles for the scavenging of heavy metals in deep-sea bottom water. Applied Geochemistry, 18, 693-710.

Lagneau, V., Pipart, A. & Catalette, H. (2005). Reactive transport modelling of CO_2 sequestration in saline aquifers. Oil and Gas Science and Technology – Rev. IFP, 60(2), 231-247.

Lai, P., Moulton, K. & Krevor, S. (2015). Pore-scale heterogeneity in the mineral distribution and reactive surface area of porous rocks. Chemical Geology, 411, 260-273.

Lambert, M.W., Berendsen, P. & Ripley, E.M. (1981). Copper sulfides in the Lower Permian redbeds of south-central Kansas. Kansas Geological Survey Bulletin 223 (2).

Lawter, A., Qafoku, N.P., Wang, G., Shao, H. & Brown, C.F. (2016). Evaluating impacts of CO_2 intrusion into an unconsolidated aquifer: I Experimental Data. International Journal of Greenhouse Gas Control, 44, 323-333.

Lee, S., Change, L., Yang, H., Chen, C. & Liu, M. (1998). Adsorption characteristics of lead onto soils. Journal of Hazardous Materials, 63(1), 37-49.

Leenheer J.A., Malcolm R.L., McKinley P.W. & Eccles L.A. (1974). Occurrence of dissolved organic carbon in selected ground-water samples in the United States. U.S. Geological Survey Journal of Research, 2: 361-369.

Lewis, M.A., Cheney, C.S. & ODochartaigh, B.E. (2006). Guide to permeability indices. British Geological Survey Open Report CR/06/160N, 1-20.

Leybourne, M.I. & Cousens, B.L. (2005). Rare earth element (REE) and Nd and Sr isotopes in groundwater and suspended sediments from the Bathurst Mining Camp, New Brunswick:

Water-rock reactions and elemental fractionation *in* Rare earth elements in groundwater flow systems. Water Science and Technology, 51, 253-293.

Long, D.T. & Larson, G.J. (1983). Field evidence for shale membrane filtration of groundwater, south-central Michigan. National Technical Information Service Institute of Water Research Completion Report: Michigan State University, East Lansing, 1-51.

Lovley, D.R. & Phillips, E.J. (1988). Novel mode of microbial energy metabolism: organic carbon oxidation coupled to dissimilatory reduction of iron or manganese. Applied and Environmental Microbiology, 54(6), 1472-1480.

Lu, J., Partin, J.W., Hovorka, S.D. & Wong, C. (2010). Potential risks to freshwater resources as a result of leakage from CO_2 geological storage: A batch-reaction experiment. Environmental Earth Sciences, 60, 335-248.

Macfarlane, A.P. (2000). Revisions to the nomenclature for Kansas aquifers. Kansas Geological Survey, Current Research in Earth Sciences Bulletin 244(2).

Mackenzie, F.T., Bishoff, W.D., Bishop, F.C., Loijens, M., Schoonmaker, J. & Wollast, R. (1983). Magnesian calcites: low-temperature occurrence, solubility, and solid solution behavior *in* Carbonates: Mineralogy and chemistry. Reviews in Mineralogy, 11, 97-144.

Mandal, B.K. & Suzuki, K.T. (2002). Arsenic round the world: A review. Talanta, 58(1), 201-235.

Meister, P., Reyes, C., Beaumont, W., Rincon, M., Collins, L., Berelson, W., Stott, L., Corsetti, F. & Nealson, K.H. (2011). Calcium and magnesium limited dolomite precipitation at Deep Springs Lake, California. Sedimentology, 58, 1810-1830.

Melhorn, J., Byrne, J.M., Kappler, A. & Planer-Friedrich, B. (2016). Time and temperature dependency of carbon dioxide triggered metal(oid) mobilization in soil. Applied Geochemistry, 74, 122-137.

Merriam, D.F. (1963). The geologic history of Kansas. Kansas Geological Survey Bulletin 162, 1-317.

Miller, K.B., McCahon, T.J. & West, R.R. (1996). Lower Permian (Wolfcampian) paleosol-bearing cycles of the U.S. midcontinent—evidence of climatic cyclicity. Journal of Sedimentary Research, 66, 71-84.

Mohan, D. & Pittman, C.U., Jr. (2007). Arsenic removal from waste/wastewater using adsorbents – a critical review. Journal of Hazardous Materials, 142(1-2), 1-53.

Moore, G.A. & Buck, D.H. (1953). The fishes of Chikaskia River in Oklahoma and Kansas. Proceedings Oklahoma Academy of Science. 34, 19-27.

Moore, R.C. (1964). Paleoecological aspects of Kansas Pennsylvanian and Permian cyclothems *in* Symposium on cyclic sedimentation. Kansas Geological Survey Bulletin 169(1-2), 287-380.

Noack, C.W., Dzombak, D.A. & Karamalidis, A.K. (2014). Rare earth element distributions in natural waters with a focus on groundwater. Environmental Science and Technology, 48, 4317-4326.

Nordstrom, D.K. (2002). Public health – Worldwide occurrences of arsenic in ground water. Science, 296(5576), 2143-2145.

O'Connor, H.G. (1971). Geology and ground-water resources of Johnson County Northeastern Kansas. Kansas Geological Survey Bulletin 203, 1-68.

O'Driscoll, M. (1991). An overview of rare earth minerals supply and applications. Materials Science Forum International Conference on Rare Earth Minerals and Minerals for Electronic Uses, Trans Tech Publications, 409-420.

Ostendorf, D.W., Hinlein, E.S., Rotaru, C. & Degroot, D.J. (2006). Contamination of groundwater by outdoor highway deicing agent storage. Journal of Hydrology, 326(1-4), 109-121.

Paikaray, S., Banerjee, S. & Mukherji, S. (2005). Sorption behavior of heavy metal pollutants onto shales and correlation with shale geochemistry. Environmental Geology, 47(8), 1162-1170.

Papangelakis, V.G. & Moldoveanu, G. (2014). Recovery of rare earth elements from clay minerals. European Rare Earth Resources Conference, 191-202.

Park, J., Sanford, R.A. & Bethke, C.M. (2006). Geochemical and microbiological zonation of the Middendorf aquifer, South Carolina. Chemical Geology, 230, 88-104.

Pope, L.M., Bruce, B.W. & Hansen, C.V. (1999). Ground-water quality in Quaternary deposits of the Central High Plains Aquifer, south-central Kansas, 1999. U. S. Geological Survey Water-Resources Investigations Report 00-4259.

Richardson, K. & Carling, P.A. (2007). A typology of sculpted forms in open bedrock channels. Area, 39(4), 551-558.

Samson, I.M., & Wood, S.A. (2004). The rare earth elements: Behavior in hydrothermal fluids and concentration in hydrothermal mineral deposits, exclusive of alkaline settings *in* Rare-Element Geochemistry and Ore Deposits. Geological Association of Canada, Short Course Notes, v. 17 (in press).

Selley, R.C. (2000). Carbonate *in* Applied sedimentology, *2nd ed.,* New York: Academic Press, 407-409.

Shannon, W.M. & Wood, S.A. (2005). The analysis of pictogram quantities of rare earth elements in natural waters *in* Rare Earth Elements in Groundwater Flow Systems. Water Science and Technology, 51, 1-37.

Sharp, Z. (2007). Principles of stable isotope geochemistry: Pearson/Prentice Hall, Upper Saddle River, NJ, 1-344.

Shearman,D.J., Khouri, J. & Taha, S. (1961). On the replacement of dolomite by calcite in some Mesozoic limestones from the French Jura. Proceedings of the Geologists' Association, 72(1), 1-12.

Smith, A.H., Lingas, E.O. & Rahman, M. (2000). Contamination of drinking-water by arsenic in Bangladesh: a public health emergency. Bulletin of the World Health Organization, 78(9), 1093-1103.

Szramek, K., McIntosh, J.C., Williams, E.L., Kanduc, T., Ogrinc, N. & Walter, L.M. (2007). Relative weathering intensity of calcite versus dolomite in carbonate-bearing temperate zone watersheds: Carbonate geochemistry and fluxes from catchments within the St. Lawrence and Danube river basins. Geochemistry, Geophysics and Geosystems, 8(4), 1-26.

Tang, J. & Johannesson, K.H. (2005). Rare earth element concentrations, speciation, and fractionation along groundwater flow paths: The Carrizo sand (Texas) and upper Floridan aquifers *in* Rare earth elements in groundwater flow systems. Water Science and Technology Library 51, 223-251.

Tang, J. & Johannesson, K.H. (2010). Rare earth elements adsorption onto Carrizo Sand: Influence of strong solution complexation. Chemical Geology, 279(3-4), 120-133.

Taylor, S.R. & McLennan, S.M. (1985). The continental crust: its composition and evolution; an examination of the geochemical record preserved in sedimentary rocks. Blackwell: Oxford, 1-312.

Thauer, R.K. (1998). Biochemistry of methanogenesis: A tribute to Marjory Stephenson. Microbiology, 144(9), 2377-2406.

Van Breugel, Y., Baas, M., Schouten, S., Mattioli, E. & Sinninghe Damste, J.S. (2006). Isorenieratane record in black shales from the Paris Basin, France: Constraints on recycling of respired CO2 as a mechanism for negative carbon isotope shifts during the Toarcian oceanic anoxic event. Paleoceanography, 21(PA4220), 1-8.

Ver Wiebe, W.A. (1937). The Wellington Formation of Central Kansas. Municipal University of Wichita, University Studies, 12(5), 3-18.

Verplanck, P.L., Nordstrom, D.K. & Taylor, H.E. (1999). Overview of rare earth element investigations in acid waters of U.S. Geological Survey abandoned mine lands watersheds. U.S. Geological Survey Water Resources Investigations Report 99-4018A, 83-92.

Verplanck, P.L. (2013). Partitioning of rare earth elements between dissolved and colloidal phases. Procedia Earth and Planetary Science, 7, 867-870.

Viessman Jr., W. & Lewis, G.L. (2002). Introduction to hydrology, 5th ed.: Pearson, Upper Saddle River, NJ, 2-31.

Volk, C., Wood, L., Johnson, B, Robinson, J., Zhu, H.W. & Kaplan, L. (2002). Monitoring dissolved organic carbon in surface and drinking waters. Journal of Environmental Monitoring, 4, 43-47.

Walters, A., Lusty, P. & Hill, A. (2011). Rare Earth Elements. British Geological Survey, Natural Environment and Research Council, 1-53.

Wang, S. & Mulligan, C.N. (2006). Occurrence of arsenic contamination in Canada: Sources, behavior and distribution. Science of the Total Environment, 366(2-3), 701-721.

Watney, W.L. (1980). Cyclic sedimentation of the Lansing-Kansas City Groups in Northwestern Kansas and Southwestern Nebraska: A guide for petroleum exploration. Kansas Geological Survey Bulletin 220, 1-72.

Watney, W.L., Guy, W.J. & Byrnes, A.P. (2001). Characterization of the Mississippian Osage Chat in south-central Kansas: American Association of Petroleum Geologists Bulletin 88(1), 85-113.

Watney, W.L., Raney, J., Birdie, T. & Victorine, J. (2015). Brief review of the hydrogeology of the shallow unconfined aquifer in North-Central Sumner County, Kansas. Kansas Geological Survey, 1-34.

Watney, W.L., Wreath, D., Birdie, T., Hildebrandt, K.F. & Harris, D. (2015). Wellington oil field small scale carbon capture and storage project Wellington, KS. Kansas Geological Survey, 1-55.

West, R.R., Miller, K.B. & Watney, W.L. (2010). The Permian System in Kansas. Kansas Geological Survey Bulletin 257, 1-82.

Whittemore, D.O. & Hathaway, L.R. (1983). Identification of saltwater sources affecting groundwater from R. Newell Irrigation Well, Reno County. Kansas Geological Society Open-File Report 83-14, 1-6.

Whittemore, D.O. (1993). Ground-water geochemistry in the mineral intrusion area of groundwater management district no. 5, south-central Kansas. Kansas Geological Survey, Open-File Report 93-2, 1-107.

Whittemore, D.O. (1995). Geochemical differentiation of oil and gas brine from other saltwater sources contaminating water resources: Case studies from Kansas and Oklahoma. Environmental Geosciences, 2(1), 15-31.

Whittemore, D.O. (2007). Fate and identification of oil-brine contamination in different hydrogeologic settings. Applied Geochemistry, 22(10), 2099-2114.

Wilkin, R.T. & Digiulio, D.C. (2010). Geochemical impacts to groundwater from geologic carbon sequestration: controls on pH and inorganic carbon concentrations from reaction path and kinetic modeling. Environmental Science and Technology, 44(12), 4821-4827.

Wollenweber, J., Alles, S., Busch, A., Krooss, B.M., Stanjek, H. & Littke, R. (2010). Experimental investigation of the CO_2 sealing efficiency of caprocks. International Journal of Greenhouse Gas Control, 2(2010), 231-241.

Zheng, L., Spycher, N., Bianchi, M., Pugh, J.D., Varadharajan, C., Tinnacher, R.M., Birkholzer, J.T., Nico, P. & Trautz, R.C. (2016). Impacts of elevated dissolved CO_2 on a shallow groundwater system: Reactive transport modeling of a controlled-release field test. Chemical Geology, 447, 117-132.

Appendix A - Well Information

ID	Township/Range /Section	Latitude	Longitude	Completion Date	Well Purpose	Screen Interval (ft. BGS)	Total Depth (ft. BGS)	Well Diameter (inches)	Estimated Yield (GPM)	Grout Interval (ft. BGS)	Sand Interval (ft. BGS)	Elevation (ft. AMSL)	Bedrock Start Depth (ft. BGS)
Ast	T31S-R1W-S34	37.31108	-97.4035	8/13/1991	Domestic - Lawn + Garden	26-46	46	5	?	0-20	26-46	1263	13
Becker	T31S-R1W-S30	37.31944	-97.4631	11/15/2013	Domestic - Lawn + Garden	23-55	55	5	10	3-20	23-55	1243	50
Shepherd	T32S-R1W-S5	37.29544	-97.4482	10/10/2013	Domestic - Household	23-47	47	5	10	3-20	23-47	1231	38
Zehr (Blubaugh)	T32S-R1W-S4	37.29656	-97.4364	4/3/2009	Domestic - General	20-60	60	5	15	3-20	20-60	1222	19
Slate Creek 1	T32S-R1W-S5	37.28817	-97.4527	N/A	N/A	N/A	N/A	N/A	N/A	N/A	N/A	1201	N/A
Slate Creek 2	T32S-R2W-S1	37.30189	-97.4759	N/A	N/A	N/A	N/A	N/A	N/A	N/A	N/A	1213	N/A
SW-3	T31S-R1W-S29	37.31811	-97.4355	2/9/2015	Monitoring	25-50	50	4	3	0-22	25-50	1255	30
SW-1	T31S-R1W-S28	37.31958	-97.4332	11/1/2014	Monitoring	50-100	100	3	4.20E-04	0-47	47-100	1260	14-15
SW-2	T31S-R1W-S33	37.319	-97.4336	11/3/2014	Monitoring	100-200	200	3	1.02E-03	0-97	97-200	1257	20
Oil Well 61	T31S-R1W-S32	37.30978	-97.4431	4/7/1937	Producing Oil Well	?	3,697	5.5	N/A	--	--	1258	?
KGS 2-32	T31S-R1W-S32	37.31056	-97.4421	6/8/2015	Active EOR - CO_2 Injection	3,664-3,706	3,860	5.5	N/A	--	--	1257	?
KGS 1-32	T31S-R1W-S32	37.31544	-97.4424	8/24/2011	Inactive EOR - CO_2 Injection	4,995-5,020	5,240	5.5	N/A	--	--	1259	?
KGS 1-28	T31S-R1W-S28	37.31948	-97.4334	8/24/2011		5,000-5,020	5,250	5.5	N/A	--	--	1257	?

Table A.1 Sample well construction details.

Appendix B - Field Water Quality Parameters

Well ID	Date	Depth to Water (feet BTOC)	Notes	Time (Military)	Purge Readings (In Order)	Sample Readings (In Order)	Turbidity (NTU)	Dissolved Oxygen (mg/L)	pH (SU)	Specific Conductivity (mS/cm)	ORP (mV)	Temperature (°C)
Ast Domestic Well (26-46') (N37°18'39.9"; W-97°24'12.7")	7/19/2016	N/A	Began purge at 1612, end of purge at 1735	1612	1	--	0	1.97	8.29	6.55	-10	28.67
				1619	2	--	0	1.76	8.27	8.21	-27	26.68
				1625	3	--	0	1.71	8.32	8.94	-20	23.66
				1633	4	--	0	1.58	8.37	8.12	-18	22.41
				1637	5	--	0	1.86	8.41	7.86	-11	20.4
				1642	6	--	0	2.12	8.4	7.27	-4	20.26
				1647	7	--	0	2.07	8.38	7.11	1	20.42
				1657	8	--	0	1.79	8.3	6.46	2	22.45
				1706	9	--	0	1.78	8.31	6.1	5	21.78
				1711	--	1	0	1.82	8.31	5.95	12	20.85
				1716	--	2	0	2.05	8.27	6.01	14	19.72
				1721	--	3	5.8	1.95	8.21	5.91	18	20.21
Becker Domestic Well (23-55') (N37°19'10.0"; W-97°27'47.1")	7/20/2016	N/A	Began purge at 1058, end purge at 1153	1058	1	--	0	5.15	8.52	1.43	94	21.67
				1106	2	--	0	5.29	8.23	1.42	109	20.89
				1111	3	--	0	4.39	8.06	1.43	119	20.75
				1116	4	--	0	4.34	8.01	1.4	124	20.59
				1120	5	--	0	4.25	7.94	1.4	128	20.69
				1123	--	1	0	5.06	7.97	1.4	129	19.43
				1125	--	2	0	5.39	7.88	1.4	135	22.85
				1153	--	3	0	4.42	7.95	1.4	139	24.88
Shepherd Domestic Well (23-47') (N37°17'43.6"; W-97°26'53.6")	10/6/2015	N/A	Began purge at 0842; End purge at 093	0842	1	--	0.33	3	6.77	3.12	473	16.5
				0847	2	--	0	3	6.18	3.02	495	16.5
				0852	3	--	0	3	6.37	3.03	529	16.5
				0900	4	--	0.01	3	6.44	3.04	515	16.5
				0905	5	--	0	3	6.51	3.05	506	16.5
				0910	6	--	0	3	6.58	3.06	493	16.4
				0935	7	--	0	3	6.58	3.06	488	16.5
				1010	--	1	0	3	6.93	3.06	430	16.8
				1030	--	2	0.42	3	6.9	3.07	438	16.9
				1035	--	3	0.67	3	6.92	3.07	434	16.9
	7/19/2016		Began purge at 1900, end purge at 1947	1900	1	--	0	2.77	7.84	3.12	101	26.77
				1908	2	--	0	9.15	7.84	3.05	103	23.22
				1912	3	--	0	7.37	7.79	3.01	106	20.89
				1917	4	--	0	3.04	7.7	3.01	113	20.65
				1922	5	--	0	2.72	7.68	3.05	113	20.79
				1927	--	1	0	2.8	7.72	3.07	112	20.71
				1937	--	2	0	2.76	7.79	3.05	112	22.29
				1947	--	3	0	2.39	7.82	3.09	112	22.31
Zehr Domestic Well (20-60') (N 37°17'47.6"; W -97°26'11.2")	10/6/2015	N/A	Began purge at 1339; End purge at 1410	1340	1	--	3.21	3	7.61	3.42	297	21.6
				1344	2	--	2.78	3	7.25	3.46	282	20.4
				1346	3	--	2.78	3	7.22	3.2	258	19.7
				1349	4	--	0.48	3	7.17	3.34	243	19.7
				1355	5	--	0	3	7.13	3.42	233	19.1
				1400	6	--	0	3	7.14	3.43	231	19.2
				1405	7	--	0.05	3	7.13	3.53	230	19.3
				1410	--	1	0.09	3	7.08	3.6	222	18.9
				1420	--	2	0.03	3	7.1	2.65	219.5	19.1
				1425	--	3	0.57	3	7.11	3.7	218.6	19.3
	7/19/2016		Began purge at 1249, ended purge at 1428	1249	1	--	0	3.27	8.63	3.45	42	24.91
				1255	2	--	0	8.64	8.09	3.11	67	24.35
				1302	3	--	0	3.96	7.92	3.00	77	23.38
				1306	4	--	0	6.96	7.86	3.16	80	22.54
				1312	5	--	0	3.13	7.77	3.14	86	22.15
				1316	6	--	0	8.46	7.72	3.27	87	22.73
				1323	--	1	0	2.45	7.72	3.36	87	22.03
				1330	--	2	0	2.27	7.76	3.36	84	23.19
				1347	--	3	5.1	2.02	7.77	3.41	83	27.04
Slate Creek 1 (N 37°17'17.4"; W -97°27'9.7")	10/6/2015	N/A	Surface Water Sample	1206	--	1	8.66	5	7.25	1.327	248	17.4
				1220	--	2	9.67	5	7.83	1.336	257	17.4
				1233	--	3	5.16	5	7.95	1.338	271	20.4
	7/18/2016		Sample collected on 7/18/16 at 1130-1230. Water quality readings collected on 7/20/16	1407	--	1	9.4	6.76	9.23	1.09	88	30.75
				1410	--	2	22	6.76	9.3	1.08	94	29.9
				1412	--	3	9.8	8.69	9.31	1.07	98	29.8
Slate Creek 2 (N 37°18'06.8"; W -97°28'33.3")	7/18/2016	N/A	Sample collected on 7/18/16 at 1130-1230. Water quality readings collected on 7/20/16	1433	--	1	274	4.38	9.35	0.256	97	32.48
				1435	--	2	245	4.2	9.36	0.241	99	32.21
				1437	--	3	277	4.77	9.27	0.238	104	32.34

Table B.1 In-field measurements of water quality parameters.

Well ID	Date	Depth to Water (feet BTOC)	Notes	Time (Military)	Purge Readings (In Order)	Sample Readings (In Order)	Turbidity (NTU)	Dissolved Oxygen (mg/L)	pH (SU)	Specific Conductivity (mS/cm)	ORP (mV)	Temperature (°C)
SW- 3 (25-50') (N 37° 19' 05.2"; W -97° 26' 07.7")	10/7/2015	8.88 @ 0745	Began purge at 0745; end purge at 0930	0820	1	--	309	5.5	6.65	49.9	287.4	16.4
		11.71 @ 0930		0900	2	--	811	6	6.47	47.5	167.8	16.7
				0923	3	--	253	6	6.51	48.1	155.8	16.9
				0953	--	1	413	5.5	6.53	46.9	162.5	17.5
				1024	--	2	262	4	6.61	48.6	164.2	17.6
				1055	--	3	115	5	6.6	48.7	159.9	18.3
	7/19/2016	9.96	Purge started at 2125 - DTW is 8.90	2127	1	--	5.1	2.01	7.62	47.0	-59	21.89
				2131	2	--	16.6	1.41	7.66	46.2	-48	20.11
		11.15		2137	3	--	48.1	1.35	7.67	45.7	-40	19.25
		11.44		2146	4	--	62.8	1.39	7.66	46.2	-34	19.33
				2155	--	1	27.5	1.26	7.62	46.4	-30	19.59
				2205	--	2	9.2	2.02	7.59	46.7	-24	23.33
SW - 1 (50-100') (N 37° 19' 10.5"; W -97° 25' 59.5")	10/6/2015	76.60 @ 1605	Began purge at 1610; end purge at ~1630	1645	--	1	181	5	6.83	80.5	301.5	19.4
		90.87 post-purge		1655	--	2	206	4	7.05	82.1	279.5	19.5
		90.17 @ 1758		1705	--	3	204	4	7.2	82.8	268.5	19
	7/19/2016	19.88	Purge began	0920	1	--	9.9	2.19	6.82	39.1	201	21.79
		31.3		0926	2	--	12.3	1.11	7.3	67.7	205	19.19
		37.7		0931	3	--	11	1.18	7.59	63.3	196	18.93
		45.5		0935	4	--	14.2	1.4	7.86	53.8	184	18.26
		48.66 @ 0938		0942	5	--	7.7	1.48	8.06	47.8	173	18.81
		49.42 @ 0939		0946	6	--	4.4	1.55	8.22	47.4	165	18.85
				0951	7	--	4.3	2.7	8.41	47.3	154	19.15
		56.0		0953	8	--	6.6	1.38	8.71	42.1	146	17.83
				1000	9	--	7.1	2.27	9.18	39.6	136	18.73
				1004	10	--	190	2.39	9.4	38.1	133	17.96
		66.5		1006	11	--	219	8.19	9.14	44.8	136	17.95
		69.8 @ 1011		1010	12	--	166	1.81	8.98	50	139	17.66
				1013	13	--	112	1.58	8.92	53.3	138	17.8
				1016	14	--	87	1.25	8.81	58.2	138	18.54
		75.0	Purge ended	1020	15	--	68.2	1.13	8.6	65.2	137	21.08
	7/20/2016	72.6 @ 2057		0957	--	1	6.2	2.00	8.00	70.2	99	23.54
		on 7/19/16		1024	--	2	124	3.05	8.36	62.7	103	21.35
		71.43 @ 0920		1030	--	3	95	2.43	8.34	62.7	104	23.14
SW - 2 (100-200') (N 37° 19' 08.4"; W -97° 26' 01.1")	10/6/2015	67.46 @ 1815	Began purge at 1830; end purge at 1955	1848	1	--	366	0.8	6.15	> 100	290.5	18.4
				1912	2	--	443	0.9	6.35	> 100	239.6	17.6
				1942	3	--	312	0.8	6.35	> 100	223.3	16.6
				2020	--	1	604	0.5	6.26	> 100	--	16.6
				2030	--	2	561	0.5	6.6	> 100	270.4	16.7
				2130	--	3	508	0.5	6.75	100	278.9	17.1
	7/19/2016	65.1	60.08 @ 1050	1055	1	--	5.6	0.96	7.37	> 100	175	20.81
		68.43		1059	2	--	5.1	0.88	7.41	> 100	165	20.32
				1107	3	--	4.1	0.95	7.42	> 100	152	20.38
		75.5		1110	4	--	3.4	3.15	7.42	> 100	143	20.46
		79.04		1112	5	--	3.3	0.68	7.4	> 100	135	21.26
		82.31		1116	6	--	0.8	0.67	7.39	> 100	124	22
		86.3		1123	7	--	0	0.85	7.43	> 100	115	20.86
		89.12		1137	8	--	19.1	0.73	7.45	> 100	104	23.04
			pump stopped at 1126	1142	9	--	21.2	5.7	7.46	> 100	80	22.31
				1147	10	--	18.1	0.8	7.49	> 100	71	21.56
				1155	11	--	14.6	2.87	7.45	> 100	36	22.6
		103.85	purge started again at 1135	1204	12	--	22.3	1.24	7.45	> 100	29	22.92
				1214	13	--	17.8	1.02	7.4	> 100	21	25.34
		107.71		1221	14	--	11.7	5.3	7.41	> 100	4	26.18
	7/20/2016	81.45	90.4 @ 2100 on 7/19/16	0736	--	1	14	2.11	5.36	> 100	209	21.24
				0830	--	2	6.8	0.96	6.71	> 100	160	20.34

Table B.2 In-field measurements of water quality parameters (continued).

Appendix C - Field Kit Analyses

Sample ID	Sample Collection Date	Alkalinity mg/L (as $CaCO_3$)	HCO_3 mg/L	SiO_2 mg/L	Cl mg/L	NO_2 mg/L	NO_3 mg/L	PO_4 mg/L	SO_4 mg/L	S mg/L	As mg/L	NH_4 mg/L	Fe^{2+} mg/L	Total Fe mg/L	Mn^{2+} mg/L
Ast	7/19/2016	200	244	> 10	--	< 0.6	< 0.6	0	> 900	0.093	0	< 0.015	0	< 0.2	0
Becker	7/20/2016	340	414	> 10	--	--	4.52	0.25	290.1	--	0	< 0.015	0	< 0.2	0
Shepherd	10/6/2015	380	463	--	--	--	--	--	--	0.025	--	0.033	--	--	0
Shepherd	7/19/2016	320	390	> 10	--	< 0.6	5.11	0.2	232.2	0.061	0	< 0.015	0	< 0.2	0
Zehr	10/6/2015	300	366	--	--	--	--	--	--	0.023	--	< 0.015	--	--	0
Zehr	7/19/2016	300	366	8	< 5,000	< 0.6	2.19	0	244.9	0.107	0	0.017	0	< 0.2	0
Slate Creek 1	10/6/2015	320	390	--	--	--	--	--	--	0.032	--	0.016	--	--	0
Slate Creek 1	7/18/2016	220	268	8	--	< 0.6	0.73	0.9	90.5	0.045	0	0.043	0.1	0.374	1.815
Slate Creek 2	7/18/2016	140	171	7	--	< 0.6	1.69	0.3	--	0.472	0	0.227	0	2.4	10.02
Oil Well 61	7/20/2016	300	366	5	< 70,000	< 0.6	> 13.5	0	755.8	0.792	--	1.089	32	> 6	> 30
SW-3	10/7/2015	140	171	--	--	--	--	--	--	0.208	--	0.634	--	--	0
SW-3	7/19/2016	160	195	8	< 20,000	< 0.6	10.67	0	> 900	0.099	0	0.41	2	2.372	> 30
SW-1	10/6/2015	140	171	--	--	--	--	--	--	0.123	--	0.288	--	--	0
SW-1	7/20/2016	160	195	3.5	< 20,000	< 0.6	0.55	0	> 900	0.047	0	0.489	0.05	< 0.2	1.077
SW-2	10/6/2015	60	73	--	--	--	--	--	--	0.568	--	1.334	--	--	0
SW-2	7/20/2016	140	171	0.6	< 85,000	< 0.6	4.13	0	> 900	0.034	0	0.041	0	0.296	1.573

-- did not analyze

Table C.1 In-field measurements of time-sensitive ions.

Appendix D - Major Ion Chromatography

Sample ID	Sample Collection Date	TDS mg/L	Water Type	Ionic Strength	Hardness mg/L	F		Cl		NO_2		Br		NO_3	
						mean mg/L	std. dev.	mean mg/L	std. dev.	mean mg/L	std. dev.	mean mg/L	std. dev.	mean mg/L	std. dev.
Ast	7/19/2016	4,819	$Na\text{-}SO_4$	0.115	1,561	0.4	--	360.2	8.8	< 0.125	--	0.5	--	< 0.25	--
Becker	7/20/2016	1,070	$Mg\text{-}HCO_3$	0.025	676	0.4	--	86.2	3.2	< 0.125	--	0.3	--	15.1	1.6
Shepherd	10/6/2015	1,995	Ca-Cl	0.045	1,079	< 0.625	--	621.4	--	< 0.625	--	3.0	--	26.7	--
Shepherd	7/19/2016	1,719	Ca-Cl	0.040	1,050	< 0.625	--	545.4	--	< 0.625	--	2.6	--	21.3	--
Zehr	10/6/2015	1,946	Mg-Cl	0.053	--	< 0.625	--	896.0	--	< 0.625	--	3.0	--	12.1	--
Zehr	7/19/2016	1,952	Ca-Cl	0.048	1,306	< 0.625	--	758.5	--	< 0.625	--	2.7	--	9.9	--
Slate Creek 1	10/6/2015	931	$Mg\text{-}HCO_3$	0.020	--	0.4	--	117.4	--	< 0.125	--	0.4	--	0.9	--
Slate Creek 1	7/18/2016	680	$Ca\text{-}HCO_3$	0.014	317	0.3	--	76.2	16.0	< 0.125	--	0.2	--	2.5	--
Slate Creek 2	7/18/2016	234	$Ca\text{-}HCO_3$	0.004	86	0.2	--	8.1	--	< 0.125	--	0.1	--	< 0.25	--
Oil Well 61	7/20/2016	175,690	Na-Cl	3.460	35,607	< 31.25	--	98,952.5	--	< 31.25	--	435.6	1.8	<62.5	--
SW-3	10/7/2015	30,992	Na-Cl	0.751	17,181	< 6.25	--	16,821.6	--	< 6.25	--	72.0	--	< 12.5	--
SW-3	7/19/2016	27,656	Na-Cl	0.657	14,347	< 6.25	--	15,363.2	--	< 6.25	--	52.4	--	< 12.5	--
SW-1	10/6/2015	67,944	Na-Cl	1.300	5,555	< 12.5	--	27,229.2	--	< 12.5	--	10.5	--	< 25	--
SW-1	7/20/2016	65,106	Na-Cl	1.250	5,234	< 12.5	--	28,845.6	--	< 12.5	--	12.6	--	< 25	--
SW-2	10/6/2015	282,882	Na-Cl	5.200	17,070	< 62.5	--	154,520.1	408.0	< 62.5	--	55.3	--	< 125	--
SW-2	7/20/2016	251,860	Na-Cl	4.650	16,280	< 62.56	--	135,600.3	988.9	< 62.56	--	53.9	--	< 125.1	--

Table D.1 DIW-corrected major ion values as measured by major ion chromatography. A dash indicates the element was unable to be quantified.

Sample ID	Sample Collection Date	PO_4		SO_4		Na		NH_4		K		Mg		Ca		Sr	
		mean mg/L	std. dev.	mean mg/L	std. dev.	mean mg/L	std. dev.	mean mg/L	std. dev.	mean mg/L	std. dev.	mean mg/L	std. dev.	mean mg/L	std. dev.	mean mg/L	std. dev.
Ast	7/19/2016	< 0.3	--	2,718.7	--	929.8	24.8	< 0.625	--	5.9	0.6	128.1	6.0	414.1	10.9	23.8	1.4
Becker	7/20/2016	0.2	--	228.9	--	100.9	11.9	< 0.625	--	1.9	--	84.5	0.3	131.5	--	6.2	0.0
Shepherd	10/6/2015	< 1.5	--	284.9	--	220.3	--	< 0.625	--	< 3.125	--	101.0	--	265.3	--	9.1	--
Shepherd	7/19/2016	< 1.5	--	172.6	21.0	214.8	21.0	< 0.625	--	3.0	--	98.5	2.3	258.0	--	13.0	1.3
Zehr	10/6/2015	< 1.5	--	290.9	--	218.8	7.8	< 0.625	--	< 3.125	--	148.0	6.2	--	--	11.6	--
Zehr	7/19/2016	< 1.5	--	155.3	16.0	213.3	15.2	< 0.625	--	3.1	--	142.6	8.7	287.7	--	13.3	--
Slate Creek 1	10/6/2015	0.7	--	258.3	--	92.2	6.1	< 0.625	--	5.0	--	51.7	4.1	--	--	13.5	--
Slate Creek 1	7/18/2016	0.3	--	156.5	--	58.2	--	< 0.625	--	9.0	--	35.3	--	68.5	--	4.6	--
Slate Creek 2	7/18/2016	< 0.3	--	9.9	--	5.2	--	< 0.625	--	10.4	--	7.8	--	21.7	--	< 1.25	--
Oil Well 61	7/20/2016	< 75	--	525.1	41.6	61,423.4	--	453.1		491.1	--	2,395.5	--	10,309.6	2,196.0	791.2	44.6
SW-3	10/7/2015	< 15	--	2,493.1	1,490.8	5,395.8	--	< 15.625	--	< 78.125	--	1,525.9	77.6	4,364.1	--	148.1	--
SW-3	7/19/2016	< 15	--	1,034.3	221.7	6,021.5	--	< 15.625	--	< 78.125	--	1,526.4	14.8	3,228.3	--	234.4	17.0
SW-1	10/6/2015	< 30	--	10,764.7	--	23,711.6	--	< 15.625	--	75.3	--	906.3	64.3	729.9	21.9	44.6	--
SW-1	7/20/2016	< 30	--	9,498.4	--	24,931.8	--	< 15.625	--	77.5	--	948.6	13.6	531.7	103.5	64.8	0.6
SW-2	10/6/2015	< 150	--	12,923.2	108.6	110,621.5	14.0	< 62.5	--	313.0	--	3,793.6	238.6	579.8	149.4	< 125	--
SW-2	7/20/2016	< 150.15	--	10,838.8	--	100,623.7	454.1	< 62.5	--	307.2	--	3,472.7	89.7	793.0	398.6	< 125	--

Table D.2 DIW-corrected major ion values as measured by major ion chromatography. A dash indicates the element was unable to be quantified (continued).

Sample ID	Sample Collection Date	TDS	Water Type	Ionic Strength	Hardness	F		Cl		NO_2		Br		NO_3	
		mg/L		M	mg/L	mean mg/L	std. dev.	mean mg/L	std. dev.	mean mg/L	std. dev.	mean mg/L	std. dev.	mean mg/L	std. dev.
Ast	7/19/2016	5,088	$Na\text{-}SO_4$	0.119	1,563	0.4	--	542.2	145.7	< 0.125	--	0.5	--	< 0.25	--
Becker	7/20/2016	1,102	$Mg\text{-}HCO_3$	0.026	676	0.5	0.2	108.0	7.1	< 0.125	--	0.3	--	17.2	0.7
Shepherd	10/6/2015	2,224	Ca-Cl	0.049	1,106	< 0.625	--	836.5	--	< 0.625	--	3.0	--	26.7	--
Shepherd	7/19/2016	1,975	Ca-Cl	0.043	1,052	< 0.625	--	739.5	--	< 0.625	--	2.6	--	24.6	--
Zehr	10/6/2015	2,165	Mg-Cl	0.042	--	< 0.625	--	1,111.1	--	< 0.625	--	3.0	--	12.1	--
Zehr	7/19/2016	2,208	Ca-Cl	0.051	1,308	< 0.625	--	952.6	--	< 0.625	--	2.7	--	13.2	--
Slate Creek 1	10/6/2015	973	$Mg\text{-}HCO_3$	0.017	--	0.4	--	160.4	--	< 0.125	--	0.4	--	0.9	--
Slate Creek 1	7/18/2016	752	$Ca\text{-}HCO_3$	0.017	387	0.3	--	95.6	16.0	< 0.125	--	0.2	--	2.5	--
Slate Creek 2	7/18/2016	234	$Ca\text{-}HCO_3$	0.004	86	0.2	--	8.1	--	< 0.125	--	0.1	--	< 0.25	--
Oil Well 61	7/20/2016	199,646	Na-Cl	3.850	37,597	< 31.25	--	118,364.0	--	< 31.25	--	435.6	1.8	<62.5	--
SW-3	10/7/2015	35,172	Na-Cl	0.813	17,235	< 6.25	--	21,122.7	--	< 6.25	--	72.0	--	< 12.5	--
SW-3	7/19/2016	32,783	Na-Cl	0.747	15,012	< 6.25	--	19,245.5	--	< 6.25	--	52.4	--	< 12.5	--
SW-1	10/6/2015	69,065	Na-Cl	1.320	5,859	< 12.5	--	31,530.3	--	< 12.5	--	10.5	--	< 25	--
SW-1	7/20/2016	69,845	Na-Cl	1.340	6,647	< 12.5	--	32,727.9	--	< 12.5	--	12.6	--	< 25	--
SW-2	10/6/2015	305,718	Na-Cl	5.550	19,080	< 62.5	--	176,025.5	408.0	< 62.5	--	55.3	--	< 125	--
SW-2	7/20/2016	272,967	Na-Cl	4.980	17,534	< 62.56	--	155,011.8	988.9	< 62.56	--	53.9	--	< 125.1	--

Table D.3 Major ion values not corrected by dilution DIW as measured by major ion chromatography. A dash indicates the element was unable to be quantified.

Sample ID	Sample Collection Date	PO_4		SO_4		Na		NH_4		K		Mg		Ca		Sr	
		mean mg/L	std. dev.	mean mg/L	std. dev.	mean mg/L	std. dev.	mean mg/L	std. dev.	mean mg/L	std. dev.	mean mg/L	std. dev.	mean mg/L	std. dev.	mean mg/L	std. dev.
Ast	7/19/2016	< 0.3	--	2,799.6	--	929.8	24.8	< 0.625	--	5.9	0.6	128.5	6.6	414.1	10.9	23.8	1.4
Becker	7/20/2016	0.2	--	237.0	--	100.9	11.9	< 0.625	--	1.9	--	84.5	0.3	131.5	--	6.2	0.0
Shepherd	10/6/2015	< 1.5	--	284.9	--	225.5	--	< 0.625	--	< 3.125	--	104.1	--	271.2	--	9.1	--
Shepherd	7/19/2016	< 1.5	--	228.8	44.0	216.3	17.3	< 0.625	--	3.0	--	99.0	3.1	258.0	--	13.0	1.3
Zehr	10/6/2015	< 1.5	--	290.9	--	221.4	11.5	< 0.625	--	< 3.125	--	149.5	8.4	--	--	11.6	--
Zehr	7/19/2016	< 1.5	--	211.6	49.1	214.8	17.3	< 0.625	--	3.1	--	143.1	9.5	287.7	--	13.3	--
Slate Creek 1	10/6/2015	0.7	--	258.3	--	92.2	--	< 0.625	--	5.0	--	51.8	4.3	--	--	13.5	--
Slate Creek 1	7/18/2016	0.3	--	176.9	--	64.2	--	< 0.625	--	9.0	--	37.5	--	93.4	--	4.6	--
Slate Creek 2	7/18/2016	< 0.3	--	9.9	--	5.2	--	< 0.625	--	10.4	--	7.8	--	21.7	--	< 1.25	--
Oil Well 61	7/20/2016	< 75	--	4,341.5	5,525.4	61,423.4	--	453.1		491.1	--	2,501.0	--	10,932.4	1,315.3	791.2	44.6
SW-3	10/7/2015	< 15	--	2,522.7	1,449.0	5,395.8	--	< 15.625	--	< 78.125	--	1,539.2	92.1	4,364.1	--	155.1	--
SW-3	7/19/2016	< 15	--	2,107.9	1,151.9	6,021.5	--	< 15.625	--	< 78.125	--	1,537.0	0.1	3,477.4	--	234.4	17.0
SW-1	10/6/2015	< 30	--	11,788.1	--	23,711.6	--	< 15.625	--	75.3	--	944.4	79.0	789.1	105.6	44.6	--
SW-1	7/20/2016	< 30	--	9,498.4	--	25,232.6	--	< 15.625	--	77.5	--	964.4	6.1	1,071.5	511.0	64.8	0.6
SW-2	10/6/2015	< 150	--	13,514.9	108.6	110,621.5	14.0	< 62.5	--	313.0	--	4,042.6	283.7	974.4	285.8	< 125	--
SW-2	7/20/2016	< 150.15	--	10,838.8	--	101,826.7	454.1	< 62.5	--	307.2	--	3,525.4	15.1	1,208.1	338.1	< 125	--

Table D.4 Major ion values not corrected by dilution DIW as measured by major ion chromatography. A dash indicates the element was unable to be quantified (continued).

Appendix E - Stable Isotopes / Dissolved Organic Carbon / CO_2 / Hydrocarbons

Sample ID	Sample Collection Date	δD H_2O ‰	$\delta^{18}O$ H_2O ‰	$\delta^{13}C$ DIC ‰	NPOC mg/L	CO_2 µg/L	Methane µg/L	Ethene µg/L	Ethane µg/L	Propylene µg/L	Propane µg/L
Ast	7/19/2016	-34.3	-5.37	--	1.5	--	--	--	--	--	--
Becker	7/20/2016	-31.4	-5.14	--	1.0	--	--	--	--	--	--
Shepherd	10/6/2015	-34.0	-5.33	--	1.2	--	--	--	--	--	--
Shepherd	7/19/2016	-33.4	-5.36	--	1.1	35,000	< 1.3	< 1.0	< 0.60	< 1.0	< 1.0
Zehr	10/6/2015	-34.0	-5.39	--	1.2	--	--	--	--	--	--
Zehr	7/19/2016	-33.3	-5.41	--	1.1	--	--	--	--	--	--
Slate Creek 1	10/6/2015	-26.2	-3.63	--	3.0	--	--	--	--	--	--
Slate Creek 1	7/18/2016	-22.4	-3.78	--	4.3	--	--	--	--	--	--
Slate Creek 2	7/18/2016	0.1	0.62	--	8.8	--	--	--	--	--	--
Oil Well 61	7/20/2016	-22.9	-2.17	-37.5	6.4	230,000	< 1.3	< 1.0	14	< 1.0	73
SW-3	2/24/2015	--	--	-7.06	--	--	--	--	--	--	--
SW-3	10/7/2015	-31.6	-4.74	--	5.3	--	--	--	--	--	--
SW-3	7/19/2016	-32.7	-5.08	-9.4	5.0	9,800	5.5	< 1.0	< 0.60	< 1.0	< 1.0
SW-1	2/24/2015	--	--	0.065	--	--	--	--	--	--	--
SW-1	10/6/2015	-45.5	-7.34	--	4.4	--	--	--	--	--	--
SW-1	7/20/2016	-46.1	-7.44	-6.9	5.2	--	--	--	--	--	--
SW-2	2/24/2015	--	--	-7.63	--	--	--	--	--	--	--
SW-2	10/6/2015	-41.0	-8.09	--	2.9	--	--	--	--	--	--
SW-2	7/20/2016	-41.1	-8.06	-8.7	3.8	--	--	--	--	--	--

Table E.1 Stable isotopic values (per mil VSMOW), dissolved organic carbon (as NPOC), dissolved CO_2, and dissolved hydrocarbons. Sample collection times before 10/6/15 were collected and analyzed by KGS.

Appendix F - Trace elements

Sample ID	Sample Collection Date	Li / 7		B / 11		Na / 23		Mg / 24		Al / 27		K / 39		Ti / 47		Cr / 52		Cr / 53		Mn / 55	
		mean µg/L	std. dev.	mean µg/L	std. dev.	mean µg/L	std. dev.	mean µg/L	std. dev.	mean µg/L	std. dev.	mean µg/L	std. dev.	mean µg/L	std. dev.	mean µg/L	std. dev.	mean µg/L	std. dev.	mean µg/L	std. dev.
Ast	7/19/2016	136.70	9.79	1,459.00	14.93	888.90	28.40	130.43	4.10	32.53	1.56	3.15	0.25	0.00	0.00	0.10	0.17	0.23	0.15	15.70	0.30
Becker	7/20/2016	19.33	0.32	146.03	19.70	88.57	0.91	87.29	1.24	27.27	7.65	0.00	0.00	0.00	0.00	0.30	0.10	0.37	0.15	0.00	0.00
Shepherd	10/6/2015	34.23	1.55	164.47	10.22	172.60	4.75	86.96	1.98	22.27	2.45	0.61	0.08	0.00	0.00	0.20	0.10	0.20	0.10	0.00	0.00
Shepherd	7/19/2016	34.13	0.15	161.67	11.63	176.00	1.45	88.46	1.13	23.07	1.76	0.82	0.13	0.00	0.00	0.50	0.53	0.57	0.90	0.00	0.00
Zehr	10/6/2015	54.57	0.67	172.10	6.70	193.77	4.90	137.30	5.31	14.77	2.31	1.36	0.21	0.00	0.00	0.00	0.00	0.00	0.00	2.13	0.15
Zehr	7/19/2016	52.07	0.96	174.00	5.48	198.33	15.01	134.23	5.33	40.33	2.87	1.68	0.60	0.00	0.00	0.00	0.00	0.00	0.00	2.97	0.55
Slate Creek 1	10/6/2015	21.47	1.44	141.23	15.14	82.96	2.89	49.21	1.53	21.67	3.13	3.32	0.07	0.00	0.00	0.00	0.00	0.00	0.00	17.47	0.65
Slate Creek 1	7/18/2016	17.53	2.05	140.93	1.15	67.44	4.25	38.40	1.06	39.77	7.34	8.46	0.52	0.00	0.00	0.00	0.00	0.00	0.00	36.77	0.93
Slate Creek 2	7/18/2016	0.97	0.46	42.27	5.21	8.88	2.44	6.59	0.28	83.17	19.83	8.22	0.35	0.37	0.47	0.00	0.00	0.10	0.17	139.00	3.52
Oil Well 61	7/20/2016	6,481.22	1,018.23	5,856.33	1,222.47	55,711.11	10,247.87	2,317.33	384.61	774.30	546.58	483.67	134.75	1.54	1.77	12.38	11.60	15.46	10.74	858.81	101.29
SW-3	10/7/2015	420.07	6.99	551.97	89.22	4,854.83	116.33	1,377.33	36.78	415.15	392.97	15.74	15.63	0.00	0.00	0.00	0.00	0.27	0.47	91.68	17.83
SW-3	7/19/2016	447.42	50.52	564.13	134.44	5,524.17	1,267.79	1,362.83	79.85	289.58	273.45	8.94	9.80	0.00	0.00	0.00	0.00	0.00	0.00	89.83	16.69
SW-1	10/6/2015	1,228.67	195.19	2,824.00	521.89	19,262.78	1,372.46	790.79	75.05	377.06	421.10	22.47	15.62	2.56	3.97	5.16	8.40	5.43	8.00	70.79	23.13
SW-1	7/19/2016	1,164.42	72.95	2,351.67	170.69	20,398.33	1,146.53	790.56	25.10	438.78	404.38	30.94	23.02	0.00	0.00	1.20	2.58	1.37	1.98	186.18	28.96
SW-2	10/6/2015	2,146.17	471.21	1,486.00	485.13	87,321.67	8,425.97	3,134.83	326.37	555.17	460.59	111.47	27.20	0.00	0.00	0.35	0.63	2.83	3.13	706.63	18.53
SW-2	7/19/2016	2,398.33	278.11	1,698.17	578.28	90,811.67	5,546.97	3,185.17	169.59	642.22	578.18	173.68	42.03	1.78	4.04	1.05	1.15	4.12	4.57	656.52	39.24

Table F.1 Trace elements as analyzed by ICP-MS values next to element indicate atomic weight of isotope.

Sample ID	Sample Collection Date	Fe / 56		Fe / 57		Co / 59		Ni / 60		Cu / 63		Zn / 64		Cu / 65		Zn / 66		As / 75		Rb / 85	
		mean µg/L	std. dev.	mean µg/L	std. dev.	mean µg/L	std. dev.	mean µg/L	std. dev.	mean µg/L	std. dev.	mean µg/L	std. dev.	mean µg/L	std. dev.	mean µg/L	std. dev.	mean µg/L	std. dev.	mean µg/L	std. dev.
Ast	7/19/2016	0.60	1.04	60.73	11.87	0.03	0.06	0.83	0.12	0.00	0.00	21.13	1.76	0.00	0.00	0.00	0.00	0.50	0.00	1.77	0.12
Becker	7/20/2016	0.00	0.00	0.00	0.00	0.00	0.00	0.03	0.06	0.00	0.00	22.80	1.01	0.00	0.00	0.03	0.06	1.47	0.06	0.40	0.10
Shepherd	10/6/2015	0.00	0.00	4.60	2.51	0.00	0.00	0.00	0.00	0.00	0.00	24.43	0.91	0.00	0.00	3.13	0.74	0.57	0.12	0.37	0.12
Shepherd	7/19/2016	0.00	0.00	12.20	5.94	0.00	0.00	0.00	0.00	0.00	0.00	27.47	2.67	0.00	0.00	6.10	2.60	0.57	0.15	0.50	0.26
Zehr	10/6/2015	0.00	0.00	31.17	4.17	0.00	0.00	0.23	0.06	0.00	0.00	55.03	2.80	0.00	0.00	34.07	2.22	1.13	0.06	1.00	0.17
Zehr	7/19/2016	0.00	0.00	25.80	13.08	0.00	0.00	0.50	0.10	0.00	0.00	36.90	1.71	0.00	0.00	14.63	1.16	1.07	0.21	1.37	0.72
Slate Creek 1	10/6/2015	0.00	0.00	0.00	0.00	0.00	0.00	0.87	0.12	0.00	0.00	6.23	6.75	0.00	0.00	0.00	0.00	6.77	0.06	0.53	0.15
Slate Creek 1	7/18/2016	0.00	0.00	0.00	0.00	0.03	0.06	2.60	0.00	0.00	0.00	5.07	1.42	0.00	0.00	0.00	0.00	6.23	0.25	1.13	0.06
Slate Creek 2	7/18/2016	33.87	14.10	29.70	12.00	0.60	0.17	2.20	0.10	0.00	0.00	0.00	0.00	0.00	0.00	0.00	0.00	6.23	0.06	0.93	0.21
Oil Well 61	7/20/2016	30,752.22	3,659.64	34,046.67	3,684.15	0.44	0.67	11.62	3.41	11.82	19.28	585.86	562.49	11.78	19.60	456.06	376.24	4.32	3.37	498.97	66.61
SW-3	10/7/2015	282.12	185.13	1,056.00	234.44	0.00	0.00	6.10	13.18	123.00	101.91	211.42	454.42	118.82	97.87	157.33	380.49	0.00	0.00	12.37	15.05
SW-3	7/19/2016	1,738.67	156.39	2,594.33	171.42	0.00	0.00	0.72	0.41	83.60	36.61	25.90	0.99	0.00	0.00	0.00	0.00	6.24	1.27	6.24	1.27
SW-1	10/6/2015	15.93	30.87	149.42	133.47	1.96	1.58	5.26	0.75	0.00	0.00	130.70	178.69	22.48	17.94	111.27	158.49	1.57	2.22	17.51	8.35
SW-1	7/19/2016	2.35	5.76	66.37	74.46	3.60	3.95	16.13	26.64	60.00	146.97	415.42	715.49	60.75	148.81	261.50	640.54	0.57	0.63	25.57	19.09
SW-2	10/6/2015	0.00	0.00	83.93	92.49	13.18	5.83	8.67	1.74	168.70	68.94	40.50	39.62	157.88	73.76	27.18	29.91	1.10	1.24	53.85	3.16
SW-2	7/19/2016	0.00	0.00	87.60	97.70	8.33	6.96	11.87	1.60	10.97	12.13	26.12	20.99	8.28	9.20	5.25	5.93	1.63	1.79	241.17	5.86

Table F.2 Trace elements as analyzed by ICP-MS values next to element indicate atomic weight of isotope (continued).

Sample ID	Sample Collection Date	Sr / 88		Mo / 95		Mo / 98		Cd / 111		Cd / 112		Sb / 121		Ba / 137		W / 182		W / 183		Hg / 200	
		mean µg/L	std. dev.	mean µg/L	std. dev.	mean µg/L	std. dev.	mean µg/L	std. dev.	mean µg/L	std. dev.	mean µg/L	std. dev.	mean µg/L	std. dev.	mean µg/L	std. dev.	mean µg/L	std. dev.	mean µg/L	std. dev.
Ast	7/19/2016	9,599.33	321.87	12.00	0.78	11.60	0.70	0.00	0.00	0.00	0.00	0.23	0.06	13.50	0.70	1.53	0.38	1.53	0.38	78.40	62.51
Becker	7/20/2016	1,052.33	22.90	0.23	0.40	0.30	0.52	0.00	0.00	0.00	0.00	0.03	0.06	62.83	0.55	0.00	0.00	0.10	0.17	10.63	2.38
Shepherd	10/6/2015	4,478.00	175.60	0.00	0.00	0.00	0.00	0.00	0.00	0.00	0.00	0.00	0.00	64.80	0.61	0.00	0.00	0.00	0.00	0.00	0.00
Shepherd	7/19/2016	4,338.67	73.08	0.00	0.00	0.00	0.00	0.00	0.00	0.00	0.00	0.00	0.00	64.70	1.56	0.00	0.00	0.00	0.00	0.00	0.00
Zehr	10/6/2015	5,177.00	189.85	0.00	0.00	0.00	0.00	0.00	0.00	0.00	0.00	0.00	0.00	91.57	2.80	0.00	0.00	0.00	0.00	0.00	0.00
Zehr	7/19/2016	5,418.33	328.00	0.00	0.00	0.00	0.00	0.00	0.00	0.00	0.00	0.00	0.00	105.13	2.93	0.00	0.00	0.00	0.00	0.00	0.00
Slate Creek 1	10/6/2015	1,200.67	19.35	0.00	0.00	0.00	0.00	0.00	0.00	0.00	0.00	0.00	0.00	157.77	4.66	0.00	0.00	0.00	0.00	0.60	0.50
Slate Creek 1	7/18/2016	853.80	11.75	0.00	0.00	0.00	0.00	0.00	0.00	0.00	0.00	0.00	0.00	175.90	4.37	0.00	0.00	0.00	0.00	3.33	1.55
Slate Creek 2	7/18/2016	166.27	7.74	0.00	0.00	0.00	0.00	0.00	0.00	0.00	0.00	0.17	0.06	77.60	1.76	0.00	0.00	0.00	0.00	0.00	0.00
Oil Well 61	7/20/2016	386,966.67	51,061.26	3.16	4.91	3.00	4.74	0.22	0.44	0.22	0.44	2.16	2.07	578.52	75.15	0.10	0.24	0.05	0.12	456.27	458.05
SW-3	10/7/2015	96,896.67	1,425.74	0.00	0.00	0.00	0.00	0.00	0.00	0.00	0.00	0.00	0.00	66.50	22.88	0.00	0.00	0.00	0.00	0.00	0.00
SW-3	7/19/2016	97,248.33	2,164.53	0.00	0.00	0.00	0.00	0.00	0.00	0.00	0.00	0.00	0.00	57.20	2.39	0.00	0.00	0.00	0.00	0.00	0.00
SW-1	10/6/2015	15,163.94	2,889.51	8.50	11.58	8.51	11.57	17.78	0.99	0.33	0.50	1.66	2.28	27.99	4.69	0.00	0.00	0.00	0.00	0.05	0.12
SW-1	7/19/2016	15,547.50	243.31	2.05	2.28	1.90	2.15	0.00	0.00	0.00	0.00	0.77	1.14	35.65	19.47	0.00	0.00	0.00	0.00	2.08	3.11
SW-2	10/6/2015	12,709.00	343.96	0.00	0.00	0.00	0.00	0.00	0.00	0.00	0.00	0.23	0.27	26.87	2.59	0.00	0.00	0.00	0.00	0.95	1.10
SW-2	7/19/2016	14,058.67	530.64	0.90	1.03	0.82	0.92	0.00	0.00	0.00	0.00	0.30	0.33	33.28	2.17	0.00	0.00	0.00	0.00	2.23	3.21

Table F.3 Trace elements as analyzed by ICP-MS values next to element indicate atomic weight of isotope (continued).

Sample ID	Sample Collection Date	Hg / 202		Pb / 206		Pb / 207		Pb / 208		U / 238	
		mean µg/L	std. dev.	mean µg/L	std. dev.	mean µg/L	std. dev.	mean µg/L	std. dev.	mean µg/L	std. dev.
Ast	7/19/2016	77.93	62.11	0.00	0.00	0.10	0.10	0.00	0.00	2.47	0.15
Becker	7/20/2016	10.83	1.96	0.00	0.00	0.00	0.00	0.00	0.00	2.43	0.06
Shepherd	10/6/2015	0.00	0.00	0.00	0.00	0.00	0.00	0.00	0.00	1.77	0.06
Shepherd	7/19/2016	0.00	0.00	0.00	0.00	0.00	0.00	0.00	0.00	1.73	0.06
Zehr	10/6/2015	0.00	0.00	0.00	0.00	0.13	0.06	0.00	0.00	0.87	0.06
Zehr	7/19/2016	0.00	0.00	0.00	0.00	0.00	0.00	0.00	0.00	0.87	0.06
Slate Creek 1	10/6/2015	0.97	0.45	0.10	0.00	0.37	0.12	0.03	0.06	2.93	0.12
Slate Creek 1	7/18/2016	3.57	1.39	0.00	0.00	0.00	0.00	0.00	0.00	2.50	0.17
Slate Creek 2	7/18/2016	0.00	0.00	0.00	0.00	0.00	0.00	0.00	0.00	0.97	0.06
Oil Well 61	7/20/2016	467.25	472.74	39.57	6.24	41.90	9.97	39.31	6.52	0.02	0.07
SW-3	10/7/2015	0.00	0.00	2.83	6.94	3.33	8.16	3.00	7.35	0.00	0.00
SW-3	7/19/2016	0.00	0.00	0.00	0.00	0.00	0.00	0.00	0.00	0.00	0.00
SW-1	10/6/2015	0.13	0.33	2.10	1.82	2.02	1.73	0.32	0.49	0.72	0.65
SW-1	7/19/2016	2.28	3.19	4.23	9.69	5.90	13.29	4.77	10.90	0.52	0.57
SW-2	10/6/2015	0.93	1.10	5.83	6.41	8.30	3.40	5.77	6.35	0.17	0.19
SW-2	7/19/2016	1.97	2.92	7.45	6.12	11.15	2.17	7.30	5.82	0.25	0.28

Table F.4 Trace elements as analyzed by ICP-MS values next to element indicate atomic weight of isotope (continued).

Appendix G - Rare Earth Elements

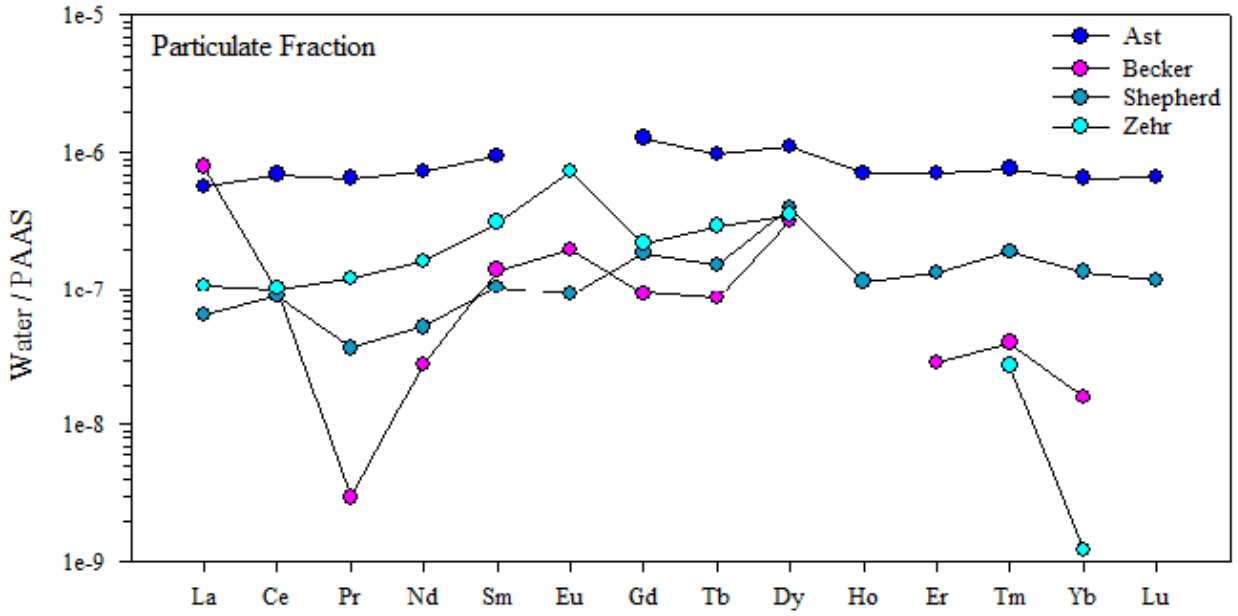

Figure G.1 'Particulate Only' fraction of domestic well samples normalized to PAAS (Taylor & McLennan, 1985). Absence of values for certain elements of specific samples indicates the dissolved concentrations exceeded total unfiltered concentrations as a result of the data nearing the instrument detection limit.

ID	Mass of sample (g)		
	before pre-concentration	after pre-concentration	Concentration factor (m/m)
SW-1 (diss.)	52.641	11.49	4.581
SW-1 (part.)	51.827	10.757	4.818
SW-2 (diss.)	59.121	11.212	5.273
SW-2 (part.)	58.769	10.695	5.495
SW-3 (diss.)	51.317	11.521	4.454
SW-3 (part.)	51.334	11.334	4.529

Table G.1 Concentration factor of high-salinity samples as based on mass of sample before pre-concentration procedure and mass of sample plus the 10 mL of 1% HNO_3 solution following the pre-concentration procedure. Factor is calculated by division of the two masses. The factor is applied to the dataset by dividing the provided factor by each individual REE for that given sample. The value is then normalized using PAAS (Taylor & McLennan, 1985). Concentration factors for low-salinity samples (domestic and surface waters) are not shown as that information rests with the performing authority (Tulane University) and was not provided with the RAW dataset but was already included.

REE	La	Ce	Pr	Nd	Sm	Eu	Gd	Tb	Dy	Ho	Er	Tm	Yb	Lu
PAAS (ng/L)	3.82E+07	7.96E+07	8.83E+06	3.39E+07	5.55E+06	1.08E+06	4.66E+06	7.70E+05	4.68E+06	9.90E+05	2.85E+06	4.10E+05	2.82E+06	4.30E+05

Table G.2 REE PAAS factors (ng/L) used in normalization of data as originally published by Taylor & McLennan, (1985).

Sample ID Dissolved / PAAS	Sample Collection Date	La mean ng/L	Ce mean ng/L	Pr mean ng/L	Nd mean ng/L	Sm mean ng/L	Eu mean ng/L	Gd mean ng/L	Tb mean ng/L	Dy mean ng/L	Ho mean ng/L	Er mean ng/L	Tm mean ng/L	Yb mean ng/L	Lu mean ng/L
Ast	7/19/2016	2.74E-07	1.66E-07	2.17E-07	2.28E-07	3.09E-07	1.82E-06	4.60E-07	5.66E-07	4.81E-07	5.15E-07	4.99E-07	4.48E-07	3.87E-07	4.27E-07
Becker	7/20/2016	1.16E-07	2.45E-08	1.03E-07	1.06E-07	1.49E-07	2.88E-07	1.82E-07	2.52E-07	2.95E-07	2.95E-07	2.12E-07	2.33E-07	1.71E-07	2.68E-07
Becker (duplicate)	7/20/2016	1.17E-07	2.43E-08	9.87E-08	1.04E-07	1.26E-07	3.24E-07	1.36E-07	1.86E-07	2.61E-07	2.71E-07	2.37E-07	2.30E-07	1.74E-07	1.84E-07
Shepherd	7/19/2016	1.89E-07	5.89E-08	1.58E-07	1.80E-07	2.71E-07	4.23E-07	3.31E-07	4.20E-07	5.49E-07	4.28E-07	4.26E-07	4.64E-07	3.38E-07	3.53E-07
Zehr	7/19/2016	2.30E-07	1.38E-07	1.64E-07	1.76E-07	2.61E-07	5.58E-07	3.82E-07	3.92E-07	5.96E-07	4.22E-07	4.62E-07	4.67E-07	3.64E-07	3.72E-07
Slate Creek 1	7/18/2016	1.14E-06	8.84E-07	1.41E-06	1.70E-06	2.50E-06	3.52E-06	3.52E-06	3.15E-06	3.15E-06	3.50E-06	3.56E-06	3.28E-06	2.85E-06	3.04E-06
Slate Creek 2	7/18/2016	7.20E-06	7.67E-06	9.35E-06	1.01E-05	1.25E-05	1.63E-05	1.42E-05	1.08E-05	8.60E-06	7.49E-06	6.94E-06	6.03E-06	5.32E-06	5.09E-06
Slate Creek 2 (duplicate)	7/18/2016	7.17E-06	7.70E-06	9.40E-06	1.01E-05	1.27E-05	1.41E-05	1.44E-05	1.13E-05	9.01E-06	7.58E-06	6.89E-06	6.28E-06	5.45E-06	5.09E-06
SW-1	7/20/2016	7.10E-07	5.92E-07	6.04E-07	6.64E-07	5.77E-07	7.80E-07	8.22E-07	8.54E-07	7.68E-07	7.51E-07	6.63E-07	6.11E-07	5.84E-07	8.70E-07
SW-2	7/20/2016	1.00E-06	8.18E-07	9.02E-07	1.02E-06	8.70E-07	9.68E-07	1.14E-06	1.32E-06	1.32E-06	1.20E-06	1.23E-06	8.95E-07	1.04E-06	1.23E-06
SW-3	7/19/2016	1.02E-06	8.06E-07	9.51E-07	1.04E-06	8.63E-07	9.17E-07	1.21E-06	1.26E-06	1.41E-06	1.14E-06	1.15E-06	1.08E-06	9.93E-07	1.33E-06

Table G.3 PAAS-normalized dissolved-only REE dataset as analyzed by medium and high resolution ICP-MS.

Sample ID Particulate / PAAS	Sample Collection Date	La mean ng/L	Ce mean ng/L	Pr mean ng/L	Nd mean ng/L	Sm mean ng/L	Eu mean ng/L	Gd mean ng/L	Tb mean ng/L	Dy mean ng/L	Ho mean ng/L	Er mean ng/L	Tm mean ng/L	Yb mean ng/L	Lu mean ng/L
Ast	7/19/2016	5.74E-07	6.99E-07	6.54E-07	7.41E-07	9.58E-07	-5.94E-07	1.29E-06	9.83E-07	1.11E-06	7.09E-07	7.13E-07	7.66E-07	6.57E-07	6.69E-07
Becker	7/20/2016	7.93E-07	1.02E-07	2.97E-09	2.83E-08	1.41E-07	1.97E-07	9.37E-08	8.67E-08	3.20E-07	-8.69E-08	2.91E-08	4.07E-08	1.62E-08	-2.66E-08
Shepherd	7/19/2016	6.49E-08	8.93E-08	3.71E-08	5.28E-08	1.05E-07	9.30E-08	1.88E-07	1.53E-07	4.04E-07	1.17E-07	1.36E-07	1.92E-07	1.37E-07	1.19E-07
Zehr	7/19/2016	1.08E-07	1.02E-07	1.23E-07	1.64E-07	3.14E-07	7.41E-07	2.22E-07	2.95E-07	3.57E-07	-2.96E-08	-4.52E-08	2.76E-08	1.22E-09	-3.58E-08
Slate Creek 1	7/18/2016	1.95E-05	2.17E-05	2.54E-05	2.75E-05	3.55E-05	3.88E-05	4.35E-05	3.43E-05	2.88E-05	2.46E-05	2.26E-05	2.09E-05	1.81E-05	1.72E-05
Slate Creek 2	7/18/2016	1.09E-04	1.27E-04	1.32E-04	1.44E-04	1.76E-04	1.93E-04	2.13E-04	1.60E-04	1.26E-04	1.10E-04	9.98E-05	9.27E-05	7.90E-05	7.42E-05
SW-1	7/20/2016	5.66E-06	6.95E-06	8.11E-06	9.57E-06	1.37E-05	1.42E-05	1.38E-05	1.48E-05	9.60E-06	8.63E-06	6.70E-06	5.88E-06	5.48E-06	7.64E-06
SW-2	7/20/2016	2.98E-06	3.30E-06	4.17E-06	4.51E-06	6.17E-06	7.29E-06	6.19E-06	7.12E-06	4.32E-06	4.78E-06	3.20E-06	3.43E-06	2.91E-06	5.27E-06
SW-3	7/19/2016	5.57E-05	7.49E-05	8.54E-05	9.50E-05	1.39E-04	1.41E-04	1.28E-04	1.09E-04	8.87E-05	7.09E-05	5.85E-05	5.77E-05	4.95E-05	4.81E-05

Negative particulate values indicate concentrations were greater in the filtered sample than in the unfiltered sample, likely due to results of that specific REE approaching the sensitivity of the analysis or method detection limit.

Table G.4 PAAS-normalized particulate-only REE dataset as analyzed by medium and high resolution ICP-MS (continued).

Concentrations in ng/L		Medium Resolution					High Resolution						
Dissolved	Isotope	La / 139	Ce / 140	Pr / 141	Nd / 143	Nd / 145	Y / 89	Nd / 146	Sm / 147	Sm / 149	Eu / 151	Eu / 153	Gd / 155
SW-1	Conc. AVG	178.79	293.78	38.46	155.15	162.89	229.39	164.45	20.33	23.56	4.52	4.55	25.06
	Conc. STD	1.84	4.35	0.76	2.84	5.86	10.17	16.31	2.95	1.37	1.08	0.34	2.55
	Conc. RSD [%]	1.03	1.48	1.97	1.83	3.60	4.43	9.91	14.52	5.82	23.80	7.39	10.16
SW-2	Conc. AVG	142.95	248.43	28.11	121.58	116.89	139.07	117.75	17.05	16.72	5.02	3.87	20.42
	Conc. STD	5.73	5.50	2.29	5.83	1.04	9.44	10.08	6.34	7.01	1.14	1.01	2.31
	Conc. RSD [%]	4.01	2.22	8.16	4.80	0.89	6.79	8.56	37.16	41.91	22.65	26.05	11.30
SW-3	Conc. AVG	170.22	290.11	35.49	148.85	152.17	211.55	160.84	22.00	21.03	4.31	5.01	24.79
	Conc. STD	3.38	4.30	0.78	8.45	12.40	0.96	5.42	3.85	2.68	0.77	0.71	7.07
	Conc. RSD [%]	1.99	1.48	2.19	5.68	8.15	0.45	3.37	17.50	12.75	17.77	14.26	28.53

Table G.5 High-salinity (shallow monitoring wells) dissolved-only (< 0.45 µm) RAW dataset of REE data analyzed at Tulane University. These data were subjected to Fe co-precipitation in addition to cation column exchange chromatography due to high concentration of interfering ions in sample matrix. Number next to element indicates atomic weight of isotope.

Concentrations in ng/L		High Resolution											
Dissolved	Isotope	Gd / 157	Gd / 158	Tb / 159	Dy / 161	Dy / 163	Ho / 165	Er / 166	Er / 167	Tm / 169	Yb / 172	Yb / 173	Lu / 175
SW-1	Conc. AVG	26.93	25.82	4.46	28.78	31.74	5.19	15.40	14.55	2.02	11.89	13.77	2.63
	Conc. STD	4.59	4.62	0.84	5.94	4.56	1.08	2.59	1.21	0.18	0.64	0.74	0.48
	Conc. RSD [%]	17.05	17.90	18.92	20.63	14.38	20.76	16.80	8.35	8.78	5.37	5.40	18.28
SW-2	Conc. AVG	21.34	18.80	3.47	18.27	19.63	3.92	10.34	9.58	nd	10.18	7.19	1.97
	Conc. STD	2.65	1.78	0.64	3.54	1.91	1.03	1.46	1.85	0.13	1.82	1.59	0.42
	Conc. RSD [%]	12.41	9.49	18.52	19.37	9.75	26.32	14.13	19.27	9.53	17.91	22.18	21.03
SW-3	Conc. AVG	22.79	23.42	4.52	28.58	26.35	5.31	17.62	13.63	nd	13.20	12.99	2.36
	Conc. STD	2.25	2.29	0.55	5.00	0.95	0.30	3.27	3.17	0.15	2.06	1.67	0.47
	Conc. RSD [%]	9.86	9.77	12.27	17.48	3.60	5.60	18.57	23.24	8.88	15.60	12.88	19.67

Table G.6 High-salinity (shallow monitoring wells) dissolved-only (< 0.45 µm) RAW dataset of REE data analyzed at Tulane University. These data were subjected to Fe co-precipitation in addition to cation column exchange chromatography due to high concentration of interfering ions in sample matrix (continued). Number next to element indicates atomic weight of isotope.

Concentrations in ng/L		Medium Resolution					High Resolution						
Particulate	Isotope	La / 139	Ce / 140	Pr / 141	Nd / 143	Nd / 145	Y / 89	Nd / 146	Sm / 147	Sm / 149	Eu / 151	Eu / 153	Gd / 155
SW-1	Conc. AVG	10,439.05	29,035.68	3,672.32	15,897.28	15,535.36	6,979.30	15,617.23	3,633.25	3,865.28	733.24	738.70	2,852.33
	Conc. STD	49.09	344.07	55.39	78.61	173.12	223.46	318.69	134.90	82.96	14.92	15.87	250.70
	Conc. RSD [%]	0.47	1.18	1.51	0.49	1.11	3.20	2.04	3.71	2.15	2.03	2.15	8.79
SW-2	Conc. AVG	1,336.76	3,300.43	422.95	1,865.64	1,787.44	968.27	2,066.82	418.52	449.71	94.01	83.52	357.80
	Conc. STD	55.20	106.25	9.25	86.16	37.92	63.41	145.65	6.16	30.02	8.99	8.34	16.05
	Conc. RSD [%]	4.13	3.22	2.19	4.62	2.12	6.55	7.05	1.47	6.68	9.56	9.99	4.49
SW-3	Conc. AVG	689.36	1,483.39	202.97	875.40	828.43	502.93	842.39	175.09	179.02	41.79	38.96	155.97
	Conc. STD	10.37	26.66	5.62	18.87	42.14	5.82	23.77	11.66	16.76	0.23	1.78	17.78
	Conc. RSD [%]	1.50	1.80	2.77	2.16	5.09	1.16	2.82	6.66	9.36	0.55	4.56	11.40

Table G.7 High-salinity (shallow monitoring wells) particulate and dissolved (unfiltered) RAW dataset of REE data analyzed at Tulane University. These data were subjected to Fe co-precipitation in addition to cation column exchange chromatography due to high concentration of interfering ions in sample matrix. Number next to element indicates atomic weight of isotope.

Concentrations in ng/L		High Resolution											
Particulate	Isotope	Gd / 157	Gd / 158	Tb / 159	Dy / 161	Dy / 163	Ho / 165	Er / 166	Er / 167	Tm / 169	Yb / 172	Yb / 173	Lu / 175
SW-1	Conc. AVG	3,008.51	2,856.07	409.01	2,068.73	1,995.36	343.50	835.13	803.72	116.09	712.25	660.84	102.49
	Conc. STD	230.58	293.59	8.77	10.57	35.20	13.21	43.01	124.91	4.71	15.85	23.87	5.47
	Conc. RSD [%]	7.66	10.28	2.14	0.51	1.76	3.85	5.15	15.54	4.06	2.22	3.61	5.34
SW-2	Conc. AVG	392.52	376.49	66.14	260.82	272.38	51.04	120.85	109.76	14.62	97.62	90.16	20.10
	Conc. STD	17.37	25.74	2.19	42.53	25.07	2.65	14.42	8.73	0.62	17.62	10.04	1.49
	Conc. RSD [%]	4.42	6.84	3.32	16.31	9.20	5.20	11.94	7.95	4.25	18.05	11.13	7.43
SW-3	Conc. AVG	148.81	159.10	29.42	119.56	119.31	26.82	57.37	57.03	8.02	51.61	49.45	12.66
	Conc. STD	10.19	13.13	3.04	6.90	0.79	0.49	2.55	11.02	1.67	6.09	3.82	0.20
	Conc. RSD [%]	6.85	8.25	10.34	5.77	0.67	1.83	4.45	19.32	20.86	11.80	7.72	1.59

Table G.8 High-salinity (shallow monitoring wells) particulate and dissolved (unfiltered) RAW dataset of REE data analyzed at Tulane University. These data were subjected to Fe co-precipitation in addition to cation column exchange chromatography due to high concentration of interfering ions in sample matrix (continued). Number next to element indicates atomic weight of isotope.

Concentrations in ng/L		Medium Resolution					High Resolution						
Particulate + Dissolved	Isotope	La / 139	Ce / 140	Pr / 141	Nd / 143	Nd / 145	Y / 89	Nd / 146	Sm / 147	Sm / 149	Eu / 151	Eu / 153	Gd / 155
DIW 1 Check 1	Conc. AVG	114.64	189.16	27.86	118.19	121.24	76.90	123.96	11.31	12.55	3.45	3.39	14.46
	Conc. STD	2.87	2.34	0.58	4.42	4.08	3.59	3.06	0.68	0.88	0.29	0.31	1.67
	Conc. RSD [%]	2.51	1.23	2.07	3.74	3.36	4.66	2.47	6.05	6.98	8.52	9.07	11.57
DIW 1 Check 2	Conc. AVG	70.10	179.87	2.02	116.56	105.05	60.85	124.84	nd	nd	nd	nd	nd
	Conc. STD	0.36	3.30	0.89	6.35	2.32	6.87	7.87	3.44	1.44	0.43	0.55	5.01
	Conc. RSD [%]	0.52	1.83	43.80	5.45	2.21	11.30	6.30	36.08	20.74	1.33	1.61	33.22
DIW 2 Check 1	Conc. AVG	67.11	165.67	nd	109.43	101.08	46.81	109.80	nd	nd	nd	nd	nd
	Conc. STD	2.68	1.12	1.63	4.22	10.57	4.79	6.35	1.00	3.74	0.46	0.26	1.52
	Conc. RSD [%]	3.99	0.67	874.67	3.86	10.46	10.23	5.78	7.35	40.32	1.44	0.72	8.53
DIW 2 Check 2	Conc. AVG	110.87	116.25	nd	68.91	64.51	35.09	68.94	nd	nd	nd	nd	nd
	Conc. STD	6.30	3.34	1.15	8.03	6.80	1.09	6.81	0.96	2.44	0.64	0.37	1.00
	Conc. RSD [%]	5.68	2.88	9.96	11.65	10.53	3.12	9.88	5.84	16.71	1.91	1.03	4.00
100ppt REE Standard Solution Check	Conc. AVG	106.71	108.43	103.52	106.52	103.53	88.12	113.36	104.46	99.22	97.61	92.72	101.64
	Conc. STD	3.55	3.34	2.89	3.60	4.06	6.28	6.37	5.73	9.01	2.83	3.79	4.43
	Conc. RSD [%]	3.33	3.08	2.79	3.38	3.92	7.13	5.62	5.48	9.08	2.89	4.09	4.36

Table G.9 RAW REE dataset of de-ionized water and standard solution checks of particulate and dissolved fraction (unfiltered) to indicate REE accuracy and repeatability. ND indicates non-detect, or under the method detection limit of 2 ppt.

Concentrations in ng/L		High Resolution											
Particulate + Dissolved	Isotope	Gd / 157	Gd / 158	Tb / 159	Dy / 161	Dy / 163	Ho / 165	Er / 166	Er / 167	Tm / 169	Yb / 172	Yb / 173	Lu / 175
DIW 1 Check 1	Conc. AVG	14.90	13.05	2.38	17.21	16.83	2.70	8.22	7.16	nd	8.65	10.28	nd
	Conc. STD	2.26	1.90	0.14	3.42	0.74	0.35	2.15	0.16	0.18	2.26	2.79	0.23
	Conc. RSD [%]	15.16	14.59	5.87	19.88	4.37	12.82	26.17	2.23	13.72	26.17	27.12	16.50
DIW 1 Check 2	Conc. AVG	nd	nd	nd	nd	nd	nd	nd	nd	nd	nd	nd	nd
	Conc. STD	3.85	2.34	0.85	4.89	0.93	1.04	2.04	2.14	0.20	0.30	1.22	0.30
	Conc. RSD [%]	23.25	9.77	2.11	52.65	5.70	6.86	12.95	46.95	7.02	3.24	4.67	0.79
DIW 2 Check 1	Conc. AVG	nd	nd	nd	nd	nd	nd	nd	nd	nd	nd	nd	nd
	Conc. STD	2.29	1.25	0.53	3.24	3.45	0.23	0.77	0.92	0.06	1.64	1.09	0.49
	Conc. RSD [%]	8.74	4.74	1.30	19.76	16.01	1.55	4.75	10.20	1.86	14.95	4.00	1.28
DIW 2 Check 2	Conc. AVG	nd	nd	nd	nd	nd	nd	nd	nd	nd	nd	nd	nd
	Conc. STD	2.74	1.78	0.46	1.71	0.25	0.24	1.10	2.74	0.13	1.90	0.61	0.21
	Conc. RSD [%]	9.01	5.25	1.11	7.77	1.14	1.48	5.52	26.85	3.64	15.78	2.01	0.55
100ppt REE Standard Solution Check	Conc. AVG	100.67	100.22	98.02	88.72	98.91	99.56	92.99	98.90	112.63	106.25	106.09	105.32
	Conc. STD	10.93	9.72	2.08	6.05	3.25	8.83	13.31	17.64	5.26	9.25	9.84	2.36
	Conc. RSD [%]	10.86	9.69	2.12	6.81	3.29	8.87	14.32	17.83	4.67	8.70	9.28	2.24

nd - non-detect, below instrument method detection limit of 2 ppt

Table G.10 RAW REE dataset of de-ionized water and standard solution checks of particulate and dissolved fraction (unfiltered) to indicate REE accuracy and repeatability. ND indicates non-detect, or under the method detection limit of 2 ppt (continued).

Concentrations in ng/L		High Resolution													
Dissolved	Isotope	La / 139	Ce / 140	Pr / 141	Nd / 144	Sm / 150	Eu / 152	Gd / 157	Tb / 159	Dy / 163	Ho / 165	Er / 167	Tm / 169	Yb / 173	Lu / 175
Ast	Conc. AVG	10.49	13.18	1.92	7.73	1.71	1.97	2.14	0.44	2.25	0.51	1.42	0.18	1.09	0.18
	Conc. STD	0.03	0.25	0.06	0.34	0.03	0.73	0.21	0.02	0.06	0.02	0.09	0.01	0.08	0.02
	Conc. RSD [%]	0.28	1.88	3.04	4.41	1.70	37.22	9.79	4.72	2.85	4.82	6.65	6.19	7.73	8.21
Becker	Conc. AVG	4.43	1.95	0.91	3.58	0.83	0.31	0.85	0.19	1.38	0.29	0.60	0.10	0.48	0.12
	Conc. STD	0.06	0.06	0.03	0.03	0.06	0.25	0.07	0.01	0.03	0.01	0.02	0.01	0.05	0.02
	Conc. RSD [%]	1.28	2.94	2.80	0.94	7.68	81.25	7.69	5.00	1.83	3.21	2.53	5.89	10.75	13.81
Becker (Duplicate)	Conc. AVG	4.46	1.93	0.87	3.53	0.70	0.35	0.63	0.14	1.22	0.27	0.68	0.09	0.49	0.08
	Conc. STD	0.07	0.05	0.04	0.10	0.06	0.23	0.03	0.02	0.08	0.02	0.04	0.03	0.08	0.00
	Conc. RSD [%]	1.60	2.73	4.59	2.70	8.23	65.18	4.00	13.94	6.45	6.41	6.10	29.84	16.65	5.52
Shepherd	Conc. AVG	7.22	4.69	1.39	6.09	1.50	0.46	1.54	0.32	2.57	0.42	1.21	0.19	0.95	0.15
	Conc. STD	0.11	0.05	0.07	0.30	0.12	0.14	0.14	0.05	0.01	0.03	0.04	0.00	0.09	0.02
	Conc. RSD [%]	1.53	1.14	5.11	4.90	7.80	30.88	8.78	15.53	0.28	7.33	3.57	1.81	9.90	11.59
Zehr	Conc. AVG	8.78	11.01	1.45	5.97	1.45	0.60	1.78	0.30	2.79	0.42	1.32	0.19	1.03	0.16
	Conc. STD	0.13	0.14	0.03	0.21	0.16	0.25	0.21	0.02	0.07	0.01	0.02	0.01	0.07	0.02
	Conc. RSD [%]	1.48	1.30	1.86	3.45	10.82	41.43	12.01	7.44	2.43	1.57	1.78	7.49	6.57	11.12
Slate Creek 1	Conc. AVG	43.57	70.38	12.49	57.74	13.88	3.80	16.41	2.43	14.74	3.47	10.14	1.34	8.03	1.31
	Conc. STD	0.58	1.23	0.23	1.07	0.31	0.92	0.21	0.05	0.22	0.03	0.15	0.05	0.21	0.05
	Conc. RSD [%]	1.32	1.75	1.88	1.86	2.22	24.28	1.26	1.89	1.50	0.78	1.52	3.70	2.58	3.56
Slate Creek 2	Conc. AVG	274.87	610.91	82.52	340.92	69.11	17.61	66.39	8.35	40.24	7.41	19.77	2.47	14.99	2.19
	Conc. STD	2.17	1.12	0.81	0.60	0.66	0.94	0.18	0.08	0.51	0.10	0.26	0.07	0.05	0.01
	Conc. RSD [%]	0.79	0.18	0.99	0.17	0.96	5.36	0.27	0.90	1.27	1.30	1.32	3.03	0.35	0.62
Slate Creek 2 (Duplicate)	Conc. AVG	273.77	613.06	83.02	342.62	70.23	15.24	67.26	8.68	42.16	7.50	19.63	2.57	15.36	2.19
	Conc. STD	2.56	3.88	0.67	1.26	1.91	0.64	1.01	0.22	0.83	0.09	0.40	0.05	0.32	0.06
	Conc. RSD [%]	0.94	0.63	0.81	0.37	2.72	4.21	1.50	2.59	1.96	1.26	2.01	1.89	2.07	2.55

Table G.11 Low-salinity (domestic and surface waters) dissolved-only (< 0.45 µm) RAW dataset of REE data analyzed at Tulane University. These data were only subjected to cation column exchange chromatography performed by Tulane University personnel to elute Fe and Ba in sample matrix.

Concentrations in ng/L		High Resolution													
Particulate	Isotope	La / 139	Ce / 140	Pr / 141	Nd / 144	Sm / 150	Eu / 152	Gd / 157	Tb / 159	Dy / 163	Ho / 165	Er / 167	Tm / 169	Yb / 173	Lu / 175
Ast	Conc. AVG	848.60	864.11	7.69	32.83	7.03	1.32	8.13	1.19	7.44	1.21	3.45	0.50	2.94	0.47
	Conc. STD	0.23	0.41	0.21	0.55	0.12	0.41	0.50	0.06	0.30	0.03	0.09	0.01	0.05	0.02
	Conc. RSD [%]	0.03	0.05	2.68	1.68	1.77	31.09	6.12	5.29	4.00	2.08	2.67	2.29	1.86	5.29
Becker	Conc. AVG	908.45	126.53	0.94	4.54	1.61	0.52	1.29	0.26	2.88	0.21	0.69	0.11	0.53	0.10
	Conc. STD	0.17	0.09	0.06	0.29	0.07	0.32	0.21	0.02	0.09	0.02	0.10	0.02	0.03	0.01
	Conc. RSD [%]	0.02	0.07	5.92	6.28	4.56	61.17	16.07	6.07	3.09	9.29	14.94	15.19	5.47	5.56
Shepherd	Conc. AVG	253.84	148.18	1.72	7.88	2.09	0.56	2.42	0.44	4.46	0.54	1.60	0.27	1.34	0.20
	Conc. STD	0.01	0.03	0.02	0.40	0.10	0.46	0.16	0.01	0.10	0.00	0.10	0.02	0.20	0.02
	Conc. RSD [%]	0.00	0.02	0.91	5.07	4.96	81.67	6.65	3.07	2.20	0.87	6.51	8.78	15.13	8.53
Zehr	Conc. AVG	338.34	240.83	2.53	11.55	3.19	1.40	2.81	0.53	4.46	0.39	1.19	0.20	1.03	0.14
	Conc. STD	0.17	0.48	0.08	0.36	0.17	0.67	0.17	0.02	0.27	0.03	0.11	0.02	0.06	0.02
	Conc. RSD [%]	0.05	0.20	3.00	3.13	5.41	47.74	6.18	4.52	6.10	7.21	9.39	7.75	5.62	12.84
Slate Creek 1	Conc. AVG	20,637.47	22,624.18	236.72	991.21	210.85	45.75	218.90	28.88	149.54	27.84	74.46	9.91	59.20	8.71
	Conc. STD	5.49	15.26	1.81	3.70	0.54	2.44	3.21	0.37	1.90	0.19	0.76	0.09	0.43	0.11
	Conc. RSD [%]	0.03	0.07	0.76	0.37	0.25	5.34	1.46	1.28	1.27	0.69	1.01	0.87	0.72	1.22
Slate Creek 2	Conc. AVG	116,361.51	134,896.84	1,248.60	5,224.10	1,046.79	226.42	1,058.98	131.27	631.28	115.97	304.27	40.47	237.64	34.08
	Conc. STD	45.59	102.64	6.93	74.65	10.23	19.42	11.89	1.45	1.73	0.43	5.94	0.54	4.01	0.62
	Conc. RSD [%]	0.04	0.08	0.56	1.43	0.98	8.58	1.12	1.11	0.27	0.37	1.95	1.33	1.69	1.83

Table G.12 Low-salinity (domestic and surface waters) particulate and dissolved (unfiltered) RAW dataset of REE data analyzed at Tulane University. These data were only subjected to cation column exchange chromatography performed by Tulane University personnel to elute Fe and Ba in sample matrix.